Petroleum Geochemistry of the Makhbaz Formation in the Offshore Well K-137, Sabratah Basin, NW Libya

By

ABDELRHMAN HAMAD ALI AL SANOSSI

Supervisor

Assist. Prof. Osama Shaltami

This Thesis was submitted in Partial Fulfillment of the Requirements for Master's Degree of Science in Geology, Geochemistry

University of Benghazi

Faculty of Science

Dec 2019

University of Benghazi **Faculty of Science**

Department of Earth Science

Petroleum Geochemistry of the Makhbaz Formation in the Offshore Well K-137, Sabratah Basin, NW Libya

By

ABDELRHMAN HAMAD ALI AL SANOSSI

This Thesis was Successfully Defended and Approved on **04.12.2019**

Supervisor

Assist. Prof. Osama Shaltami

Signature: ....

Prof. Ahmed M. Muftah **(Internal Examiner)**

Signature: ....

Assist. Prof. Rahel G. Rahel **(External Examiner)**

Signature: ....

Dean of Faculty **Director of Graduate Studies and Training**

University of Benghazi

Director of Graduate Studies and Training

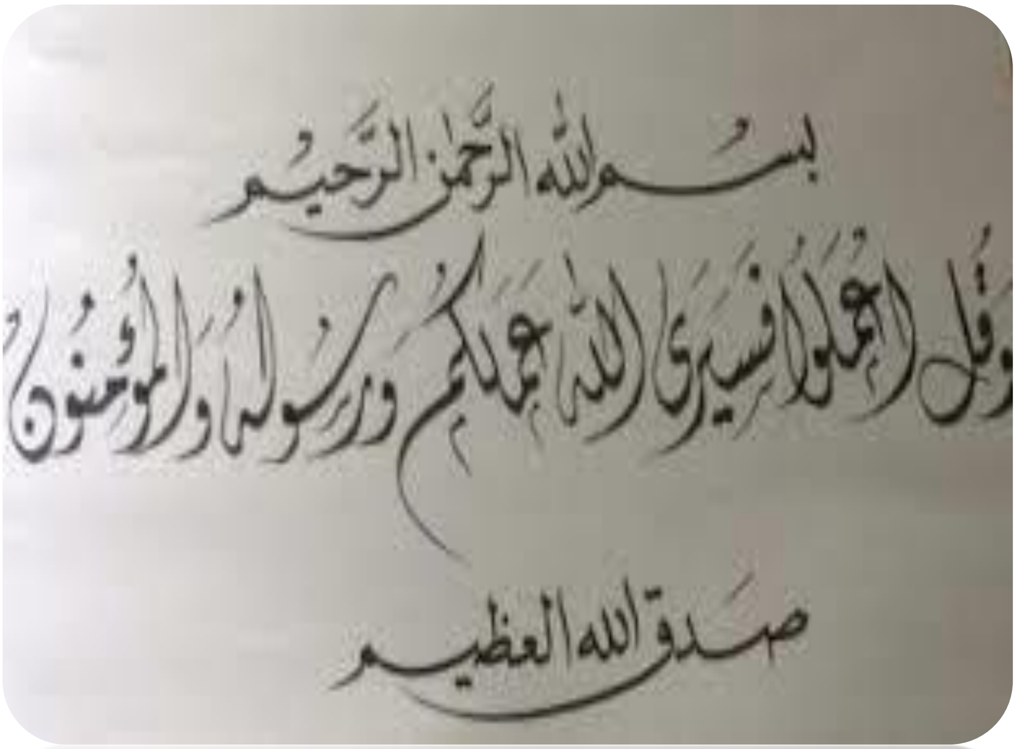

سورة التوبة ، الآية (105)

AKNOWLEDGEMENT

This work would not have been possible without the help of my supervisor, Assist. Prof. Osama Shaltami Long staff, thank you, sir, for your guidance, motivation, patience and immense knowledge throughout my project.

I would like to thank AGIP company for giving samples.

I would also like to thank the laboratory of Chemostratigraphy and Organic Geochemistry (LGQM), State University of Rio de Janeiro (UERJ), Brazil. For preparing and analyzing samples.

I dedicated my work to people who have been my pillars of strength throughout my life, my parents, and my other family member.

I would also like to thank my lovely friends and Staff Members of the Department of the Earth Sciences, Faculty of Science, Benghazi University, for their help during the academic years of my study at this department.

LIST OF CONTENTS

LIST OF TABLES

LIST OF FIGURES

ABBREVIATION

TOC = total organic carbon (wt. %)

S_1 = amount of free hydrocarbons in sample (mg/g)

S_2 = amount of hydrocarbons generated through thermal cracking (mg/g) – provides the quantity of hydrocarbons that the rock has the potential to produce through diagenesis

S_3 = amount of CO_2 (mg of CO_2/g of rock) - reflects the amount of oxygen in the oxidation step

T_{max} = the temperature at which maximum rate of generation of hydrocarbons occurs

Hydrogen index: HI = 100 * S_2 / TOC

Oxygen index: OI = 100 * S_3 / TOC

Production index: PI = S_1 / (S_1 + S_2)

Semi-quantitative index: GP = S_1 / S_2

Ro = vitrinite reflectance (wt. %)

Pr/Ph = Pristane/Phytane

Carbon preference index: CPI = $2(C_{23} + C_{25} + C_{27} + C_{29})/(C_{22} + 2[C_{24}+ C_{26} + C_{28}] + C_{30})$

Waxiness index: WI = $\Sigma(n\text{-}C_{21}\text{-}n\text{-}C_{31})/\Sigma(n\text{-}C_{15}\text{-}n\text{-}C_{20})$

TPP = tetracyclic polyprenoid

Petroleum Geochemistry of the Makhbaz Formation in the Offshore Well K-137, Sabratah Basin, NW Libya

By

ABDELRHMAN HAMAD ALI AL SANOSSI

Supervisor

Assist. Prof. Osama Shaltami

ABSTRACT

This study is a geochemical evaluation of the Makhbaz Formation in the offshore well K137, Sabratah Basin, NW Libya. The TOC content indicated that the Makhbaz Shale is an excellent source rock. The organic matter is thermally mature and characterized by the sovereignty of type II kerogen. The most abundant gas in the petroleum inclusions of the Makhbaz Limestone (reservoir) is C_1 with lesser amounts of C_2, C_3, nC_4, iC_4, N_2, CO_2 and H_2S. There are two oil families in the petroleum inclusions. The Makhbaz Shale is the main source rock of Family I oils (heavy oils), whereas Family II oils (light oils) were probably derived from the Bilal Formation. All oils are thermally mature. There are two episodes of oil charging took place in the Makhbaz Reservoir.

Keywords: petroleum Geochemistry, Source Rock, Reservoir, Makhbaz Formation, Sabratah Basin, Libya.

CHAPTER ONE
INTRODUCTION

1.1. General

The Sabratah Basin, which lies on the Pelagian Shelf extending from Tunisian waters into the northwest Libya offshore (Fig. 1.1), has oil and gas accumulations in Eocene carbonate reservoirs and gas in Upper Cretaceous reservoirs (Hallett and Clark-Lowes, 2016). These are present in a basin developed on the north side of the Nafusah Arch/Jifarah Terrace against the major Jifarah fault system (Hallett and Clark-Lowes, 2016, Fig. 1.2).

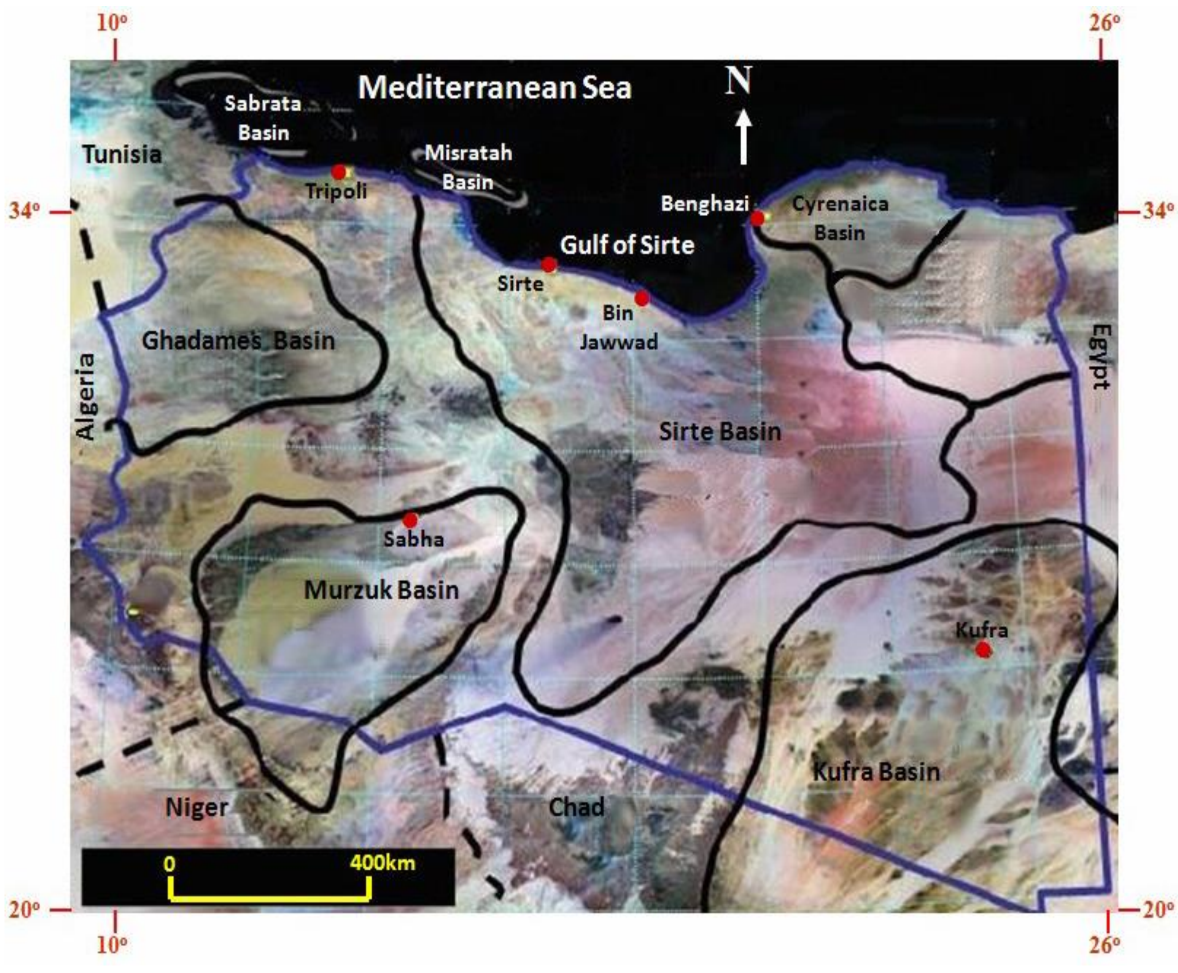

Fig. 1.1: Satellite image showing the sedimentary basins in Libya (after Shaltami, 2012).

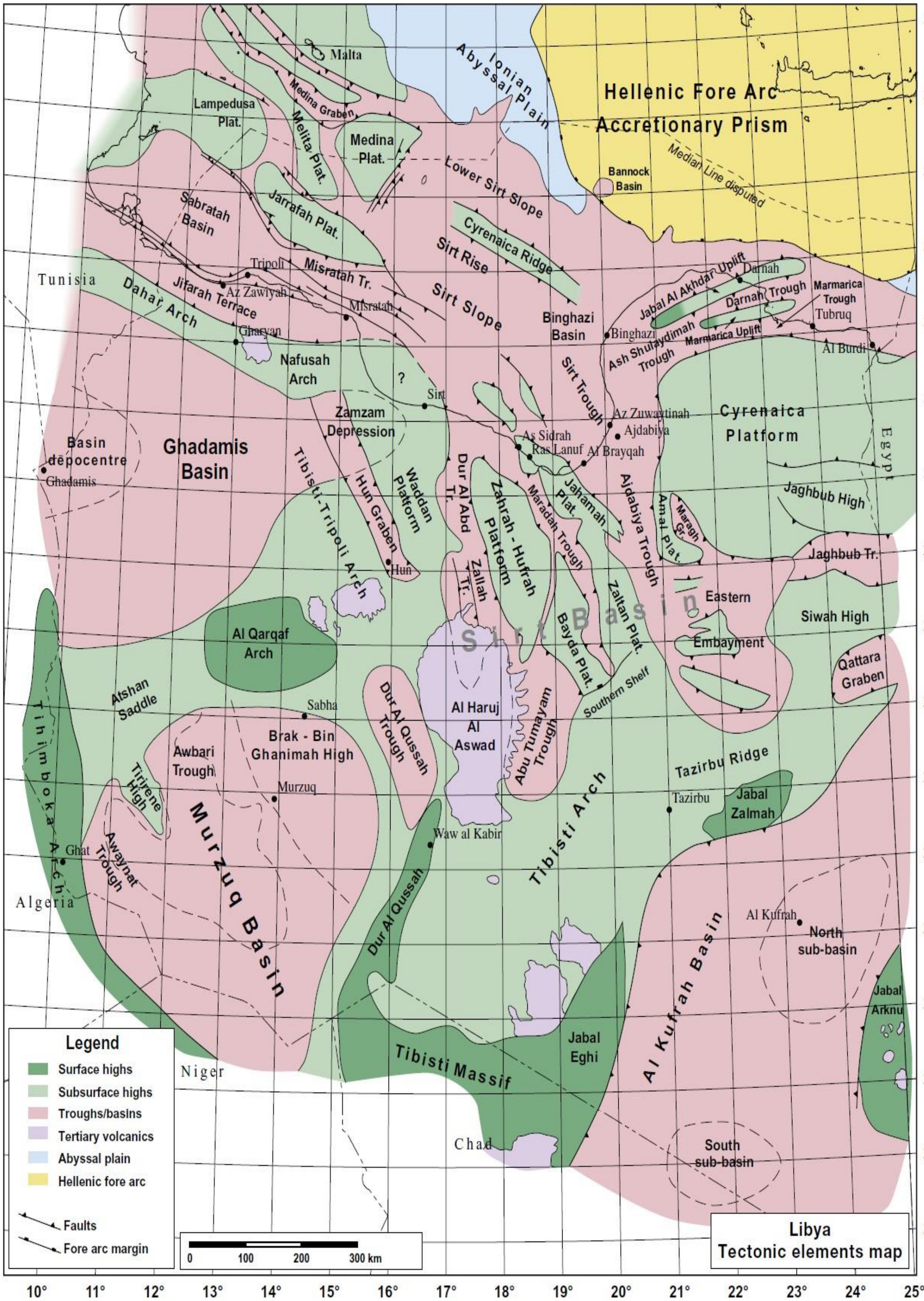

Fig. 1.2: Libya tectonic elements (after Hallett and Clark-Lowes, 2016).

The Mesozoic/Cenozoic sedimentary succession of the Sabratah Basin comprises passive continental margin deposits including Late Triassic to Early Jurassic evaporites with halite and Late Cretaceous and Paleogene platform carbonates and shales, these becoming more distal in character towards the north (Hallett and Clark-Lowes, 2016, Figs. 1.3-4).

The Neogene section comprises a mixed siliciclastic/carbonate/shale succession, detritus derived in part from the rising Alpine orogenic belt to the north. The main reservoir is an oil and gas bearing nummulitic limestone of the Ypresian Jdeir (or called El Garia in Tunisia) Formation which is present in a belt extending from Sfax to the Misratah Basin and is buried to a depth of 9000-11000ft (Hallett and Clark-Lowes, 2016). It has been postulated that the reservoir might extend further eastwards into the Misratah Basin and beyond but this has not been confirmed by drilling. Other reservoirs are present in the Upper Cretaceous in the Turonian to Santonian Makhbaz and Douleb formations and in the Middle and Upper Eocene Dahman and Samdun formations, these being gas-bearing carbonate reservoirs (Hallett and Clark-Lowes, 2016). Sealing lithologies are present as interbedded shales within the Eocene and Upper Cretaceous successions. Halokinetic movement of late Triassic to early Jurassic salt is thought to be responsible not only for contemporaneous bathymetric shoaling that allowed the Ypresian nummulitic banks to develop but also for the subsequent development of structural traps (Hallett and Clark-Lowes, 2016). The source rock for the oil reservoired in the Jdeir Formation is the distallyequivalent Hallab and Bilal (or called Bou Dabbous in Tunisia) shales, located in the Zohra Graben region (Hallett and Clark-Lowes, 2016). The source kitchen for the gas present in Cretaceous and Eocene reservoirs comprises Turonian Makhbaz (or called Bahloul in Tunisia) source rock located in the Ashtart sub-basin kitchen (Hallett and Clark-Lowes, 2016). Similarly mature Makhbaz Shale is most probably present centrally in the Sabratah Basin (Hallett and Clark-Lowes, 2016, Fig. 1.5).

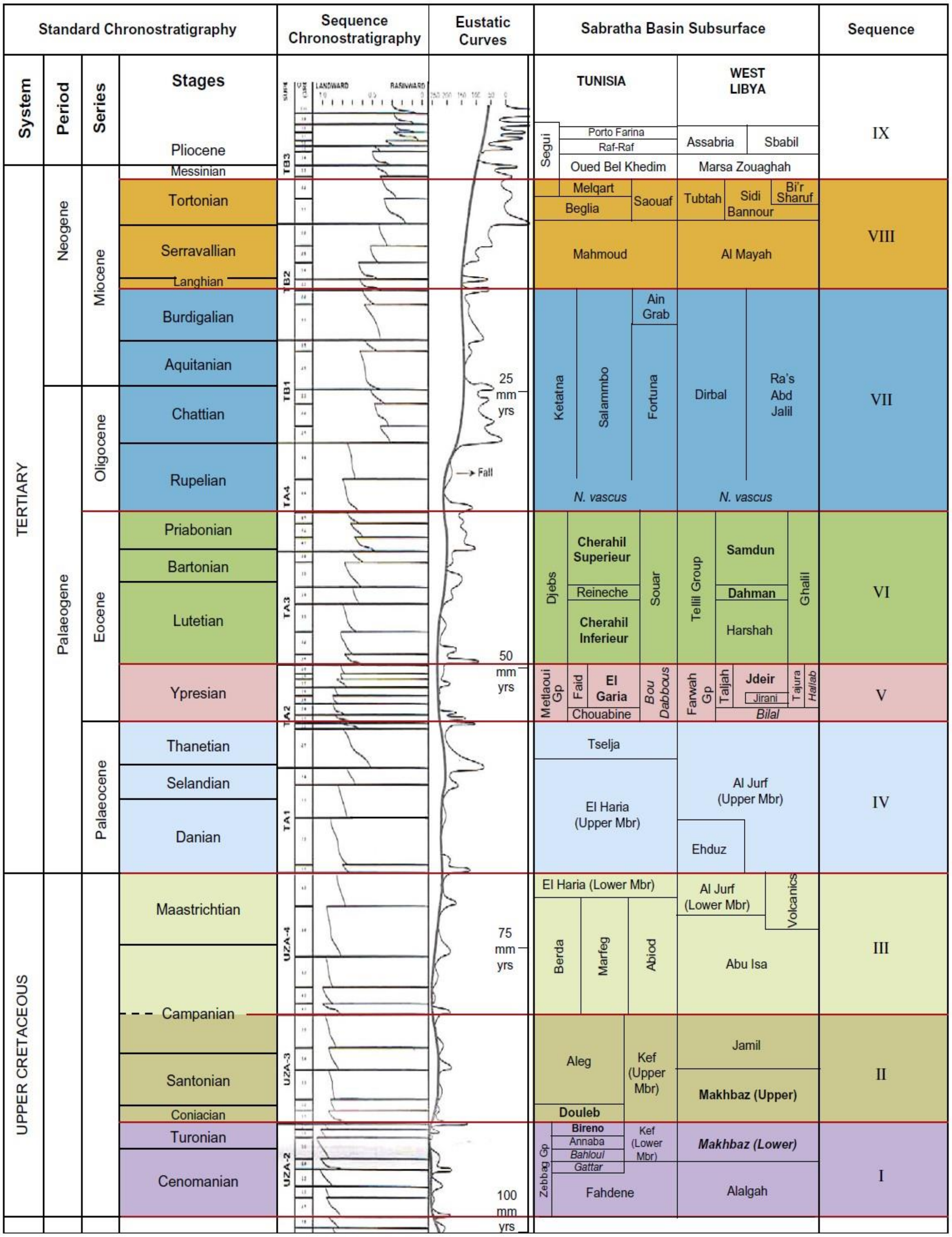

Fig. 1.3: Libyan north-western offshore, time stratigraphic summary chart (after Hammuda et al., 1985; Haq et al., 1988; Hassan and Kendall, 2014).

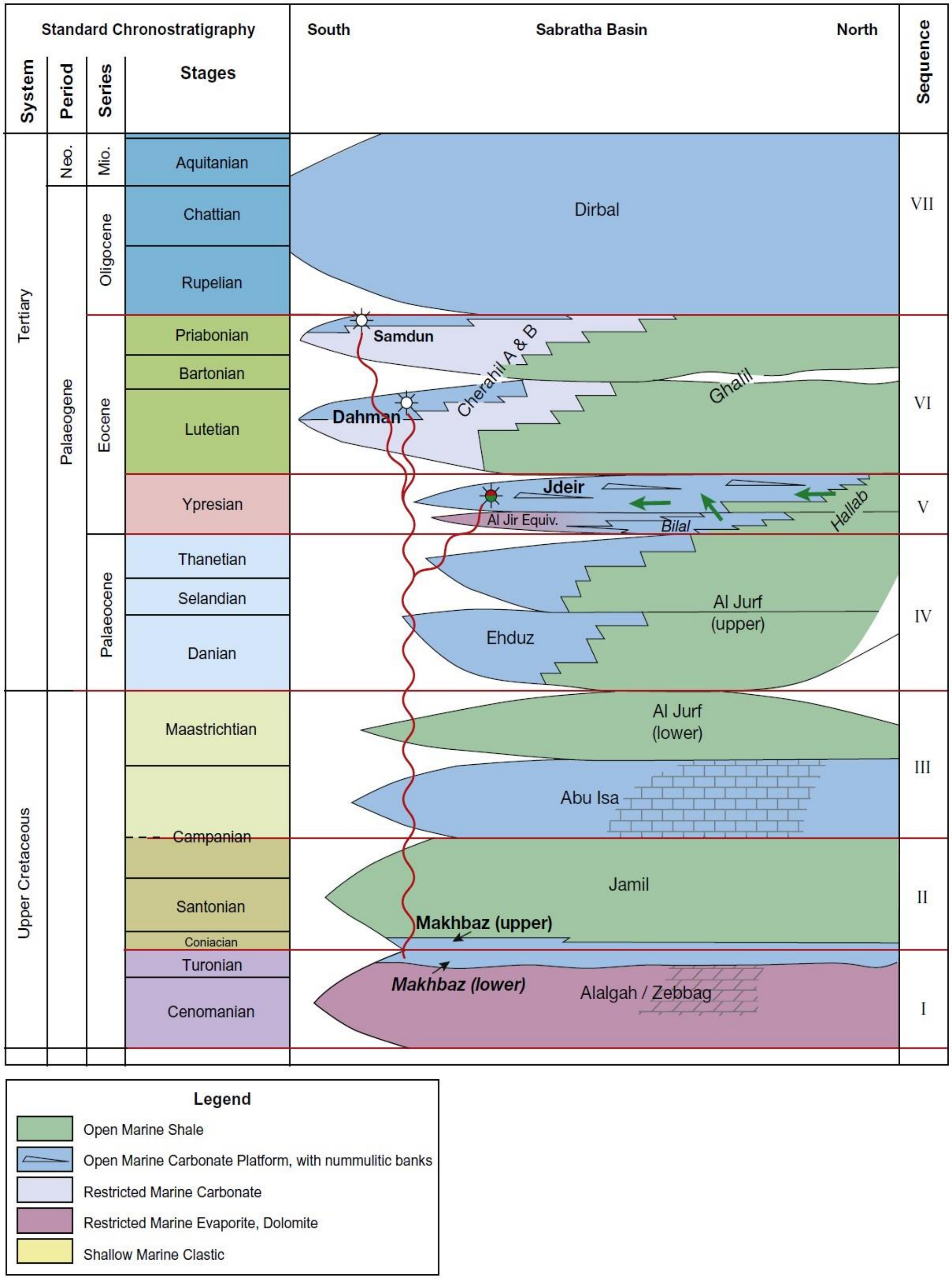

Fig. 1.4: Libyan north-western offshore, schematic chronostratigraphic framework (after Ricchiuto and Pajola, 2003; Fornaciari, 2007).

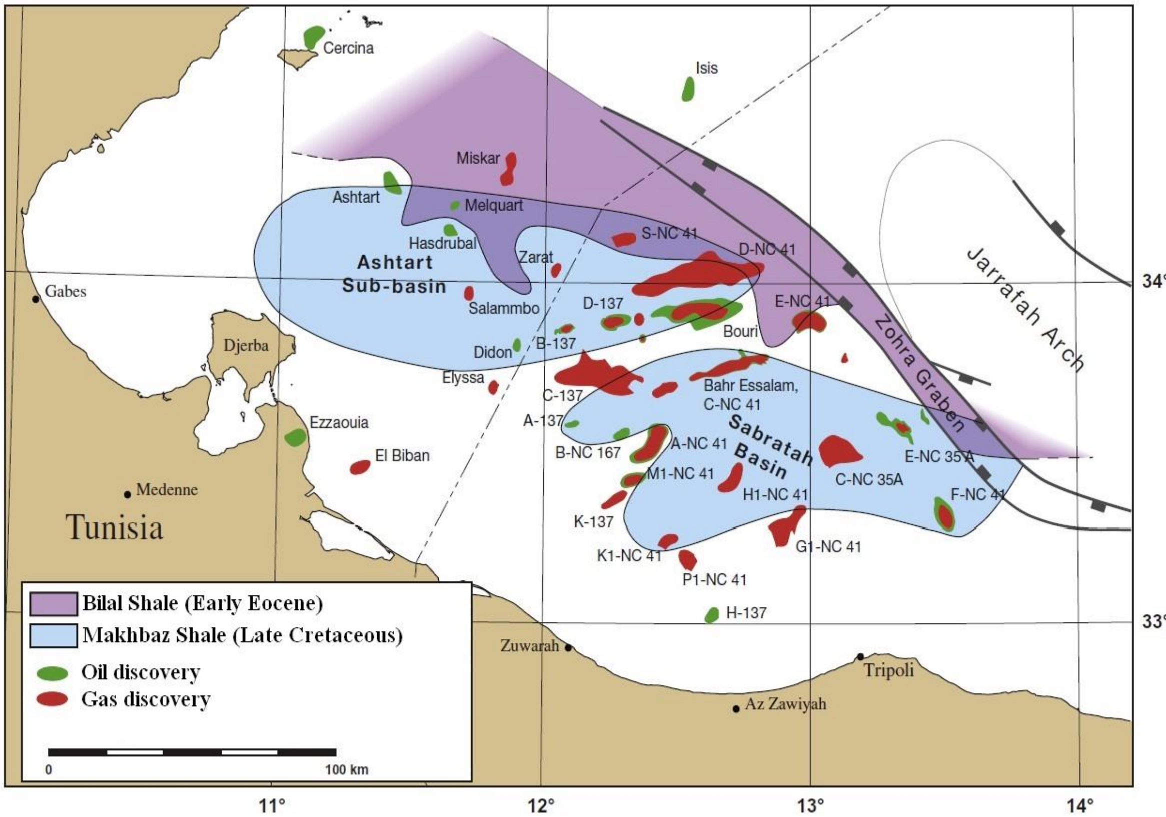

Fig. 1.5: Cretaceous and Eocene Source Rocks in the Sabratah Basin (after Bishop, 1988; Bailey et al., 1989; Sbeta, 1990; El Ghoul, 1991; Anketell and Mriheel, 2000; Racey et al., 2001).

1.2. Oil and Gas Fields in the Sabratah Basin

1.2.1. Bouri Field

The Bouri oil and gas field ranks 17th among Libya's 21 giant fields in terms of oil reserves. It is located 115 km offshore in the Sabratah Basin, 10 km south of the D-NC 41 discovery and 18 km north of the Bahr Essalam field, in a water depth of 480-580 ft (Hallett and Clark-Lowes, 2016). The structure is an east-west anticline formed by flowage in the underlying Late Triassic-Early Jurassic salt, on trend with the Al Jawf oil pool (Hallett and Clark-Lowes, 2016, Fig. 1.6). Oil and gas were found in the nummulitic facies of the Lower Eocene Jdeir Formation, with more than one reservoir zone. The reservoir was charged laterally from the Hallab shale facies located seaward of the nummulitic Jdeir trend, whilst gas charge is thought to be by vertical migration from Late Cretaceous source rocks beneath (Hallett and Clark-Lowes, 2016).

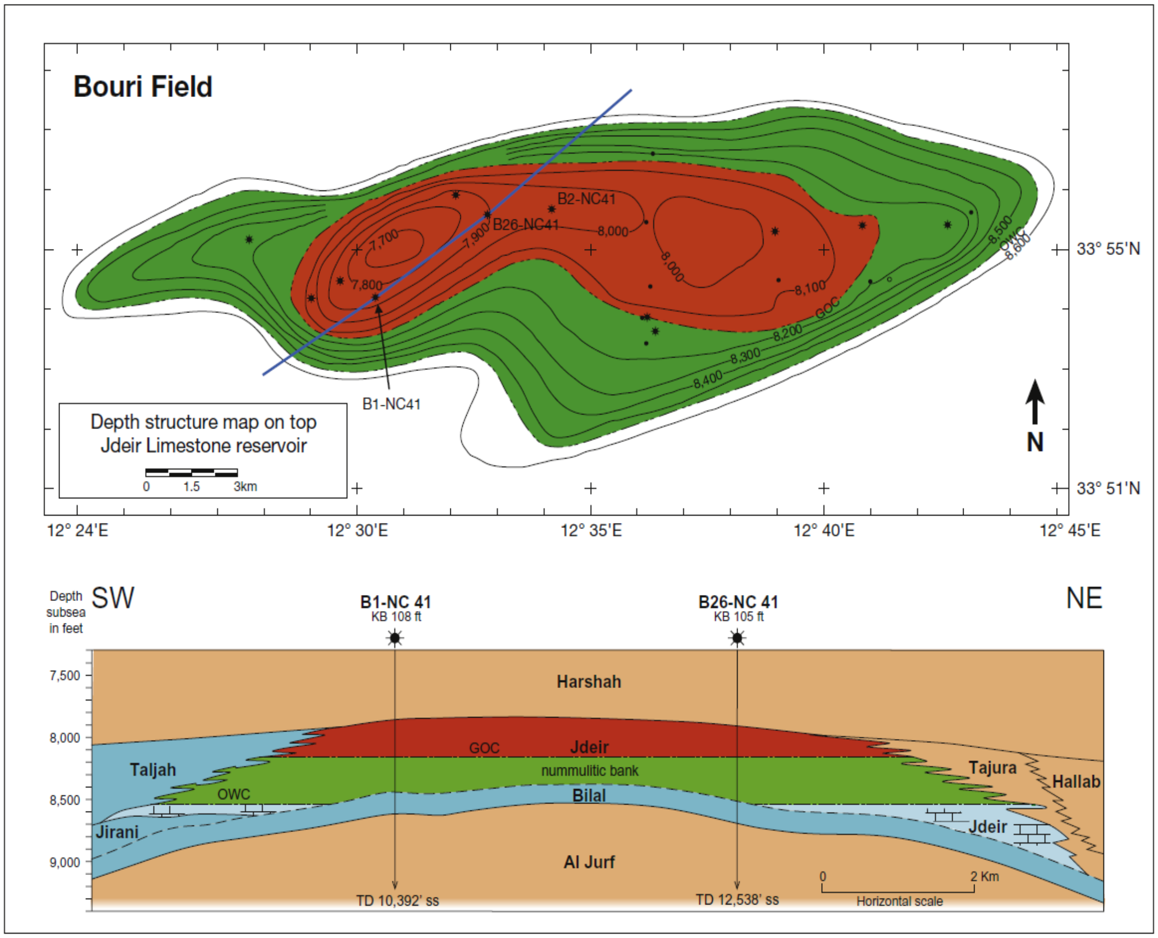

Fig. 1.6: Depth structure map on top Jdeir Limestone reservoir in the Bouri Field with south-west to north-east cross-section (contour interval 100ft, after Hallett and Clark-Lowes, 2016).

The discovery was made by Agip in January 1977 with the B1-NC 41 well. Agip drilled the successful B2 appraisal well 7km to the north-east in the same year (Hallett and Clark-Lowes, 2016). Five more successful appraisal wells were drilled in the period 1985-88. In 1988 the decision was taken to develop the field and two fixed steel platforms were installed with the eastern platform connected to a floating production storage and offloading vessel with a capacity of 1.5 MMB (Hallett and Clark-Lowes, 2016). The field came on stream in 1988 and peak production was reached in 1991 with 84,000 bopd. Since 1988, 38 development wells have been drilled and tied-in to the 2 production platforms. Production problems have been experienced with rapid pressure drop and with water and gas encroachment, and production levels have not matched expectation. It has been shown that porosity rapidly decreases off-structure and the expected water drive is much weaker than predicted. It has also been established that overall porosity is lower than anticipated, and that microfractures play a key role in permeability distribution. Further problems have been encountered with significant amounts of H_2S and the presence of wax in the crude (Hallett and Clark-Lowes, 2016).

ENI North Africa took over operatorship in 2004, and in 2008 ENI converted their Libyan licenses into EPSA IV licenses, and the name of their Libyan operating company to Mellitah Oil and Gas BV (Hallett and Clark-Lowes, 2016). Production in December 2010 was about 40,000 bopd and 100 MMscf/day. The field was shut in during the war from April to October 2011, but by December the field was producing about 5,500 bopd and 40 MMscf/day from its DP 4 platform, the DP 5 platform being shut-in. By December 2012 production was almost back to pre-war levels. The original oil in place figure of 2,570 MMB and production to end 2013 of about 570 MMB give a recovery at that time of 22%. It is thought that, without enhanced oil recovery techniques, this carbonate reservoir will only achieve recovery of 25%. However, with enhanced oil recovery techniques, recovery could possibly be increased up to 30%. Gas production to 2013 is about 37% of the estimated free and associated gas reserves of 2,200 BCF. The gas is exported via Bahr Essalam to Mellitah, and then by the GreenStream gas pipeline to Sicily (Hallett and Clark-Lowes, 2016).

1.2.2. Bahr Essalam Field

The Bahr Essalam oil and gas field is the largest gas field in Libya (when both pools are included) (Hallett and Clark-Lowes, 2016, Table 1.1). It is located 100km offshore in the Sabratah Basin, 18km south of the Bouri oil field and 15km west of the E-NC 41 gas discovery, in a water depth of 475-620 ft (Hallett and Clark-Lowes, 2016). Like Bouri, the structure is a salt supported anticline aligned WSW-ENE, on trend with the A-137 oil pool. It is composed of two closures on the same trend, the Eastern Pool (C2 pool) being the most significant with a large gas cap and small oil leg, and the subsidiary Western Pool (C1 pool) hosting a significant free gas accumulation (Fig. 1.7). Oil and gas were found in the nummulitic facies of the Lower Eocene Jdeir Formation, and gas in the chalky limestones of the Middle Eocene Dahman Formation. Like the Bouri Field described above, gas charge is thought to be by vertical migration from Upper Cretaceous source rocks. The oil leg is charged laterally from the Hallab shale facies located seaward of the nummulitic Jdeir trend (Hallett and Clark-Lowes, 2016). The discovery was made by Agip in April 1978 with the C1-NC 41 well which tested gas on the Western Pool. In the following year the C2 well tested oil and gas on the Eastern Pool, 24km to the east of C1 (Hallett and Clark-Lowes, 2016). Fourteen years elapsed before any further appraisal drilling was undertaken, but in 1993/94 six further wells were drilled which proved the field to extend for 45km from east to west, including both structures, and the decision was taken to develop these accumulations as one field. Seismic data demonstrated a complex structure which is heavily cross faulted and with most faults aligned NNW-SSE (Hallett and Clark-Lowes, 2016).

Table 1.1: Gas fields in Libya with ORR Greater than 1 TCF. Gas fields with greater than 1 TCF of reserves, listed by originally recoverable reserves of gas (conventional recovery). Color coded basins: mauve fields lie in the Sirt Basin, tan in the Murzuq Basin and blue in the Sabratah Basin (after Hallett and Clark-Lowes, 2016)

	Field name	Location	Hydrocarbons	Field description (HC phase)	Gas production	Originally recoverable reserves (conventional recovery) BCF
1	*Bahr Essalam (C2-NC 41 and C1-NC 41)*	Northwest Offshore	Oil and Gas (C2-NC 41) and Gas (C1-NC 41)	Oil and associated gas (C2-NC 41) and Non associated gas (C1-NC 41)	Production from C2-NC 41	4,010 (C2-NC 41) and 1,300 (C1-NC 41)
2	*Al Wafaa (A-NC 169)*	South Ghadamis Basin	Oil, Gas and Condensate	Associated gas and gas cap	Production	4,060
3	D-NC 41	Northwest Offshore	Gas	Non associated gas (CO2 rich)	No production	4,000
4	Attahadi (FF-6)	Zaltan Platform	Gas (and Oil)	Non associated gas (and oil pool)	Production	3,220
5	Hutaybah (S-6)	Zaltan Platform	Gas	Non associated gas	Production	3,080
6	*Bouri (B-NC 41)*	Northwest Offshore	Oil and Gas	Oil with associated gas and gas cap	Production	2,200
7	C-137N	Northwest Offshore	Gas	Non associated gas	No production	1,880
8	Kalanshiyu Argub (EE-59, 5I-59 & 5H-59)	Eastern Embayment	Oil and Gas	Oil with associated gas and gas cap	Production	1,220
9	E-NC 41	Northwest Offshore	Oil and Gas	Oil with associated gas and gas cap	No production	1,220
10	*Raqubah (E-20)*	Bayda Province	Oil and Gas	Oil with associated gas and gas cap	Production	1,210
11	*Zahrah-Hufrah*	Zahrah Hufrah Platform	Oil and Gas	Oil with associated gas and gas cap	Production	1,140

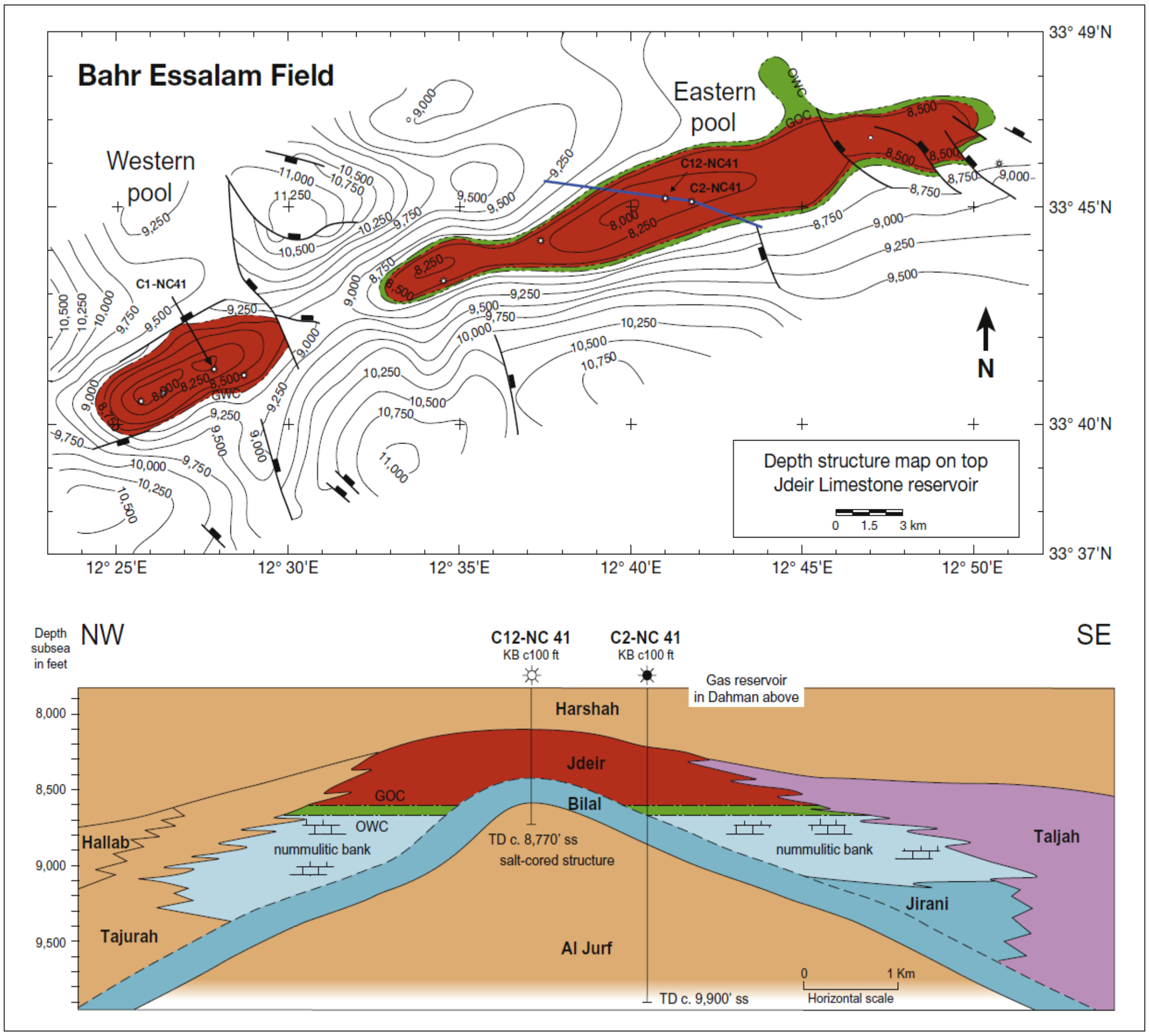

Fig. 1.7: Depth structure map on top Jdeir Limestone reservoir in the Bahr Essalam Fieldwith north-west to south-east cross-section (contour interval 250ft, after Hallett and Clark-Lowes, 2016).

In 2005 a 663ft high fixed steel platform, named Sabratah, was constructed and installed on the Eastern Pool (Hallett and Clark-Lowes, 2016). Twenty-six wells have been drilled, 15 from the platform, and 11 are sub-sea completions. A 36 in. gas pipeline and a 10 in. liquids pipeline were laid to a shore facility at Mellitah, where provision was also made to receive gas from Bouri. The production wells were tied in to the platform and the field came on stream in Aug. 2005. The gas is sour, with 15% CO_2 and 2% H_2S (Hallett and Clark-Lowes, 2016).

In 2004 operatorship passed to ENI North Africa, and in 2008 an agreement was signed converting ENI's Libyan licenses to EPSA IV licenses, and changing the name of the company to Mellitah Oil and Gas BV (Hallett and Clark-Lowes, 2016). By December 2010 gas production at Bahr Essalam was over 950 MMscf/day. Although Bahr Essalam is principally a gas producing field, cumulative liquids production to end 2010 was greater than 40 MMB (7% of the original oil in place of 590 MMB) and daily production about 20,000 bopd. Future liquids production using conventional techniques should allow recovery of about 30% of the total oil in place (Hallett and Clark-Lowes, 2016).

The field was shut-in during the war from March to January 2011, but by December 2011 the field was producing gas at approximately two-thirds of pre-war levels. By 2013 cumulative production of gas from the Eastern Pool was about 1,150 BCF (about 30% of the recoverable gas) whilst the 1,300 BCF of recoverable gas in the Western Pool remains to be produced (Hallett and Clark-Lowes, 2016).

Gas production from Bahr Essalam and Bouri is piped to the Mellitah Complex where it is processed for local and export markets (Hallett and Clark-Lowes, 2016). The exported gas passes through the 32 in. subsea GreenStream gas pipeline from Mellitah and Gela in Sicily which handles gas from both the offshore Sabratah Basin fields and from Al Wafaa, and has a capacity of 770 MMscf/day (281 BCF/year) (Hallett and Clark-Lowes, 2016).

1.3. Makhbaz Formation

In the offshore southern Sabratah Basin the Alalgah Formation (Late Cretaceous) is overlain by a series of micritic to finely-crystalline limestones, sometimes dolomitic, with thin intercalations of calcareous shales (Hallett and Clark-Lowes, 2016). Hammuda *et al.*, (1985) named this unit the Makhbaz Formation and defined a type section in the I1-137 well close to the Tunisian border. The thickness in the type well is 184m. It has been penetrated by many wells on the southern margin of the basin, as far east as well Jl-NC 35a in the Misratah Basin. No diagnostic fauna has been reported, but on stratigraphic grounds it has been assigned to the Turonian-Coniacian (Hallett, 2002). It is believed to equate approximately with the Qasr Tigrinnah Formation of northwest Libya and with the Upper Zebbag and Douleb carbonates of Tunisia, which contain both reservoir and source rocks (Hammuda *et al.*, 1985).

1.3.1. Makhbaz Gas Play

Fig (1.8) shows the Makhbaz/Bahloul gas play. The Libyan gas-condensate discoveries located along a belt of restricted low-energy shelf deposits that back the Jdeir nummulitic trend of the Sabratah Basin, have Makhbaz, Dahman and Samdun reservoirs (Hallett and Clark-Lowes, 2016). These gas-condensate discoveries (in concessions 137 and NC 41) are believed to have been charged by Upper Cretaceous source rocks, the Turonian Makhbaz Formation being the most likely (Hallett and Clark-Lowes, 2016). These three gas petroleum systems, two in the younger Eocene section and one in the Upper Cretaceous, are much less significant in terms of reserves than the Jdeir oil and gas play (Hallett and Clark-Lowes, 2016).

Much of the gas in the Jdeir reservoir such as at Bahr Essalam is also thought to have been sourced from the Makhbaz Formation. The Makhbaz source rock is mature for gas generation in two depocentres of the Greater Sabratah Basin. These shales are late-mature in the Ashtart sub-basin and are gas generative. A similar late-mature kitchen is thought to be present in the Libyan Sabratah Basin south of Bouri (Hallett and Clark-Lowes, 2016). The Makhbaz Formation is dark-grey, laminated, globigerinid marl to black limestone which is a proven source rock in Tunisia, charging gas accumulations at Isis and elsewhere in the Zebbag carbonate reservoir, including the Miskar gas field (Hallett and Clark-Lowes, 2016). It has TOC values ranging from 4 to 8%. A zone of organically rich Makhbaz source rock extends from Sfax into Libyan territory, extending along a northwest–southeast trend into the Bouri area (Hallett and Clark-Lowes, 2016). The eastern extension of the source facies in Libya is as yet undefined. The depth to the top of the oil window for the Makhbaz Formation is around 8250ft and to the top of the gas zone about 13000ft (Hallett and Clark-Lowes, 2016). Around the basin margin the peak-mature shales have probably sourced the oils found at Isis, Rhemoura, Gremda and El Ain in Tunisia (Hallett and Clark-Lowes, 2016).

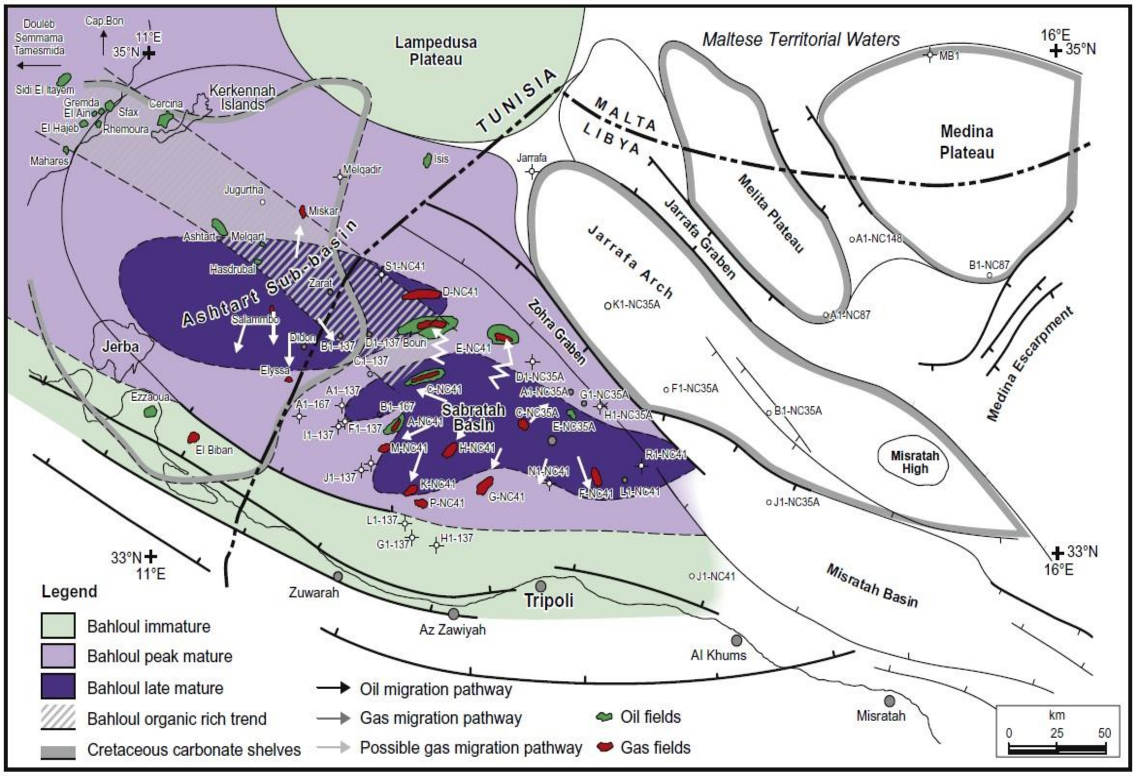

Fig. 1.8: Makhbaz/Bahloul gas play (after Finetti, 1982; Bishop, 1988; Bailey et al., 1989; El Ghoul, 1991; Pratsch, 1994; Bishop and Debono, 1996).

Typical traps of these gas-condensate accumulations are structural anticlines located over salt swells and salt walls which have generated fractures and faults in the Upper Cretaceous and Paleocene section thereby providing migration routes for hydrocarbons to pass from the Turonian source rock to the younger reservoirs (Hallett and Clark-Lowes, 2016). Generation and migration of gas is thought to have occurred during the Oligocene and Miocene (Hallett and Clark-Lowes, 2016).

1.4. Objectives

It is clear that the lower part (shale) of the Makhbaz Formation represents the source rock, while the upper part (limestone) represents the reservoir. The goal of the current work is the geochemical evaluation of source rock and reservoir of the Makhbaz Formation in the offshore well K-137, Sabratah Basin, NW Libya (Fig. 1.9). The reservoir was evaluated using petroleum inclusions. The geochemical assessment can give the following information:

1) Depositional environment, paleosalinity and paleo-oxygenation.

2) Source rock quality.

3) Kerogen type.

4) Thermal maturation of organic matter.

5) Origin of organic matter.

6) History of migration.

7) Charging times.

8) Types of natural gas in the Makhbaz Reservoir.

1.5. Previous Work

Based on the published papers, this work is considered the first geochemical evaluation of the Makhbaz Formation in the offshore well K-137, because I did not find any paper related to this subject.

1.6. Stratigraphy

The total thickness of the Makhbaz Formation in the offshore well K-137 is 185m (Fig. 1.10). The formation in this well consists of limestone and shale beds. The thickness of the source rock bed (lower shale) is 51m, while the thickness of the reservoir bed (limestone) is 25m. In the studied well, the lower boundary of the Makhbaz Formation is conformable with the underlying Alalgah Formation (Late Cretaceous), while the upper boundary is conformable with the overlying Jamil Formation (Late Cretaceous).

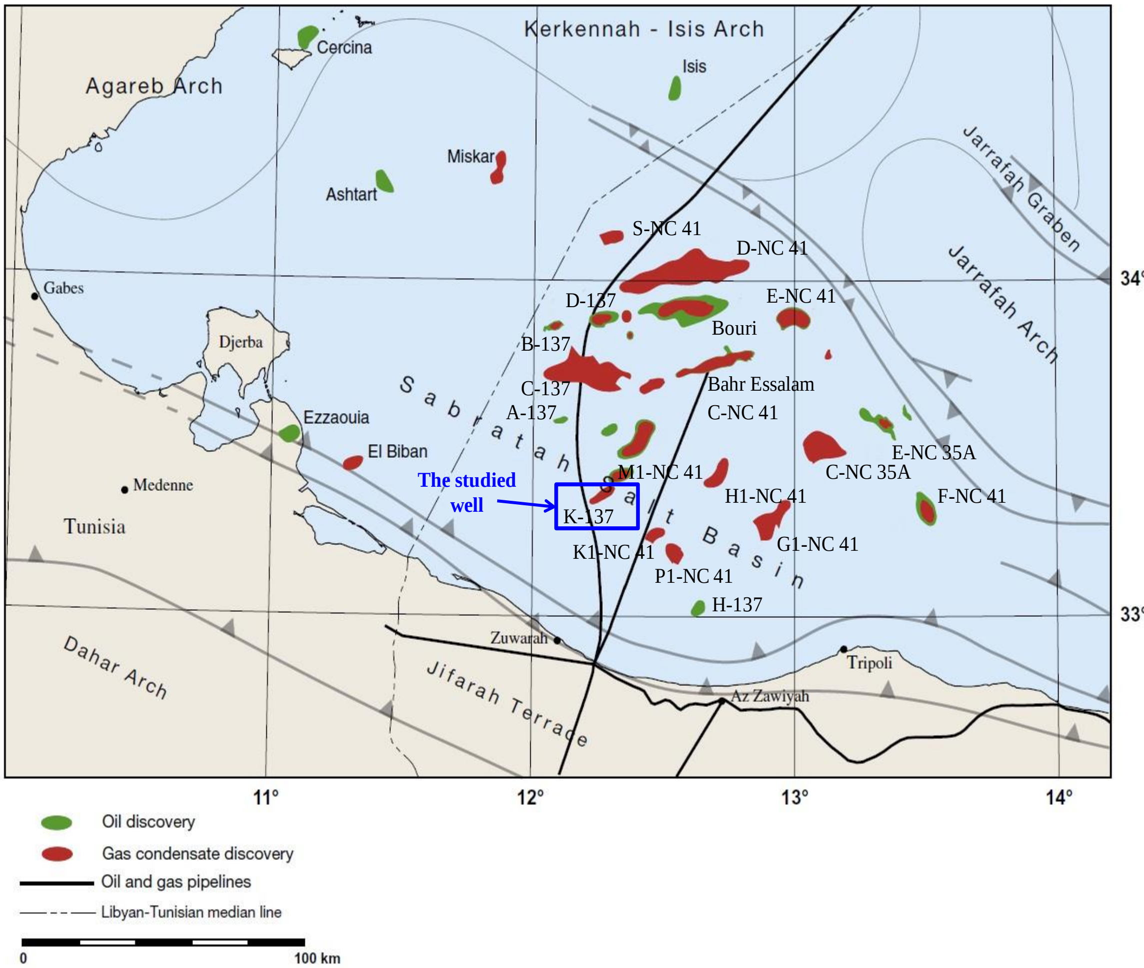

Fig. 1.9: Well location map of the Sabratah Basin showing the location of the offshore well K-137 (modified after Bishop, 1988; Bailey et al., 1989; Sbeta, 1990; Anketell and Mriheel, 2000; Racey et al., 2001).

1.7. Methodology

The data used in this work were obtained from the Agip Company. Twelve samples were selected from the source rock (shale) and four samples from the reservoir (limestone). The laboratory of Chemostratigraphy and Organic Geochemistry (LGQM), State University of Rio de Janeiro (UERJ), Brazil, performed all analyses used in this work.

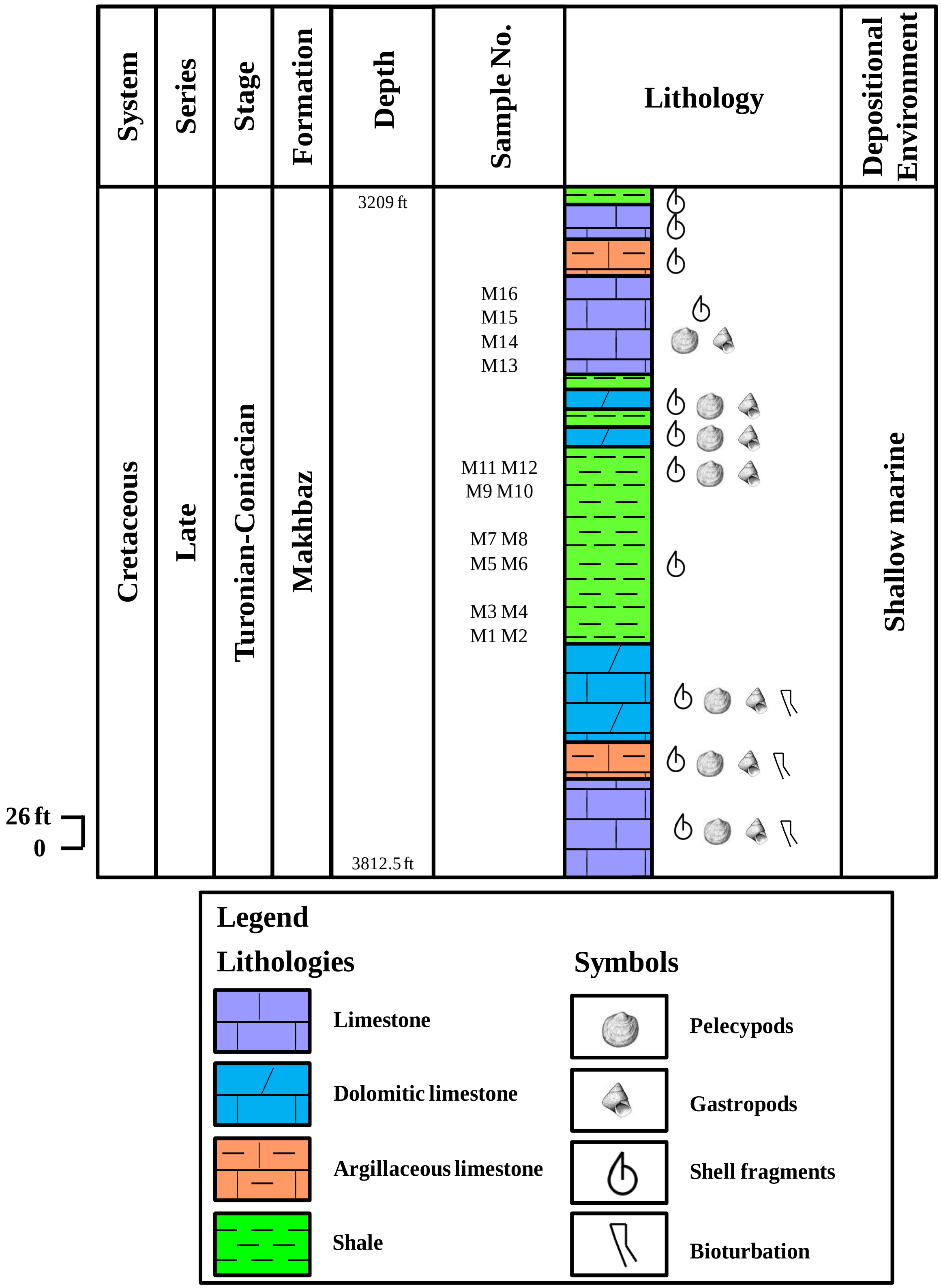

Fig. 1.10: Lithostratigraphic column of the Makhbaz Formation in the offshore well K-137.

1.7.1. Petrographic Analysis

The limestone samples were prepared for petrographic analysis (Fig. 1.11). They were cut to 30-microns thick, and polished. Two main methods, transmitted and reflected-light microscopy, were used to describe the thin sections. This petrographical study was done to detect the petroleum inclusions.

Fig. 1.11: Thin section instrument.

1.7.2. Scanning Electron Microscope (SEM)

The petroleum inclusions were described in the thin sections using the scanning electron microscope (Fig. 1.12). The samples were coated with 20 to 30nm of high purity carbon. Special operating conditions using an accelerating voltage of 30kV, a working distance of 3.3mm, and an operating chamber gas pressure of 0.8Torr were found to achieve the best signal to noise ratio at the highest resolution for SEM imaging of the petroleum inclusions.

Fig. 1.12: Scanning electron microscope instrument.

1.7.3. LECO Analysis

The LECO analysis (Fig. 1.13) is one of the most successful analyses used to estimate total organic carbon (TOC) content. In the present study, the TOC content in the shale samples was measured using this analysis. Approximately 250-500mg of pulverized rock was required for the LECO analysis. To remove inorganic carbon in the form of carbonates, chemical treatment of the sample was required prior to analysis. To achieve this, samples were treated with hydrochloric acid (HCl) for 12-24h with intermittent stirring. At the end of this time or when the dissolution of carbonates was observed to be complete (no effervescence with stirring or additional acid), the samples were rinsed free of the HCl solution by using distilled water. The samples were then dried to eliminate moisture prior to analysis. Prepared samples were then combusted at ~1100°C inside the oven of a LECO SC-632 analyzer and the amount of carbon dioxide (CO_2) generated was measured by an infrared cell.

Fig. 1.13: LECO instrument.

1.7.4. Rock Eval Pyrolysis

Rock-Eval (Fig. 1.14) is a pyrolysis tool that is designed to measure hydrocarbon potential and generative history from whole-rock samples. This method provides several measurable parameters like S_1, S_2, S_3, T_{max}, HI, OI, and PI. The main point in using this method is to calculate the quantity of the organic matter content that is detected by a flame ionization detector (FID) during pyrolysis, and predict the quantity of hydrocarbon that would be produced during rock maturation. This analysis was used to determine the parameters mentioned above in the studied shale samples. Briefly, for each sample 60mg of pulverized material were first thermally decomposed in a pyrolysis oven to obtain the weight % of pyrolyzable carbon (PC) and pyrolyzable mineral-carbon. Hydrocarbons and both CO_2 and CO were simultaneously detected via a flame ionization detector (FID for hydrocarbons) and infrared cells (IR cells for CO_2 and CO). Subsequently, each sample was combusted in an oxidation oven to obtain the weight % of residual carbon (RC) and oxidized mineral-carbon. The temperature program for pyrolysis was 300°C isothermal for three minutes followed by a 25°C/min ramping from 300 to 650°C; oxidation program was 300°C isothermal for 30s followed by a 25°C/min ramping from 300 to 850°C, held isothermal for 5min at 850°C.

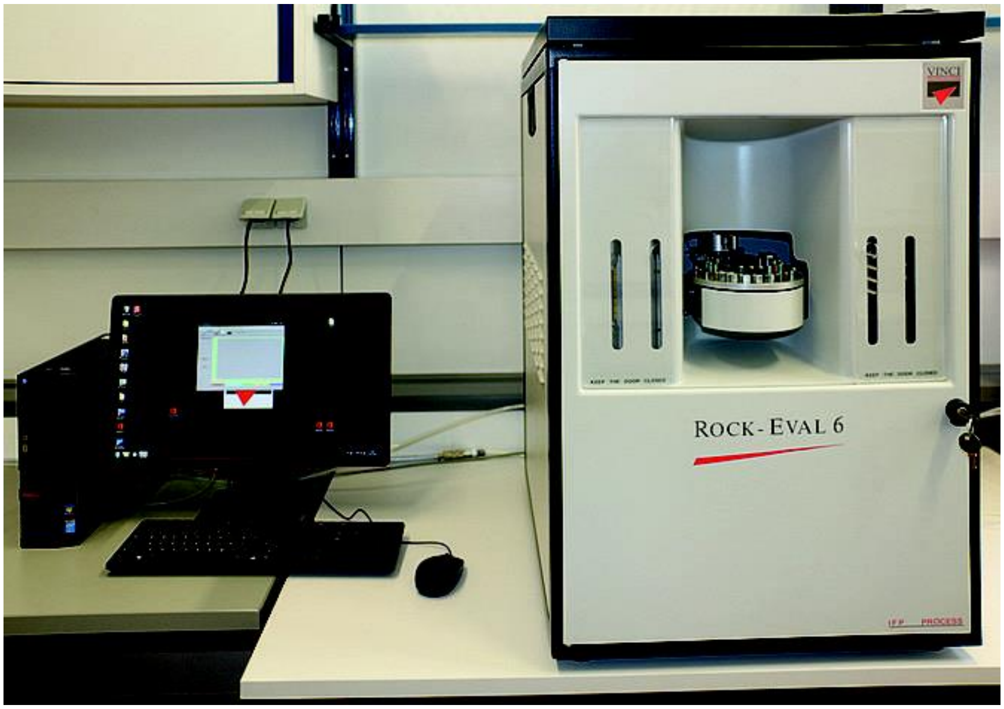

Fig. 1.14: Rock-Eval 6 instrument.

1.7.5. Gas Chromatography-Mass Spectrometry (GC-MS)

The GC-MS analysis (Fig. 1.15) was used to evaluate organic matter in the samples of shale, crude oil and natural gas. Eight oil samples and eight gas samples were taken from the petroleum inclusions using a special syringe. The GC-MS analysis was performed on a 7890A/5975C GC/MS analyzer (Agilent Technologies). Pyrolysis interface and GC injection port were kept at 290°C. Analytes were separated by an HP-5MS column (30m × 0.25mm × 0.25µm). The chromatographic oven temperature was programmed from 50 to 290°C at a rate of 10°C/min after an initial 2.5min isothermal period. Then the oven was kept at the final temperature for 5min. Selected ion monitoring (SIM) was used to identify the biomarkers by monitoring m/z 85 and 217 ions. The ion source was at 230°C and positive ions were analyzed in full scan mode.

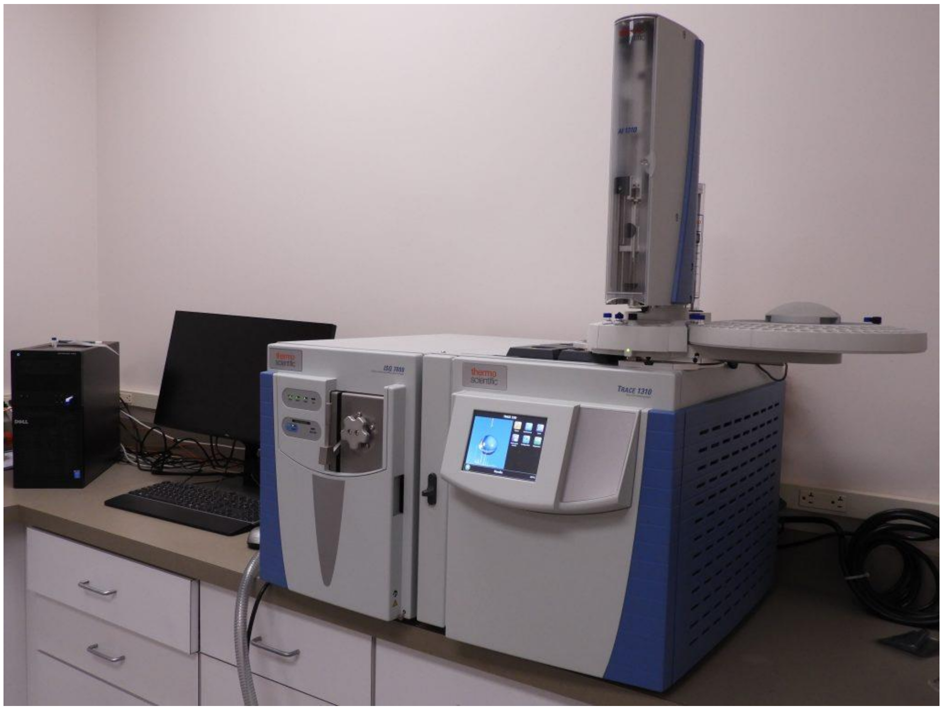

Fig. 1.15: Gas chromatography-mass spectrometry instrument.

1.7.6. Fluorescence Spectrophotometry

The reservoir samples were analyzed through the techniques of Quantitative Grain Fluorescence (QGF) and Quantitative Grain Fluorescence on Extract (QGF-E). The QGF and QGE-E technique applies fluorescence spectrophotometry (Fig. 1.16) to identify hydrocarbon migration pathways. The experiments are carried out by using a Varian Cary-Eclipse Spectrophotometer. QGF is measured on dry, disaggregated reservoir grains (63μm-1mm) after a pre-cleaning procedure removes surface contaminants, and records the fluorescence emission spectra (300-600nm) of petroleum inclusions in the grains during UV excitation at 254nm. QGF-E is measured on the solvent extract from the QGF cleaned grains, and measures the fluorescence emission spectra of the extractable hydrocarbons during UV excitation at 260nm. QGF index and QGF-E intensity are the two key parameters. QGF index is the average spectral intensity between the wavelength of 375nm and 475nm normalized to the spectral intensity at 300nm. QGF-E intensity is the maximum spectral intensity normalized to weight and volume. The higher the QGF index, the higher the abundance of oil inclusions and the greater the oil saturation will be. QGF indexes greater than 4 with the peak wavelength (λ_{max}) of 375-475nm generally indicate paleo or current oil reservoirs, while the values ranging from 0 to 4 generally correspond to water-bearing zones or carrier beds. However, the QGF index within some late-charged current oil reservoirs may be less than 4, since inclusion formation is a function of time, to some extent. The QGF-E intensity may be used to approximate relative oil saturation. Residual and current oil reservoirs have distinct QGF-E spectra with λ_{max} generally at about 370 nm, and their QGF-E intensities are usually greater than 20 photometer counts (pc). However, the QGF-E intensities are rarely over 40 pc within water zones and carrier beds, and the λ_{max} is around 300-500nm. The API gravity was calculated as: API gravity = (141.5/speciflc gravity at 15.6^{o}C)-131.5.

Fig. 1.16: Fluorescence spectrophotometer instrument.

CHAPTER TWO
SOURCE ROCK GEOCHEMISTRY

2.1. Introduction

Sedimentary rocks commonly contain minerals and organic matter with the pore space occupied by water, bitumen, oil, and/or gas (Tiem *et al.,* 2008; Ahmed *et al.,* 2014; Grotheer *et al.,* 2019). Kerogen is the particulate fraction of organic matter remaining after extraction of pulverized rock with organic solvents (Tissot and Welte, 1984; Peters and Cassa, 1994). Kerogen can be isolated from carbonate- and silicate-bearing rocks by treatment with inorganic acids, such as HC1 and HF (Peters and Cassa, 1994; Aycard *et al.,* 2003). This is only an operational definition because the amount and composition of insoluble organic matter or kerogen remaining after extraction depends on the types and polarities of the organic solvents (Peters and Cassa, 1994). Kerogen is a mixture of macerals and reconstituted degradation products of organic matter. Macerals are the remains of various types of plant and animal matter that can be distinguished by their chemistry and by their morphology and reflectance using a petrographic microscope (Stach, 1982; Peters and Cassa, 1994). This term was originally applied to components in coal but has been extended to sedimentary rocks. Palynomorphs are resistant, organic-walled microfossils such as spores, pollen, dinoflagellate cysts, and chitinozoa (Peters and Cassa, 1994; Dutta *et al.,* 2013; Tahouna and Mansour, 2019).

Applied organic geochemistry provides the information needed to make maps of the richness, type, and thermal maturity of a source rock (Peters and Cassa, 1994; Liu *et al.,* 2008; Abarghani *et al.,* 2018). These maps are a necessary step toward determining the stratigraphic and geographic extent of a pod of active source rock in a petroleum system, and they are based on geochemical analyses of rock samples from outcrops and wells that are displayed on logs (Peters and Cassa, 1994). These geochemical well logs are based on Rock-Eval pyrolysis, total organic carbon, vitrinite reflectance, and other rapid, inexpensive "screening" methods. The logs define the following:

1) Potential, effective, and spent petroleum source rock.

2) The thermal maturation gradient, including immature, mature, and postmature zones. 3) In situ and migrated petroleum shows.

Useful geochemical logs require proper sample selection, preparation, analysis, and interpretation. Detailed studies, including oil-source rock correlations by biomarker and supporting techniques, are undertaken on selected samples only after the screening methods are completed (Peters and Cassa, 1994; Curtis *et al.*, 2004; Mashhadi and Rabbani, 2015; Xiao *et al.*, 2019).

2.2. Organic Geochemistry

As I mentioned in the first chapter that part of the Makhbaz Formation is a source rock (shale) and another part is considered a reservoir (limestone). In this chapter I will discuss the source rock quality, kerogen type, thermal maturity, organic matter input, depositional environment, paleosalinity and paleo-oxygenation. The evaluation of the source rock was done using several techniques such as LECO analysis, Rock-Eval pyrolysis and gas chromatography-mass spectrometry (GC-MS). Tables (2.1-7) illustrate the results of the chemical analysis.

2.2.1. Statistical Treatment

Statistical analysis of source rock data gives several information such as thermal maturity (Rabbani and Kamali, 2005; Gurgey and Canbolat, 2017). Three types of statistical analysis were used in this chapter, namely descriptive statistics (Table 2.8 and Fig. 2.1), correlation matrix (Table 2.9 and Fig. 2.2) and principal component analysis (PCA, Table 2.10 and Fig. 2.3). These analyses were performed using the SPSS© program.

Table 2.1: LECO and Rock Eval pyrolysis data of the Makhbaz Shale

Sample No.	TOC	T_{max}	Ro	S_1	S_2	S_3	HI	OI	GP	PI
M1	5.18	457	0.75	6.14	21.18	2.21	408.88	42.66	27.32	0.22
M2	5.30	455	0.80	7.30	21.29	1.98	401.70	37.36	28.59	0.26
M3	4.71	453	0.77	5.70	17.25	1.46	366.24	31.00	22.95	0.25
M4	4.77	452	0.82	4.74	17.17	1.54	359.96	32.29	21.91	0.22
M5	4.50	452	0.85	4.55	18.00	1.09	400.00	24.22	22.55	0.20
M6	4.42	454	0.85	4.49	19.14	0.90	433.03	20.36	23.63	0.19
M7	5.33	453	0.80	8.21	20.46	1.76	383.86	33.02	28.67	0.29
M8	5.24	453	0.80	7.24	20.67	1.83	394.47	34.92	27.91	0.26
M9	4.75	455	0.78	4.58	17.40	1.52	366.32	32.00	21.98	0.21
M10	4.68	456	0.71	5.61	19.09	1.59	407.91	33.97	24.70	0.23
M11	4.70	454	0.72	6.53	18.46	1.66	392.77	35.32	25.00	0.26
M12	4.52	454	0.74	6.44	17.00	1.51	376.11	33.41	23.44	0.27

Table 2.2: Gas chromatogram data of normal alkanes and isoprenoids ratios of the Makhbaz Shale (calculated on m/z 85)

Sample No.	Pr/Ph	$(Pr+n\text{-}C_{17})/(Ph+n\text{-}C_{18})$	$Pr/n\text{-}C_{17}$	$Ph/n\text{-}C_{18}$	$\sum(n\text{-}C_{12}\text{-}n\text{-}C_{20})/(\sum(n\text{-}C_{12}\text{-}n\text{-}C_{20})+\sum(n\text{-}C_{12}\text{-}n\text{-}C_{29}))$	CPI	WI
M1	0.44	0.65	0.27	0.43	0.82	0.65	0.71
M2	0.61	0.54	0.31	0.39	0.88	0.63	0.78
M3	0.71	0.60	0.34	0.54	0.91	0.75	0.68
M4	0.65	0.33	0.31	0.56	0.90	0.77	0.64
M5	0.64	0.39	0.40	0.56	0.90	0.74	0.62
M6	0.67	0.41	0.42	0.58	0.87	0.71	0.66
M7	0.64	0.67	0.29	0.41	0.82	0.73	0.80
M8	0.72	0.32	0.23	0.38	0.84	0.79	0.81
M9	0.55	0.30	0.38	0.59	0.87	0.66	0.59
M10	0.55	0.30	0.35	0.57	0.95	0.73	0.64
M11	0.66	0.51	0.29	0.55	0.92	0.69	0.65
M12	0.63	0.45	0.29	0.56	0.84	0.71	0.67

Table 2.3: Gas chromatogram data of steranes and diasteranes of the Makhbaz Shale (calculated on m/z 217)

Sample No.	C_{27}	C_{28}	C_{29}	C_{29} (ßß/ßß+αα)	C_{29} ßα(S+R)-dia/ (C_{28} ßα(S+R)-dia+ C_{27} ßα(S+R)-dia)	C_{30} sterane index
M1	54.91	32.00	13.07	0.77	0.49	0.11
M2	53.58	34.77	11.65	0.70	0.34	0.12
M3	69.28	4.97	25.75	0.53	0.33	0.10
M4	69.50	4.49	26.01	0.61	0.31	0.10
M5	76.60	11.42	11.98	0.62	0.48	0.13
M6	75.85	13.84	10.31	0.58	0.40	0.11
M7	60.28	24.87	14.85	0.68	0.42	0.10
M8	57.62	27.81	14.57	0.71	0.42	0.14
M9	60.85	22.29	16.86	0.62	0.51	0.14
M10	69.77	21.39	8.84	0.60	0.60	0.11
M11	66.39	9.39	24.22	0.57	0.43	0.10
M12	65.47	10.73	23.80	0.55	0.46	0.13

Table 2.4: Gas chromatogram data of terpanes, hopanes and TPP ratios of the Makhbaz Shale (calculated on m/z 217)

Sample No.	C_{31}R/ C_{30}H	C_{32} 22S/ (22S+22R)	G/C_{30}	C_{31} 22R/H	C_{35}/C_{34} homohopanes	Hopanes/ (Hopanes+ ∑20R steranes)	TPP
M1	0.47	0.62	0.53	0.57	1.05	0.34	0.18
M2	0.50	0.60	0.54	0.54	1.00	0.29	0.15
M3	0.46	0.69	0.52	0.68	1.33	0.21	0.11
M4	0.45	0.66	0.51	0.61	1.12	0.25	0.10
M5	0.51	0.76	0.50	0.62	1.23	0.26	0.13
M6	0.48	0.70	0.50	0.54	1.09	0.24	0.13
M7	0.49	0.70	0.52	0.49	0.93	0.39	0.16
M8	0.49	0.56	0.53	0.50	0.88	0.42	0.16
M9	0.46	0.59	0.52	0.50	0.79	0.22	0.10
M10	0.47	0.55	0.50	0.47	1.11	0.25	0.09
M11	0.47	0.76	0.50	0.61	0.90	0.21	0.09
M12	0.48	0.76	0.51	0.53	0.87	0.26	0.09

Table 2.5: Continued

Sample No.	$(C_{19}+C_{20})/(C_{23}+C_{24})$ TT	C_{24} TeT/ C_{26} TT	$(C_{19}+C_{20})/$ C_{23} TT	$C_{23}/$ C_{21} TT
M1	1.10	1.53	1.19	0.28
M2	0.97	1.33	1.05	0.31
M3	1.23	1.91	0.93	0.31
M4	0.81	2.00	0.97	0.29
M5	0.89	1.42	1.11	0.43
M6	1.19	1.51	1.20	0.40
M7	1.31	1.38	1.20	0.40
M8	1.00	1.88	1.07	0.34
M9	0.92	1.67	0.89	0.37
M10	1.32	1.72	0.92	0.27
M11	1.05	1.98	1.12	0.29
M12	0.87	1.36	0.98	0.44

Table 2.6: Continued

Sample No.	C_{29} TT/ C_{30} hopane	C_{28} TT/ C_{30} hopane	C_{25} TT/ C_{24} TeT	C_{24} TeT/ $(C_{24}$ TeT+ C_{26} TT)
M1	0.04	0.03	0.71	0.90
M2	0.04	0.07	0.49	0.72
M3	0.07	0.04	0.55	0.75
M4	0.05	0.04	0.50	0.89
M5	0.05	0.06	0.61	0.63
M6	0.03	0.06	0.72	0.72
M7	0.05	0.04	0.71	0.69
M8	0.06	0.05	0.63	0.60
M9	0.07	0.05	0.53	0.60
M10	0.07	0.04	0.47	0.81
M11	0.04	0.03	0.45	0.88
M12	0.05	0.04	0.70	0.67

Table 2.7: Continued

Sample No.	C_{30} diahopane/ C_{30} hopane	C_{29} diahopane/ C_{29} hopane
M1	0.51	0.39
M2	0.47	0.43
M3	0.38	0.40
M4	0.38	0.52
M5	0.39	0.52
M6	0.47	0.46
M7	0.49	0.38
M8	0.50	0.42
M9	0.50	0.50
M10	0.46	0.44
M11	0.39	0.44
M12	0.44	0.37

Where:

TOC = total organic carbon (wt. %)

S_1 = amount of free hydrocarbons in sample (mg/g)

S_2 = amount of hydrocarbons generated through thermal cracking (mg/g) – provides the quantity of hydrocarbons that the rock has the potential to produce through diagenesis

S_3 = amount of CO_2 (mg of CO_2/g of rock) - reflects the amount of oxygen in the oxidation step

T_{max} = the temperature at which maximum rate of generation of hydrocarbons occurs

Hydrogen index: HI = 100 * S_2 / TOC

Oxygen index: OI = 100 * S_3 / TOC

Production index: PI = S_1 / (S_1 + S_2)

Semi-quantitative index: GP = S_1 / S_2

Ro = vitrinite reflectance (wt. %)

Pr/Ph = Pristane/Phytane

Carbon preference index: CPI = $2(C_{23} + C_{25} + C_{27} + C_{29})/(C_{22} + 2[C_{24}+ C_{26} + C_{28}] + C_{30})$

Waxiness index: WI = $\Sigma(n\text{-}C_{21}\text{-}n\text{-}C_{31})/\Sigma(n\text{-}C_{15}\text{-}n\text{-}C_{20})$

TPP = tetracyclic polyprenoid

Table 2.8: Descriptive statistics of organic parameters of the Makhbaz Shale

Parameters	N	Minimum	Maximum	Mean	Std. Deviation
TOC	12	4.42	5.33	4.84	0.33
T_{max}	12	452	457	454	1.54
Ro	12	0.71	0.85	0.78	0.05
S_1	12	4.49	8.21	5.96	1.24
S_2	12	17.00	21.29	18.93	1.63
S_3	12	0.90	2.21	1.59	0.35
HI	12	359.96	433.03	390.94	21.41
OI	12	20.36	42.66	32.54	5.74
PI	12	0.19	0.29	0.24	0.03

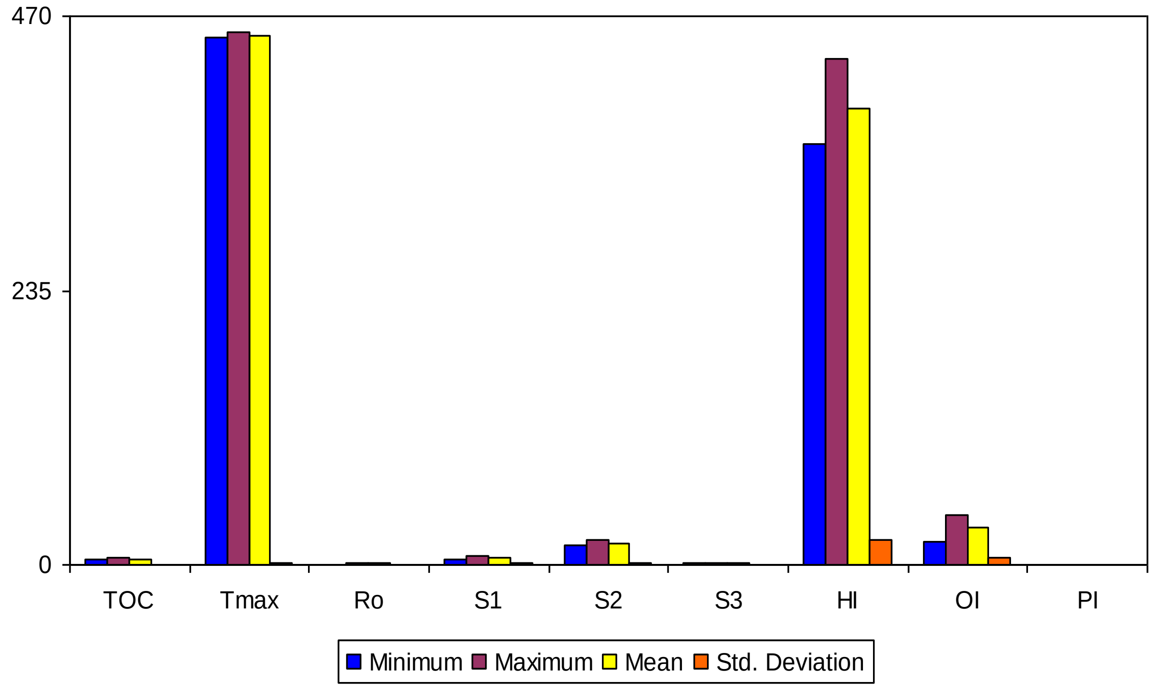

Fig. 2.1: Descriptive statistics of organic parameters of the Makhbaz Shale.

Table 2.9: Correlation matrix of organic parameters of the Makhbaz Shale

Parameters	TOC	T_{max}	Ro	S_1	S_2	S_3	HI	OI	PI
TOC	1.00								
T_{max}	0.20	1.00							
Ro	-0.03	-0.59	1.00						
S_1	0.77	0.09	-0.29	1.00					
S_2	0.79	0.42	0.04	0.62	1.00				
S_3	0.83	0.50	-0.48	0.67	0.61	1.00			
HI	-0.03	0.40	0.14	-0.01	0.59	-0.13	1.00		
OI	0.68	0.55	-0.64	0.58	0.44	0.97	-0.20	1.00	
PI	0.55	-0.10	-0.41	0.91	0.24	0.53	-0.32	0.50	1.00

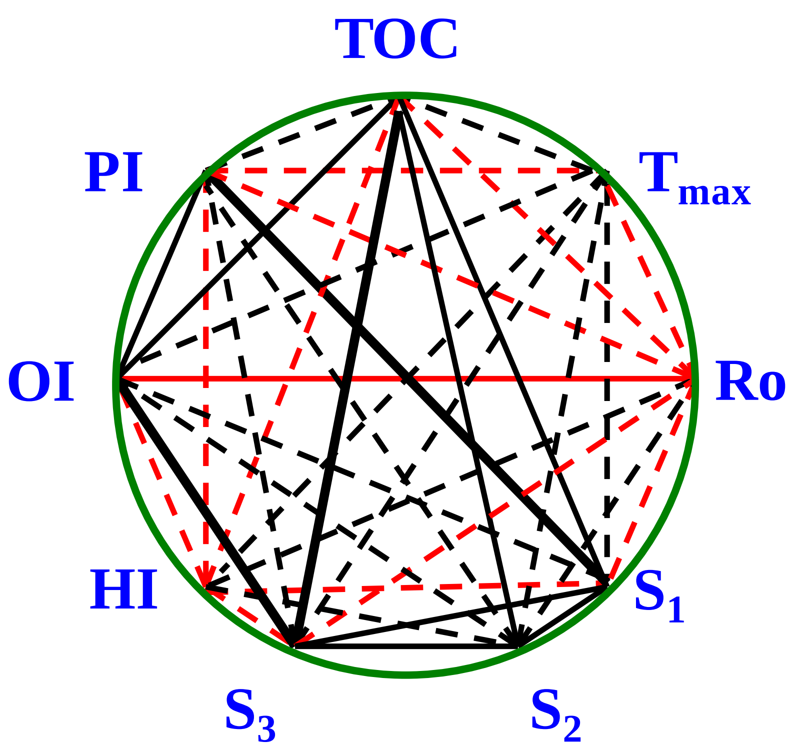

Fig. 2.2: Correlations among the organic parameters of the Makhbaz Shale (intensity of lines corresponds to the strength of the correlation coefficient (<0.4 to >0.8)) (red line means inverse relation).

Table 2.10: Principal component analysis of organic parameters of the Makhbaz Shale

Eigenvalues	4.56	2.50	2.00
% of Variance	45.64	24.95	20.19
Cumulative %	45.64	70.59	90.78
Principal components	PC1	PC2	PC3
TOC	0.89	0.09	0.29
T_{max}	0.46	0.25	-0.82
Ro	-0.43	0.48	0.65
S_1	0.87	-0.11	0.36
S_2	0.77	0.62	0.09
S_3	0.92	-0.17	-0.17
HI	0.08	0.91	-0.21
OI	0.84	-0.31	-0.33
PI	0.69	-0.47	0.38

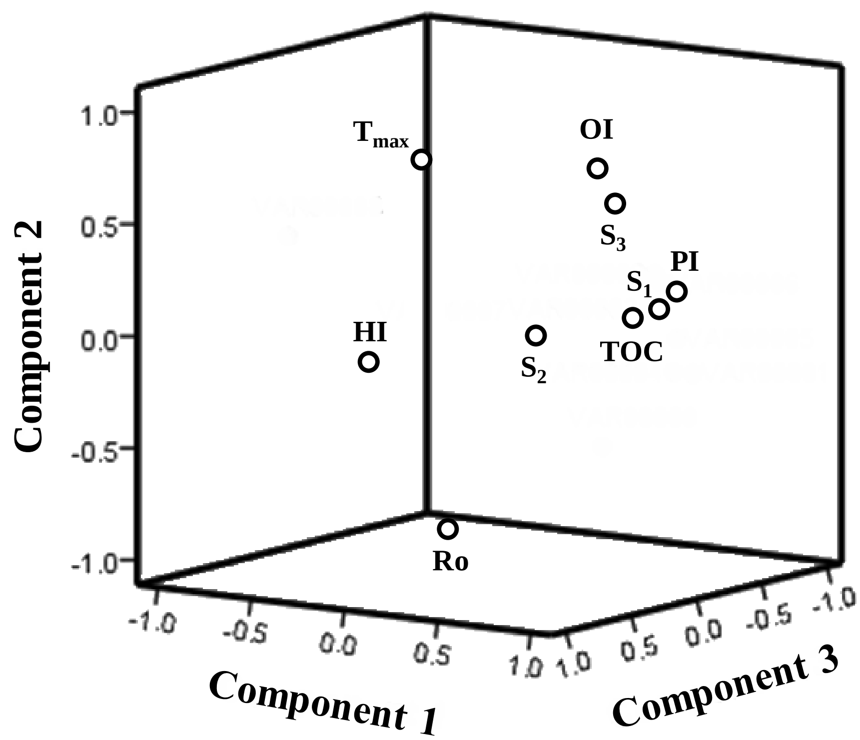

Fig. 2.3: Plot of PC loadings of organic parameters of the Makhbaz Shale.

2.2.1.1. Descriptive Statistics

Descriptive statistics are brief descriptive coefficients that summarize a given data set, which can be either a representation of the entire or a sample of a population. Descriptive statistics can be useful for two purposes: 1) to provide basic information about variables in a dataset and 2) to highlight potential relationships between variables.

In the current work, the descriptive statistics (Table 2.8 and Fig. 2.1) show that there is a slight difference in the organic parameter values (except for HI and OI), indicating the homogeneity of the organic chemical composition of the Makhbaz Shale.

2.2.1.2. Correlation Matrix

A correlation matrix is a table showing correlation coefficients between variables. Each cell in the table shows the correlation between two variables. A correlation matrix is used as a way to summarize data, as an input into a more advanced analysis, and as a diagnostic for advanced analyses.

In the present study, the TOC is positively correlated with S_1 and S_2 ($r = 0.77$ and 0.79, respectively, Table 2.9 and Fig. 2.2), suggesting the involvement of S_1 and S_2 from TOC. The independence of the amount of organic matter from the maturity of the Makhbaz Shale is evident through the weak correlation between TOC and each of HI, OI and PI ($r =$ -0.03, 0.68 and 0.55, respectively).

2.2.1.3. Principal Component Analysis (PCA)

Principal component analysis (PCA) is a technique for reducing the dimensionality of such datasets, increasing interpretability but at the same time minimizing information loss. It does so by creating new uncorrelated variables that successively maximize variance. Finding such new variables, the principal components, reduces to solving an eigenvalue/eigenvector problem, and the new variables are defined by the dataset at hand, not a priori, hence making PCA an adaptive data analysis technique. It is adaptive in another sense too, since variants of the technique have been developed that are tailored to various different data types and structures. This article will begin by introducing the basic ideas of PCA, discussing what it can and cannot do. It will then describe some variants of PCA and their application. In this work, three principal components (PCs) were performed describing 90.78% total variance of data.

First principal component (PC1): It accounts for about 45.64% of the total variables. It shows positive loading for TOC, S_1, S_2, S_3, OI and PI. It can be nominated as the component of the organic richness.

Second principal component (PC2): It accounts for 24.95% of the total variables. This component seems to be significant in interpreting the organic matter type where its loads positively for S_2 and HI.

Third principal component (PC3): It represents only 3.8% of the total variables. It shows positive loading for Ro and negative loading for T_{max}. This component expresses the thermal maturity of organic matter.

2.2.2. Richness, Type and Maturity of Organic Matter

According to Seiter *et al.,* (2004) total organic carbon (TOC) is the amount of carbon found in an organic compound and is often used as a non-specific indicator of water quality or cleanliness of pharmaceutical manufacturing equipment. TOC may also refer to the amount of organic carbon in soil, or in a geological formation, particularly the source rock (Seiter *et al.,* 2004). The amount of TOC present in a rock is a determining factor in a rock's ability to generate hydrocarbons. Furthermore, the quantity of organic matter in the source rocks is also evaluated by measuring of the pyrolysis derived (S_1 and S_2, Kruge *et al.,* 1996; Schulz *et al.,* 2002; Balbinot and Kalkreuth, 2010; El Nady *et al.,* 2016; Xia *et al.,* 2019). Peters and Cassa (1994) reported that the samples which contain TOC less than 0.5 are considered poor source rocks. Samples containing from 0.5 to 1% TOC are fair source rocks. Meanwhile, those containing TOC from 1 to 2 are good source rocks and samples that contain from 2 to 4% TOC are considered very good source rocks. They added that excellent source rocks contain more than 4% TOC. Table (2.11) shows average TOC values for different sedimentary rock types. The LECO analysis data show that All shale samples contain high TOC content (>4%), which suggests that the Makhbaz Shale is considered to be an excellent source rock. The binary plots of TOC versus S_2 (Fig. 2.4) and TOC versus GP (Fig. 2.5) supporting the above assumption. Additionally, the Makhbaz

Shale falls in the field of potential source rock in the binary plots of TOC versus S_1+S_2 (Fig. 2.6) and TOC versus HI (Fig. 2.7).

Table 2.11: Average TOC values for different sedimentary rock types (after Chinn, 1991)

Rock type	TOC value, %
Average for all shales	0.8
Average for shale source rocks	2.2
Average for calcareous shale source rocks	1.8
Average for carbonate source rocks	0.7
Average for all source rocks	1.8

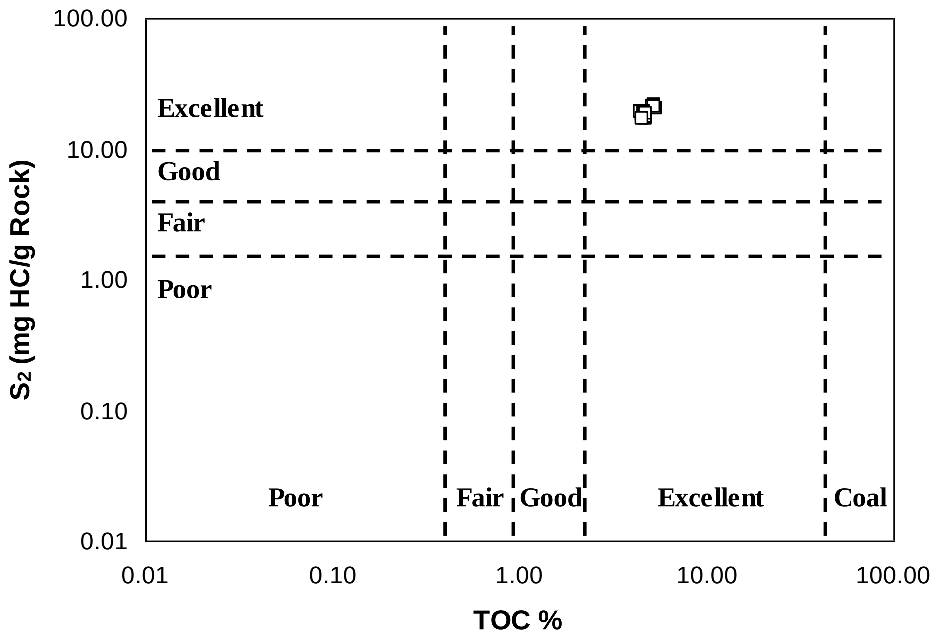

Fig. 2.4: Plot of TOC vs. S_2 showing the hydrocarbon potentialities for the Makhbaz Shale (fields after Dembicki, 2009).

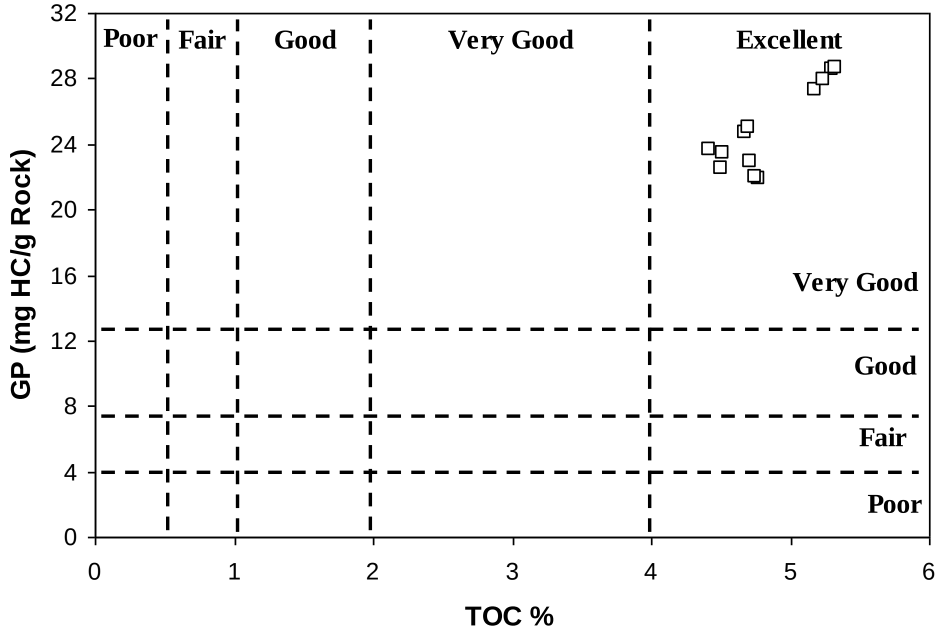

Fig. 2.5: Plot of TOC vs. GP showing the hydrocarbon potentialities for the Makhbaz Shale (fields after Ghori, 2002).

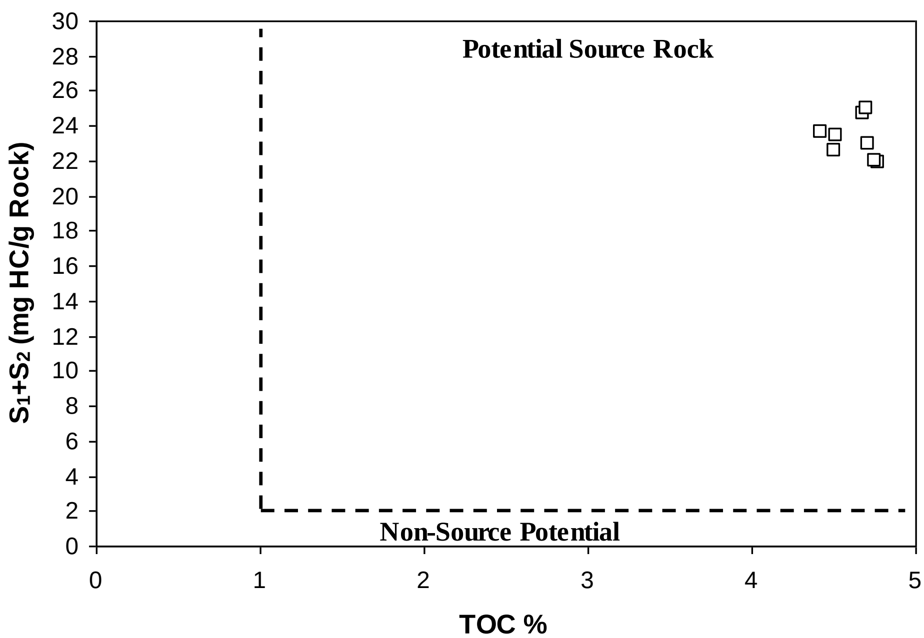

Fig. 2.6: Plot of TOC vs. S_1+S_2 showing the hydrocarbon potentialities for the Makhbaz Shale (fields after El Nady et al., 2016).

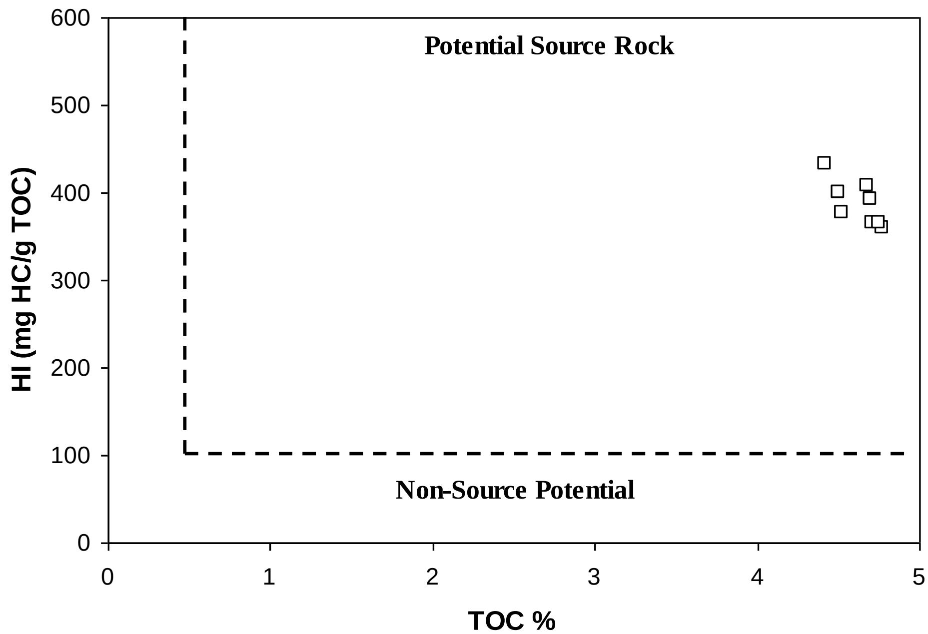

Fig. 2.7: Plot of TOC vs. HI showing the hydrocarbon potentialities for the Makhbaz Shale (fields after El Nady et al., 2016).

The type of organic matter (kerogen) is considered the second most important parameter in evaluating the source rock (Peters and Cassa, 1994; Schulz *et al.*, 2002; Lewan and Roy, 2011; El Nady *et al.*, 2016; Longbottom *et al.*, 2019). The kerogen type is defined by plotting the OI versus HI (Van Krevelen, 1961). Moreover, the binary plots of TOC versus S_2 and T_{max} versus HI can also be used to identify the kerogen type (Longford and Blanc-Valleron, 1990; Hall *et al.*, 2016). The plots of OI versus HI and TOC versus S_2 are less definitive than the plot of T_{max} versus HI (El-Kammar *et al.*, 2015; Aviles *et al.*, 2019).

The three models were used in the current work and all indicated that the Makhbaz Shale contains type II kerogen with moderate HI and very low OI (Figs. 2.8-10). This means that marine organic matter is prevalent in the Makhbaz Shale as I will explain later in this chapter.

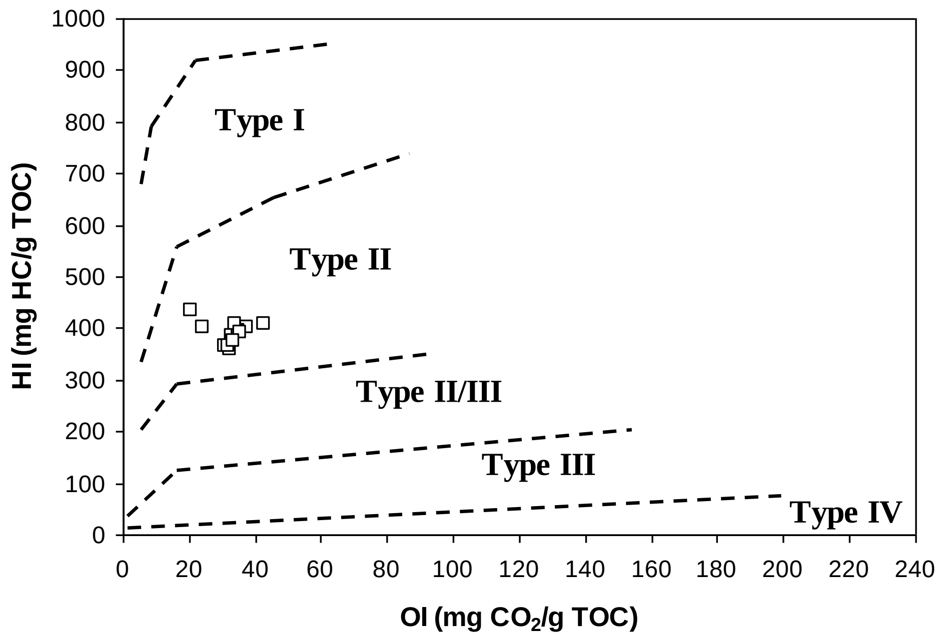

Fig. 2.8: Plot of OI vs. HI showing the kerogen type for the Makhbaz Shale (fields after Van Krevelen, 1961).

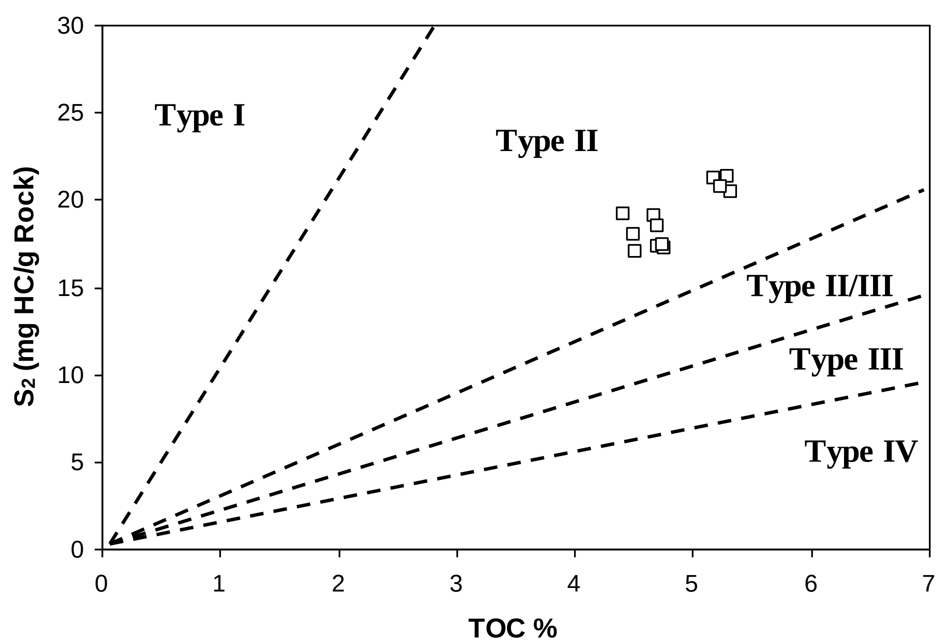

Fig. 2.9: Plot of TOC vs. S_2 showing the kerogen type for the Makhbaz Shale (fields after Longford and Blanc-Valleron, 1990).

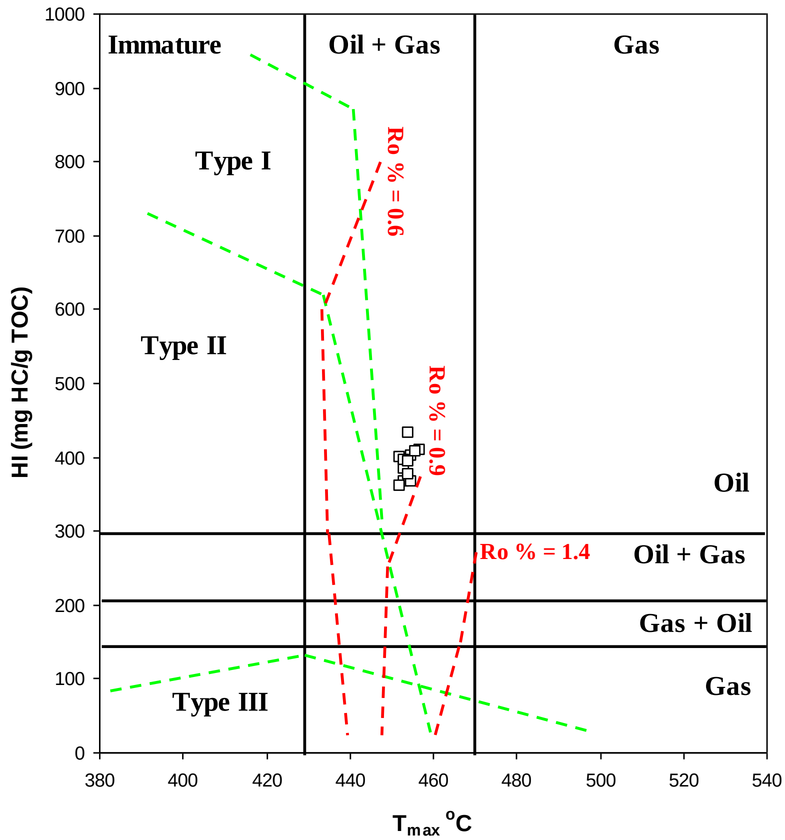

Fig. 2.10: Plot of T_{max} vs. HI showing the thermal maturity and kerogen type for the Makhbaz Shale (fields after Hall et al., 2016).

Thermal maturity is defined as the geothermal-driven reactions that modify the physical properties and chemical composition of organic matter in sedimentary rocks with increasing depth of burial with time to form a range of petroleum compounds (Tissot and Welte, 1984; Hunt, 1996; Peters *et al.*, 2012). Different maturity indices, such as vitrinite reflectance (Ro), pyrolysis-estimated T_{max} temperature, biomarkers, gas chromatography, and spore coloration are used to assess the level of thermal maturity of the organic matter (Tissot and Welte, 1984; Hunt, 1996; Peters *et al.*, 2005). For a very comprehensive review of thermal maturity indicators, readers are referred to Hartkopf-Froder *et al.*, (2015). There is no doubt that the thermal maturity appraisals are of great interest to many palynologists, coal petrologists, and hydrocarbon explorationists. During the last few decades, there has been a remarkable evolution in the classical thermal maturity indices; however, they are still expensive and time-consuming. In the meantime, it is crucial to cope with the technical revolution of the ideas and digital methodologies concerning maturation measurements. This shows the real need for such a modern, simple, accessible, and responsive index that can work side-by-side with other classic, expensive, and time-consuming techniques (Hartkopf-Froder *et al.*, 2015).

The data of Ro, T_{max}, HI, PI, and C_{32} 22S/(22S+22R) homohopane and C_{29} (ßß/ßß+αα) sterane for the Makhbaz Shale were used to indicate the phases of hydrocarbon generation. The T_{max}, PI and Ro values rang from 452 to 457°C, 0.19 to 0.29 and 0.71 to 0.85%, respectively, indicating mature organic matter. Moreover, the plots of T_{max} versus HI (Fig. 2.10), T_{max} versus Ro (Fig. 2.11), T_{max} versus PI (Fig. 2.12) and C_{32} 22S/(22S+22R) homohopane versus C_{29} (ßß/ßß+αα) sterane (Fig. 2.13) confirm the previous assumption.

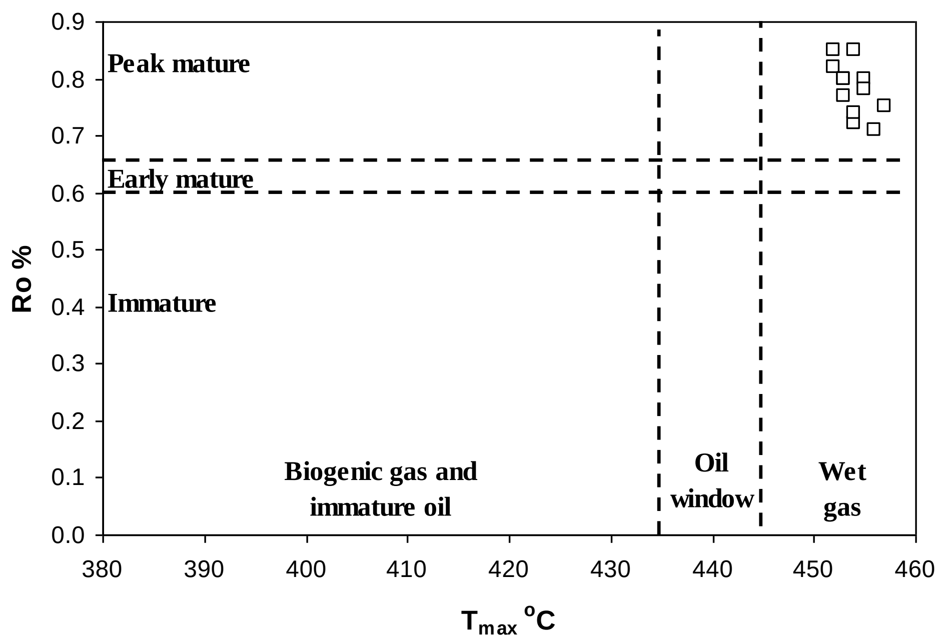

Fig. 2.11: Plot of T_{max} vs. Ro showing the thermal maturity for the Makhbaz Shale (fields after Atta-Peters and Garrey, 2014).

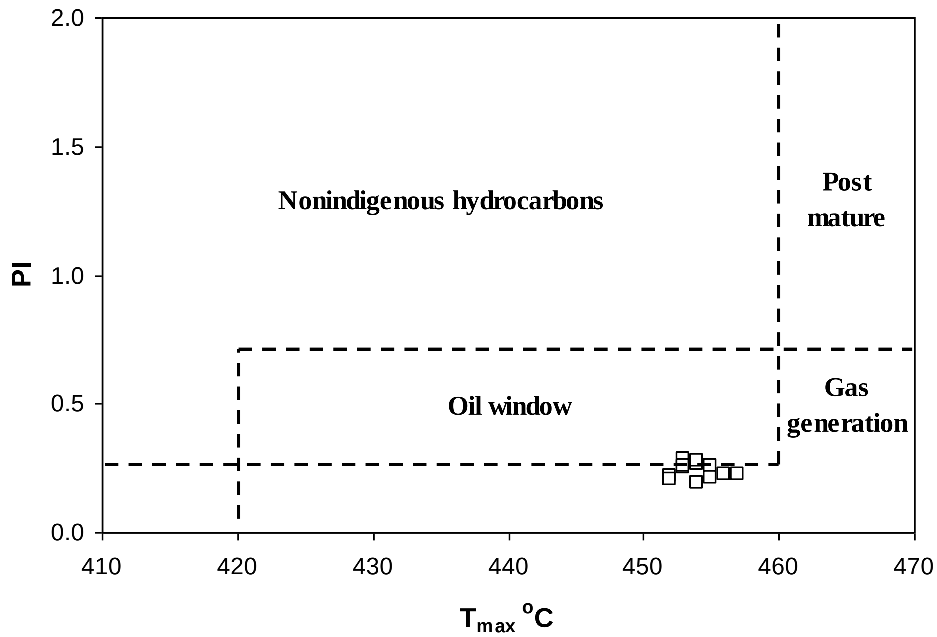

Fig. 2.12: Plot of T_{max} vs. PI showing the thermal maturity for the Makhbaz Shale (fields after El Nady et al., 2016).

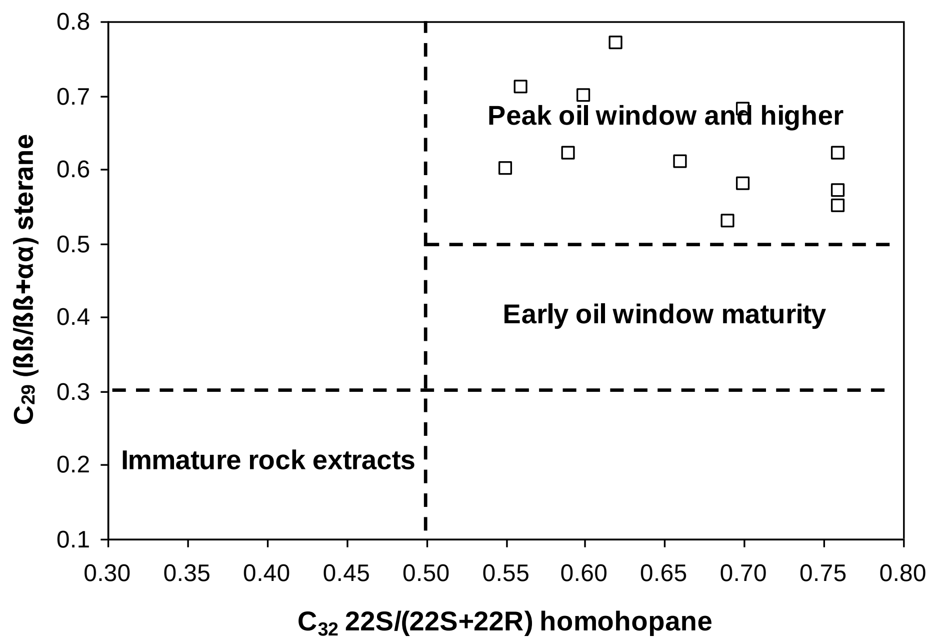

Fig. 2.13: Plot of C_{32} 22S/(22S+22R) homohopane vs. C_{29} (ββ/ββ+αα) sterane showing the thermal maturity for the Makhbaz Shale (fields after Peters and Moldowan, 1993).

2.2.3. Organic Matter Input and Depositional Environment

Organic geochemistry, using biological marker compounds, must help identify various paleoenvironmental conditions, examples may include; marine or nonmarine environments, anaerobic subaqueous conditions, and paleosalinity (Moldowan *et al.*, 1996; Peters *et al.*, 2005; Sousa *et al.*, 2019). Different depositional environments may have different assemblages of organisms, and thus contribute different biomarkers to the sediment (Baydjanova and George, 2019). Terrigenous, marine, deltaic, and hypersaline environments all show characteristic differences in biomarker compositions (Peters *et al.*, 2005). *n*-Alkane indices in conjunction with sterane and aromatic ratios can help to distinguish between terrigenous and marine organic matter inputs, the ratio of hopanes to steranes help to differentiate prokaryotic versus eukaryotic input, and various biomarker and aromatic hydrocarbon ratios help to discern thermal maturity, lithology, and the depositional environments (Baydjanova and George, 2019). There are some limitations to the biomarker method; however, including that biomarker ratios could be influenced by both organic source inputs and thermal maturity (Peters *et al.*, 2005; Sousa *et al.*, 2019). To evaluate the depositional environment, paleosalinity, paleooxygenation condition and organic matter input, the following models were used in this chapter: 1) The binary plots of Pr/Ph versus CPI (Fig. 2.14), Pr/Ph versus WI (Fig. 2.15), Pr/Ph versus C_{29}/C_{27} regular steranes (Fig. 2.16), Ph/n-C_{18} versus Pr/n-C_{17} (Fig. 2.17), Pr/Ph versus $\sum$(n-C_{12}-n-C_{20})/($\sum$(n-C_{12}-n-C_{20})+$\sum$(n-C_{12}-n-C_{29})) (Fig. 2.18) and Pr/Ph versus C_{29} ßα(S+R)-dia/(C_{28} ßα(S+R)-dia+C_{27} ßα(S+R)-dia) (Fig. 2.19) and the ternary plot of C_{27}-C_{28}-C_{29} regular steranes (Fig. 2.20) were used to determine the redox condition and organic matter input,
2) The binary plots of Pr/Ph versus C_{31}22R/C_{30}- Hopane (Fig. 2.21), Pr/Ph versus (Pr+n-C_{17})/(Ph+n-C_{18}) (Fig. 2.22) and Hopanes/(Hopanes+$\sum$20R steranes) versus TPP (Fig. 2.23) were used to define the depositional environment, and 3) The binary plot of Pr/Ph versus G/C_{30} (Fig. 2.24) was used to identify the paleosalinity. These models suggest the following: 1) The Makhbaz Shale contains marine organic matter formed in anoxic conditions, and 2) The Makhbaz Shale was deposited in a medium-saline marine environment.

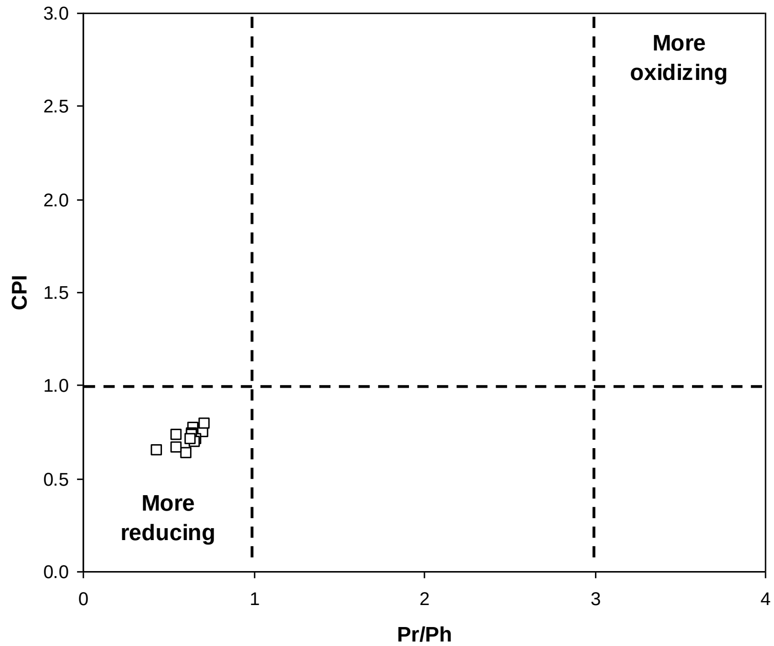

Fig. 2.14: Plot of Pr/Ph vs. CPI showing the organic matter origin and redox conditions for the Makhbaz Shale (fields after Akinlua et al., 2007).

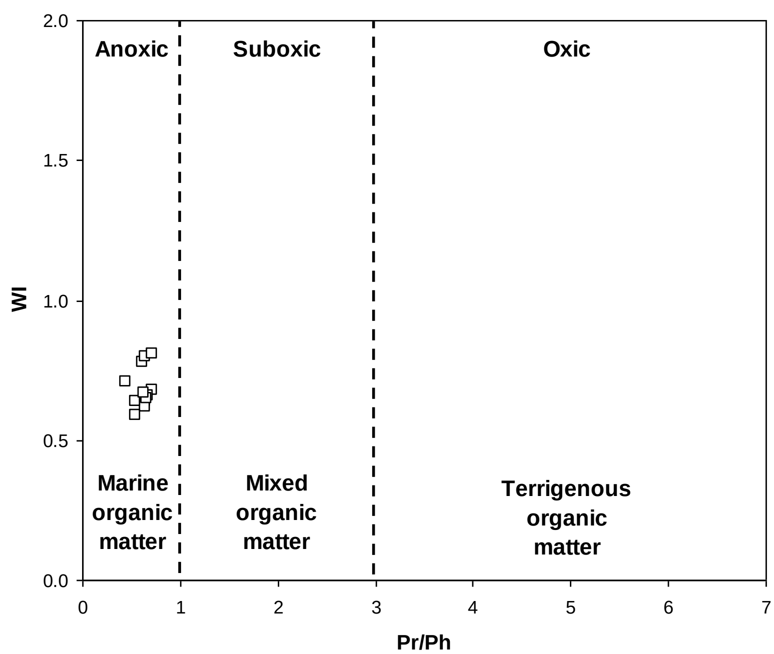

Fig. 2.15: Plot of Pr/Ph vs. WI showing the organic matter origin and redox conditions for the Makhbaz Shale (fields after El Diasty and Moldowan, 2012).

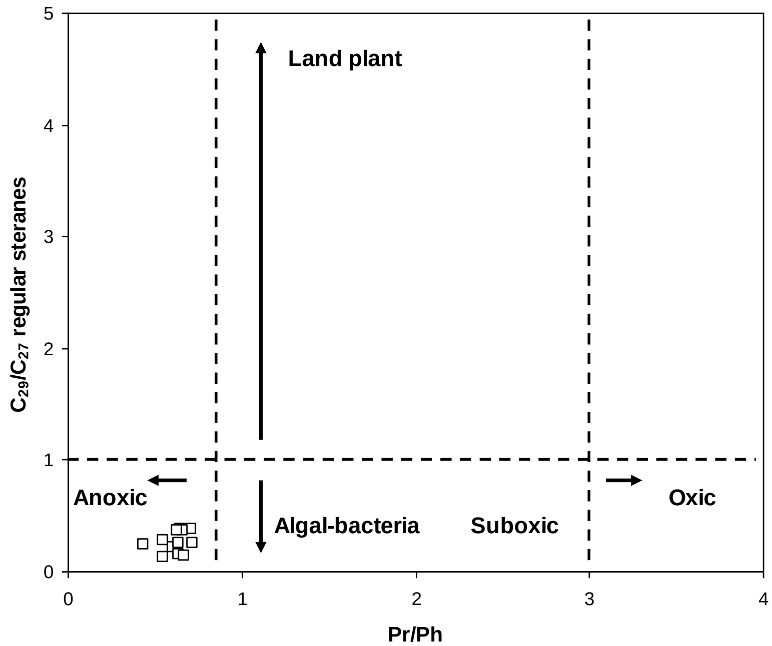

Fig. 2.16: Plot of Pr/Ph vs. C_{29}/C_{27} regular steranes showing the organic matter origin and redox conditions for the Makhbaz Shale (fields after Yandoka et al., 2015).

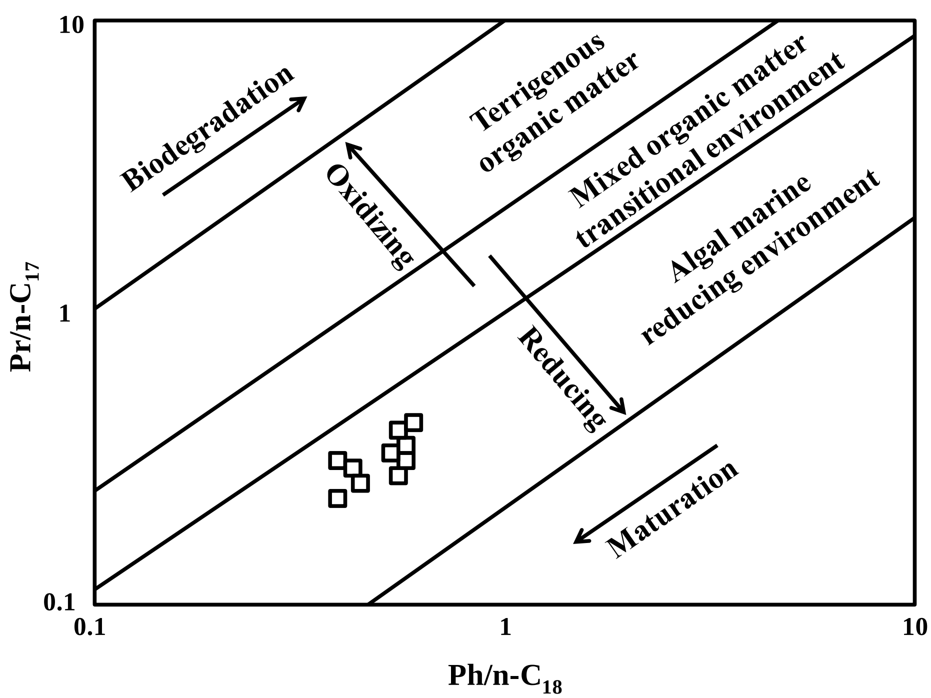

Fig. 2.17: Plot of Ph/n-C_{18} vs. Pr/n-C_{17} showing the organic matter origin and redox conditions for the Makhbaz Shale (fields after Shanmugam, 1985).

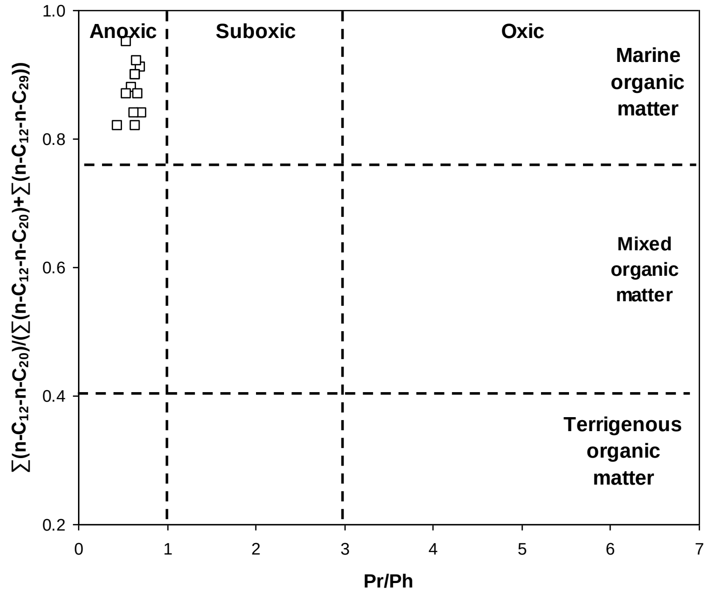

Fig. 2.18: Plot of Pr/Ph vs. n-alkane SLR ($\Sigma n\text{-}C_{12\text{-}20}$)/($\Sigma n\text{-}C_{12\text{-}29}$) showing the organic matter origin and redox conditions for the Makhbaz Shale (fields after Shaltami et al., 2019).

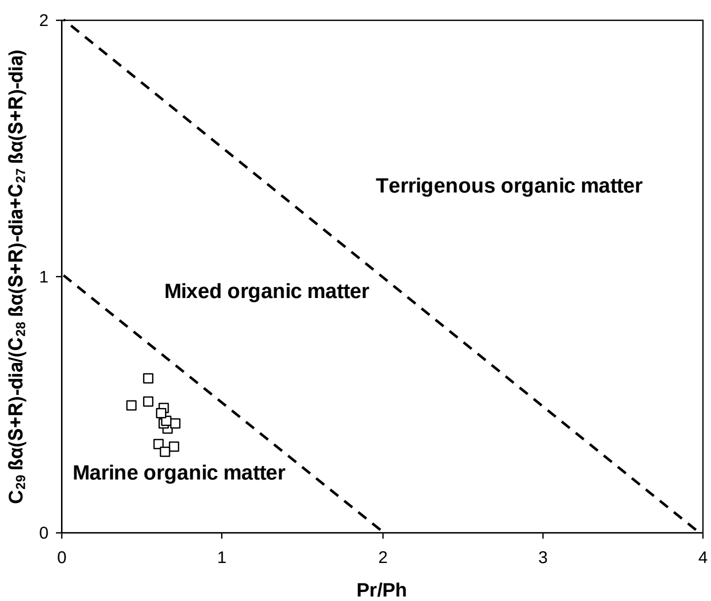

Fig. 2.19: Plot of Pr/Ph vs. predominance of C_{29} -components amongst diasteranes showing the organic matter origin for the Makhbaz Shale (fields after Shaltami et al., 2019).

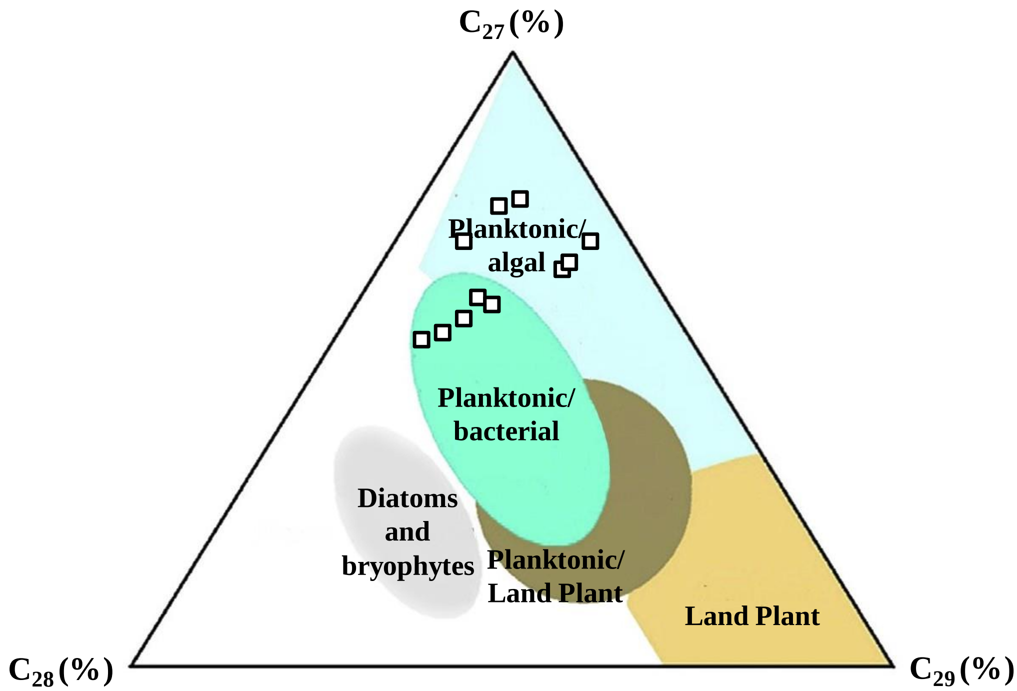

Fig. 2.20: Ternary diagram of C_{27}-C_{28}-C_{29} regular steranes showing the organic matter origin for the Makhbaz Shale (fields after Huang and Meinschein, 1979).

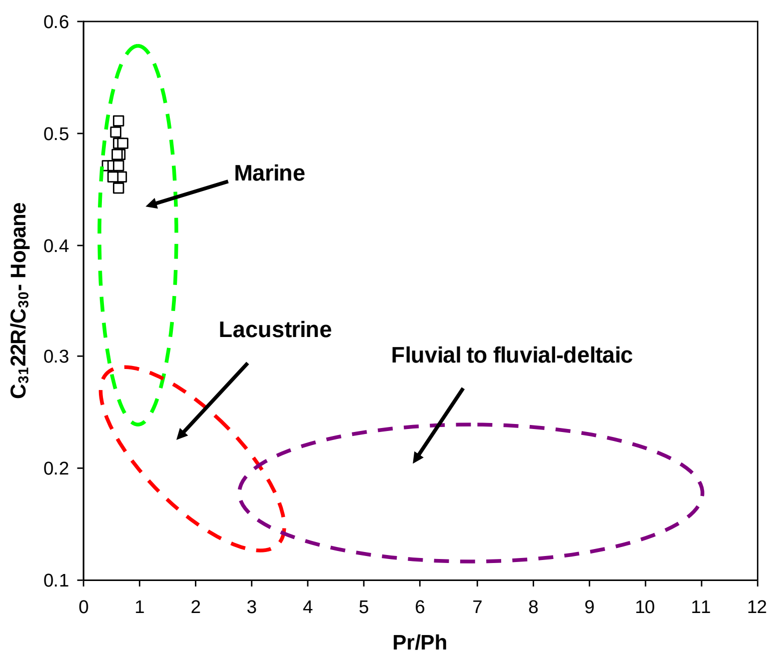

Fig. 2.21: Plot of Pr/Ph vs. $C_{31}R/C_{30}$ hopane showing the depositional environment of the Makhbaz Shale (fields after Peters et al., 2005).

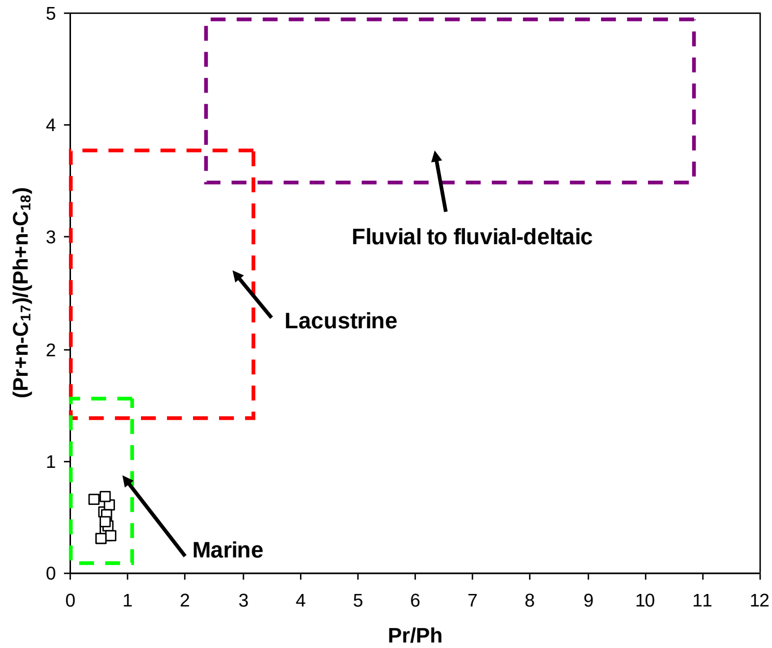

Fig. 2.22: Plot of Pr/Ph vs. (Pr+n-C_{17})/(Ph+n-C_{18}) showing the depositional environment of the Makhbaz Shale (fields after Shaltami et al., 2019).

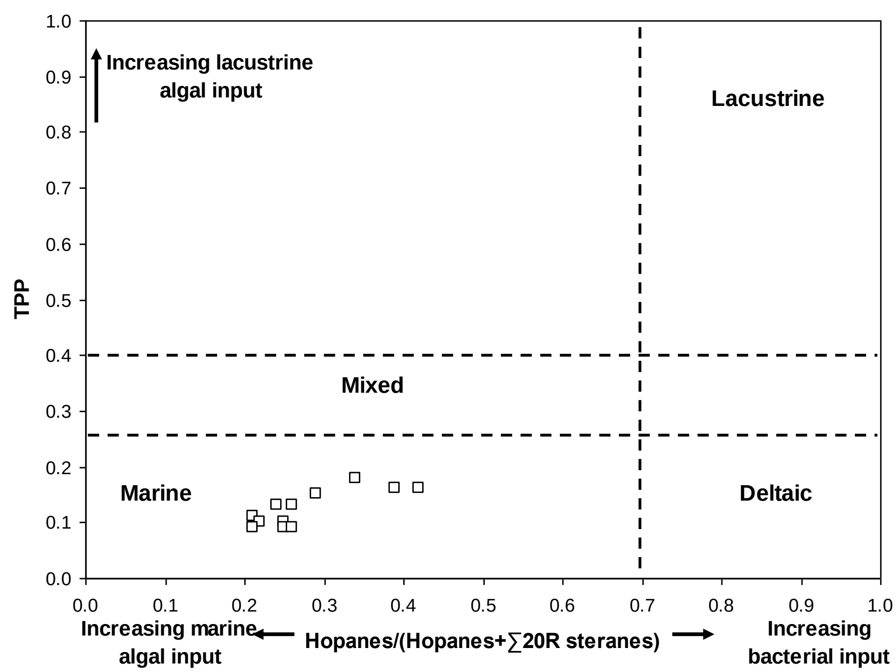

Fig. 2.23: Plot of TPP vs. hopane/(hopanes+Σ20R steranes) showing the depositional environment of the Makhbaz Shale (fields after Holba et al., 2003).

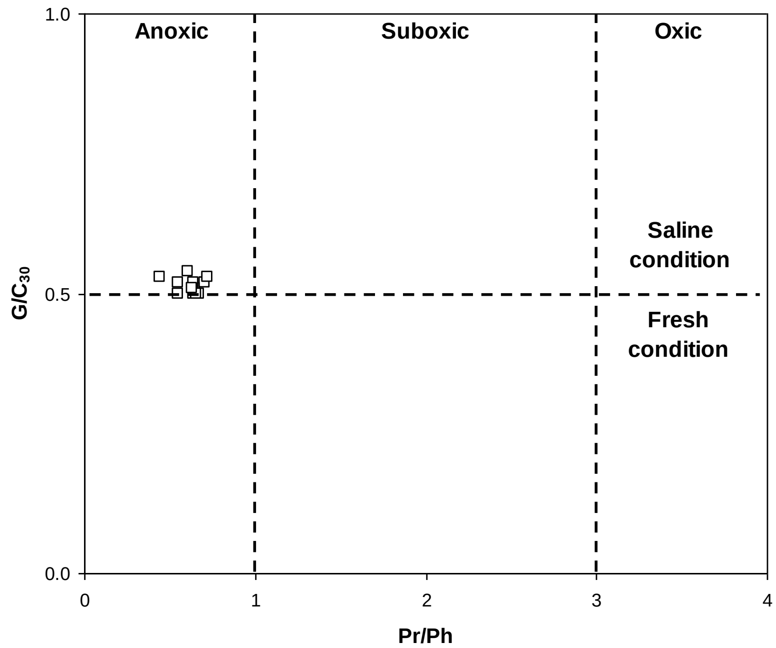

Fig. 2.24: Plot of Pr/Ph vs. G/C_{30} showing the paleosalinity and redox conditions for the Makhbaz Shale (fields after Zhou and Huang, 2008).

CHAPTER THREE
RESERVOIR GEOCHEMISTRY

3.1. Introduction

Reservoir fluid geochemistry, or reservoir geochemistry, is the measurement and application of compositional variations in subsurface reservoir fluids (oil, water, gas) to the solution of practical problems in the energy and environment sector (Larter *et al.,* 1997; Larter *et al.*, 2010; Li *et al.,* 2018). Reservoir geochemical applications in the energy sector are now many and diverse with petroleum geochemical applications dominating, but with water geochemistry being increasingly applied to problems related to well scale, well and reservoir breaching during production and reservoir souring. Reservoir geochemistry, while now a successful mainstream industrial application area, with a defined commercial presence outside of major oil company research groups (Larter *et al.*, 2010; Yang *et al.*, 2019), continues to be an area of active research and development in industry and academia. The next decade promises great developments as more refractory unconventional resources become development targets, more high tech analytica come online and reactive enhanced oil recovery becomes more common via microbiological, chemical, thermal and/or electrical means (Larter *et al.,* 2008). While the industry continues to search for ever deeper or more complex plays, there is still a push to more accurately predrill predict petroleum location and quality, to scavenge stranded resources, and to monitor recovery operations in situ real time as carbon management issues become a priority in all aspects of fossil fuel recovery (Bennett *et al.*, 2008). To date, reservoir geochemical activity has been traditionally petroleum production related and that will continue, but in the future, there will be greater focus on applications related to subsurface carbon sequestration and radioactive and other waste disposal in the deep subsurface (Baba *et al.,* 2019). In particular, measurement, monitoring and verification (MMV) of subsurface carbon sequestration as part of globally regulated climate change mitigation activities will become a huge area of research and application for reservoir geochemists of all subdisciplines (Shea *et al.,* 2007).

Reservoir geochemistry grew out of our ability to correlate distributions of key chemical species with system state variables for fundamental processes in petroleum systems or production (Larter *et al.,* 2010). While most early work was qualitative, we have seen a persistent trend towards the use of absolute quantification of petroleum components for reservoir geochemical applications (Larter *et al.,* 2010). Such studies are reliant on excellent calibration data sets, which require unaltered, carefully handled, representative samples prepared for high resolution compositional imaging and quantification with state of the art analytica (Bennett *et al.,* 2008). Typically, these days, sophisticated data processing using both traditional chemometric tools and supervised learning methods is used to build robust models of reservoir behavior from fluid analyses. While there have been failures, there has been considerable success in developing such models and deciphering the mechanics of petroleum systems using petroleum geochemistry, aided considerably by a consistent increase in the use of absolute rather than relative component abundance data, i.e. component concentrations rather than just component ratios (Baba *et al.,* 2019).

Petroleum inclusions are small encapsulations of oil and gas that offer an invaluable opportunity to better constrain the evolution of petroleum systems (Volk and George, 2019). Insights into paleo fluid compositions complement observations on present day fluid compositions, which represent only the end-point of complex cumulative processes throughout basin history (Burruss, 1981; Pironon *et al.,* 1995; Munz, 2001; Arouri *et al.,* 2009; Liu *et al.,* 2014; Shaltami *et al.,* 2018). Petroleum inclusions are the latest technologies used in reservoir evaluation (Larter *et al.,* 1997; Volk *et al.,* 2002; George *et al.,* 2007; Liu *et al.,* 2014; Pestilho *et al.,* 2018). There are two stages in assessing petroleum inclusions: 1) Identify the type of inclusions using a petrographic microscope or SEM, and 2) Perform chemical analysis of fluids.

Shaltami *et al.,* (2018) applied the technique of petroleum inclusions to evaluate the Achabiyat and Hawaz reservoirs in the Dur Al Qussah area, Murzuq Basin, SW Libya, and this was the first application of this technology in Libya.

3.2. Petroleum Inclusions

In the studied reservoir (Makhbaz Limestone), the petroleum inclusions are abundant in calcite. Most inclusions contain two types of fluid namely, natural gas and crude oil (Figs. 3.1-4), and some of which contain water. It is clear that the studied inclusions differ in the chemical composition because they have different shapes. Most inclusions are irregular in shape and some are rounded. The BSE images (Figs. 3.1-4) also show that at least there are two different types of crude oil in the petroleum inclusions, which will be discussed later in this chapter. Different types of oil may indicate different source rock.

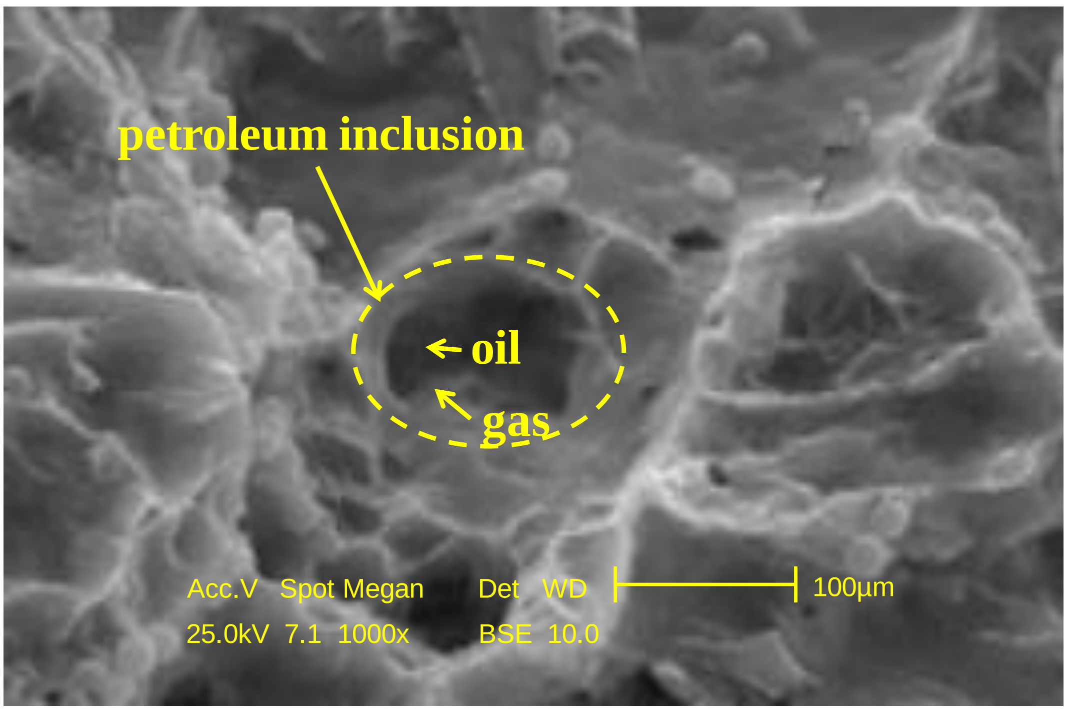

Fig. 3.1: BSE image of rounded petroleum inclusion in the Makhbaz Reservoir (Sample M13).

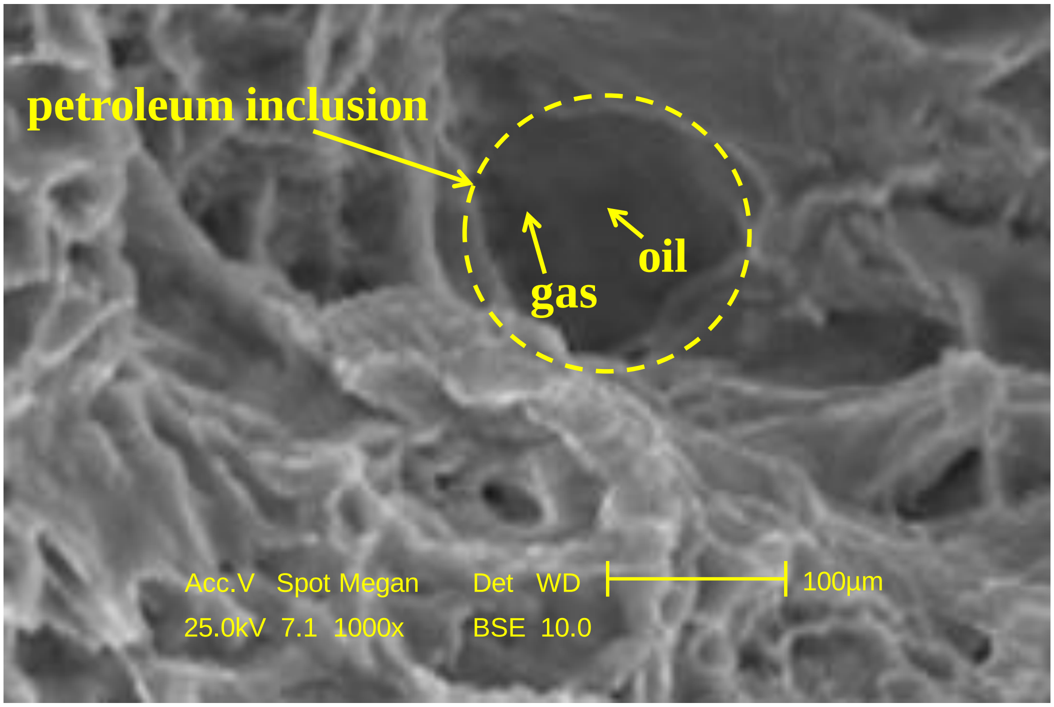

Fig. 3.2: BSE image of irregular petroleum inclusion in the Makhbaz Reservoir (Sample M14).

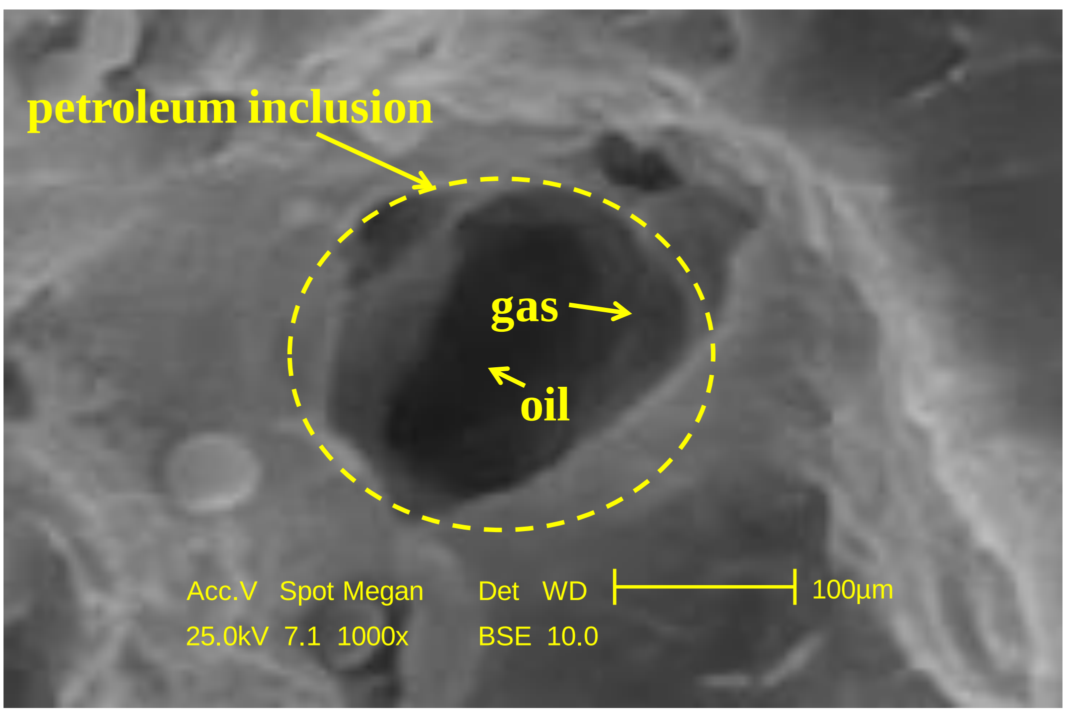

Fig. 3.3: BSE image of subrounded petroleum inclusion in the Makhbaz Reservoir (Sample M15).

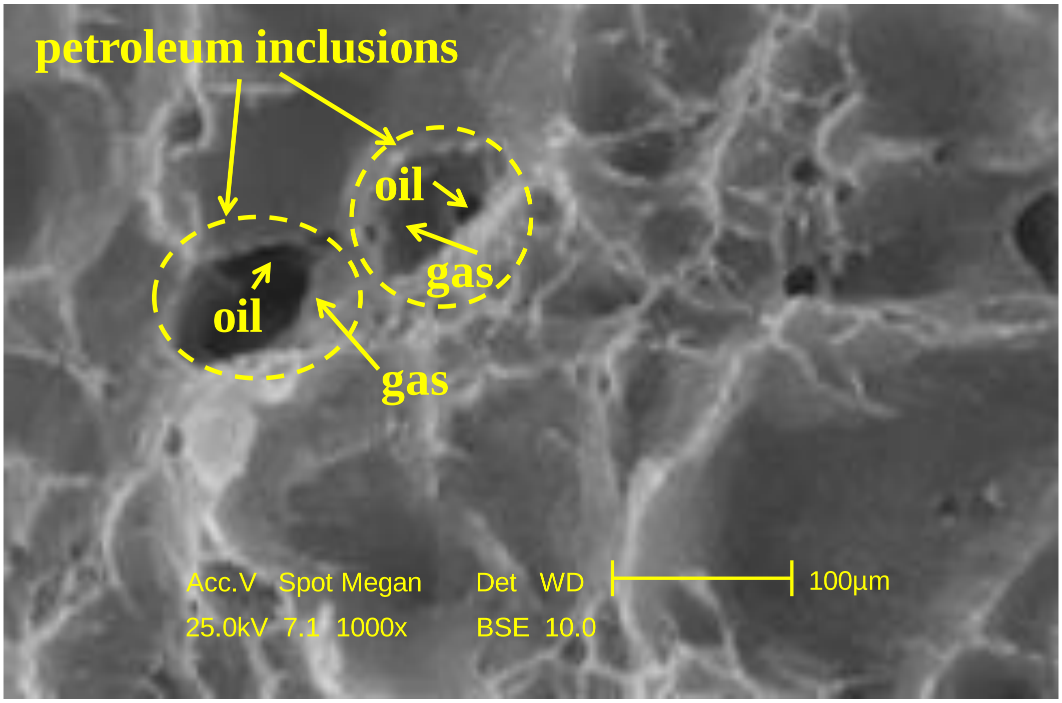

Fig. 3.4: BSE image of two irregular petroleum inclusions in the Makhbaz Reservoir (Sample M16).

3.3. Types of Natural Gas

According to Claypool and Kvenvolden (1983) and Selley (1998) there are two different classifications of natural gas:

1) The first classification divides natural gas into two types: a) Hydrocarbon gases (methane (CH_4), ethane (C_2H_6), propane (C_3H_8), butane (C_4H_{10}), pentane (C_5H_{12}) and hexane (C_6H_{14})), and b) Non-hydrocarbon gases (hydrogen (H_2), nitrogen (N_2), carbon dioxide (CO_2), hydrogen sulfide (H_2S) and inert gases (helium (He), argon (Ar), krypton (Kr) and radon (Rn)).

2) The second classification depends on the origin and therefore the natural gases are divided into three types: a) Inorganic source (nitrogen and inert gases), b) organic source (hydrogen and hydrocarbons), and 3) mixed source (carbon dioxide and hydrogen sulfide).

The hydrocarbon gases are primarily methane with smaller quantities of other hydrocarbons (Asomaning *et al.*, 2014; Samani *et al.*, 2019). Based on the methane content, there are two general types of hydrocarbon gases:

1) Biogenic gas (±95% methane), or dry gas, which was formed by bacterial decay at shallow depth.

2) Thermogenic gas (<95% methane), or wet gas, which is a lower quality gas formed at high temperatures. Wet gas on the other hand contains compounds such as ethane and butane, in addition to methane.

Table (3.1) shows the types of natural gas in the petroleum inclusions of the Makhbaz Reservoir. Obviously, the reservoir contains high concentration of hydrocarbon gases (C_1, C_2, C_3, nC_4 and iC_4) with small amounts of non-hydrocarbon gases (H_2, N_2, CO_2 and H_2S) (Fig. 3.5). C_1 represents the most abundant gas.

Table 3.1: Components of gases (%) in the Makhbaz Reservoir inclusions

Sample No.	C_1	C_2	C_3	nC_4	iC_4	H_2	N_2	CO_2	H_2S
M13(1)	82.14	4.92	0.49	1.05	0.52	2.55	0.66	5.21	2.46
M13(2)	81.47	4.41	0.30	1.05	0.49	3.56	0.61	5.06	3.05
M149(1)	68.59	13.34	6.29	2.08	0.71	2.60	0.53	4.42	1.44
M14(2)	83.09	3.95	0.24	0.87	0.53	3.83	0.60	4.91	1.98
M15(1)	82.25	3.79	0.29	0.92	0.51	3.23	0.56	5.10	3.35
M15(1)	70.09	13.97	6.58	2.12	0.74	1.76	0.68	3.39	0.67
M16(1)	68.26	13.67	8.12	2.32	0.87	2.43	0.61	3.16	0.56
M16(2)	69.00	13.16	8.00	2.39	0.76	1.94	0.70	3.05	1.00

Where:

C_1 = methane

C_2 = ethane

C_3 = propane

nC_4 = normal butane

iC_4 = isobutene

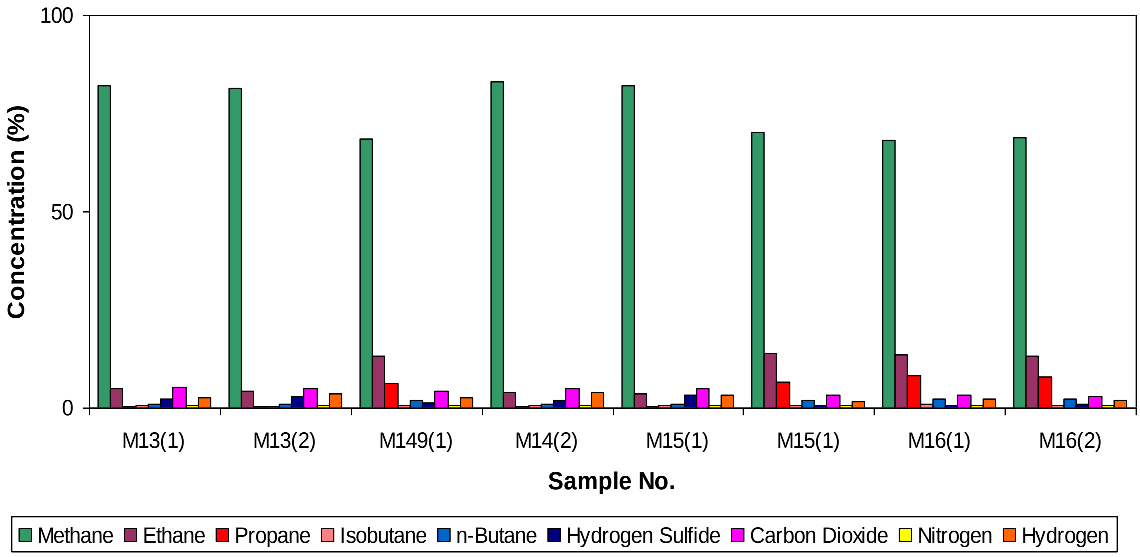

Fig. 3.5: Concentration of natural gas in the Makhbaz Reservoir inclusions.

3.4. Oil Families

Cluster analysis is a class of techniques that are used to classify objects or cases into relative groups called clusters. It is also called classification analysis or numerical taxonomy. In cluster analysis, there is no prior information about the group or cluster membership for any of the objects. Tables (3.2-10) illustrate the chemical analysis data of the crude oil in the Makhbaz Reservoir inclusions. The oil families were identified using cluster analysis. This analysis was done using biomarkers. The cluster analysis shows two different oil families (Fig. 3.6). These families have been termed Family I and Family II.

Based on the API gravity, Martinez *et al.*, (1984) classified crude oils into light oils (API gravity>31.1°), medium oils (27.3°<API gravity<31.1°) and heavy oils (API gravity<27.3°), while Waples (1985) classified crude oils into biodegraded oils (API gravity<20°) and condensate oils (API gravity>45°). Figs (3.7-10) show that Family I oils are heavy oils (biodegraded oils) while Family II oils are of light oils (condensate oils). This assumption is also supported by the binary plot of C_6H_6/C_6H_{12} vs. C_7H_8/C_7H_{14} (Fig. 3.11). Generally, Family II oils are depleted in toluene and benzene and there are indications of oil-water interactions.

Table 3.2: API gravity and SARA values of the studied crude oil

Sample No.	API (°)	SAT (%)	ARO (%)	NSO (%)
M13a	17.53	46.89	32.24	20.87
M13b	19.27	49.38	32.50	18.12
M14a	18.64	52.45	28.06	19.49
M14b	16.10	60.33	28.72	10.95
M15a	48.49	59.46	28.20	12.34
M15b	45.88	48.09	32.91	19.00
M16a	46.27	50.80	29.08	20.12
M16b	46.00	51.00	30.11	18.89

Table 3.3: Commission Internationale de l'Elcairage (CIE) values of the studied crude oil

Sample No.	CIE X	CIE Y
M13a	0.39	0.42
M13b	0.37	0.43
M14a	0.34	0.38
M14b	0.36	0.36
M15a	0.34	0.32
M15b	0.32	0.33
M16a	0.30	0.33
M16b	0.30	0.30

Table 3.4: Peak wavelength (λ_{max}), Q_{F535} and $Q_{650/500}$ values of the micro-beam fluorescence spectra of the studied crude oil

Sample No.	λ_{max} (nm)	$Q_{650/500}$	Q_{F535}
M13a	551	0.66	1.24
M13b	549	0.60	1.10
M14a	545	0.69	1.05
M14b	554	0.64	1.16
M15a	502	0.44	0.75
M15b	501	0.39	0.67
M16a	504	0.50	0.88
M16b	507	0.41	0.73

Table 3.5: Biomarker analysis data of the studied crude oil (calculated on m/z 217)

Sample No.	C_{29} steranes: ßß/(αα+ßß)	C_{29} steranes: 20S/(20S+20R)	C_{30} sterane index	C_{35}/C_{34} homohopanes	C_{31} 22R/H
M13a	0.87	0.51	0.12	1.00	0.66
M13b	0.83	0.50	0.14	1.51	0.65
M14a	0.91	0.50	0.14	1.17	0.63
M14b	0.91	0.56	0.12	1.25	0.62
M15a	0.89	0.59	0.07	0.60	0.32
M15b	0.88	0.50	0.05	0.52	0.28
M16a	0.88	0.50	0.09	0.47	0.21
M16b	0.80	0.55	0.08	0.40	0.19

Table 3.6: Continued

Sample No.	Ts/ (Ts+Tm)	29Ts/ (29Ts+30NH)	Pr/Ph	C_6H_6/ C_6H_{12}	C_7H_8/ C_7H_{14}
M13a	0.71	0.55	0.64	0.81	1.19
M13b	0.70	0.57	0.42	0.84	1.23
M14a	0.74	0.59	0.63	0.81	1.30
M14b	0.72	0.53	0.79	0.81	1.27
M15a	0.72	0.49	1.55	0.24	0.22
M15b	0.77	0.50	1.61	0.28	0.34
M16a	0.71	0.52	1.70	0.23	0.26
M16b	0.69	0.48	1.88	0.19	0.33

Table 3.7: Continued

Sample No.	$(C_{19}+C_{20})$/ $C_{23}+C_{24})$ TT	C_{24} TeT/ C_{26} TT	$(C_{19}+C_{20})$/ C_{23} TT	C_{23}/ C_{21} TT	C_{29} TT/ C_{30} hopane
M13a	0.92	1.40	0.90	0.32	0.06
M13b	1.09	1.87	1.22	0.29	0.03
M14a	0.89	1.66	0.95	0.34	0.05
M14b	1.33	1.37	1.08	0.45	0.05
M15a	0.66	0.56	0.67	1.54	0.12
M15b	0.54	0.50	0.44	1.50	0.11
M16a	0.59	0.43	0.56	1.69	0.15
M16b	0.43	0.49	0.60	1.72	0.13

Table 3.8: Continued

Sample No.	C_{28} TT/ C_{30} hopane	C_{25} TT/ C_{24} TeT	C_{24} TeT/ (C_{24} TeT+ C_{26} TT)	C_{30} diahopane/ C_{30} hopane	C_{29} diahopane/ C_{29} hopane
M13a	0.04	0.44	0.61	0.35	0.52
M13b	0.07	0.75	0.91	0.33	0.50
M14a	0.07	0.66	0.76	0.56	0.37
M14b	0.06	0.69	0.82	0.49	0.41
M15a	0.11	1.12	0.42	0.21	0.25
M15b	0.15	1.45	0.47	0.18	0.29
M16a	0.12	1.33	0.29	0.16	0.21
M16b	0.12	1.20	0.21	0.20	0.18

Table 3.9: Continued

Sample No.	MDI	MAI	DMAI-2	TMAI-2	Diamondoids (ppm)
M13a	0.23	0.29	0.25	0.29	1200.00
M13b	0.40	0.59	0.45	0.44	7700.89
M14a	0.33	0.52	0.42	0.40	6089.11
M14b	0.30	0.43	0.31	0.33	4222.67
M15a	0.40	0.59	0.43	0.42	6880.45
M15b	0.28	0.40	0.33	0.36	2800.23
M16a	0.31	0.47	0.39	0.41	3408.00
M16b	0.25	0.24	0.27	0.30	1700.71

Table 3.10: Continued

Sample No.	HOP/STER	GAM/H30	21/23TRI	TRIC/HOP	TET24/TR26	H28/H29
M13a	9.00	0.15	1.05	1.87	0.28	0.10
M13b	9.50	0.43	1.12	1.15	0.34	0.11
M14a	8.14	0.34	1.09	1.94	0.30	0.09
M14b	8.85	0.17	1.20	1.55	0.30	0.10
M15a	2.11	0.98	0.70	1.05	0.69	0.05
M15b	1.40	0.66	0.77	1.20	0.52	0.05
M16a	1.20	0.71	0.80	1.20	0.60	0.07
M16b	3.20	0.74	0.72	1.17	0.54	0.06

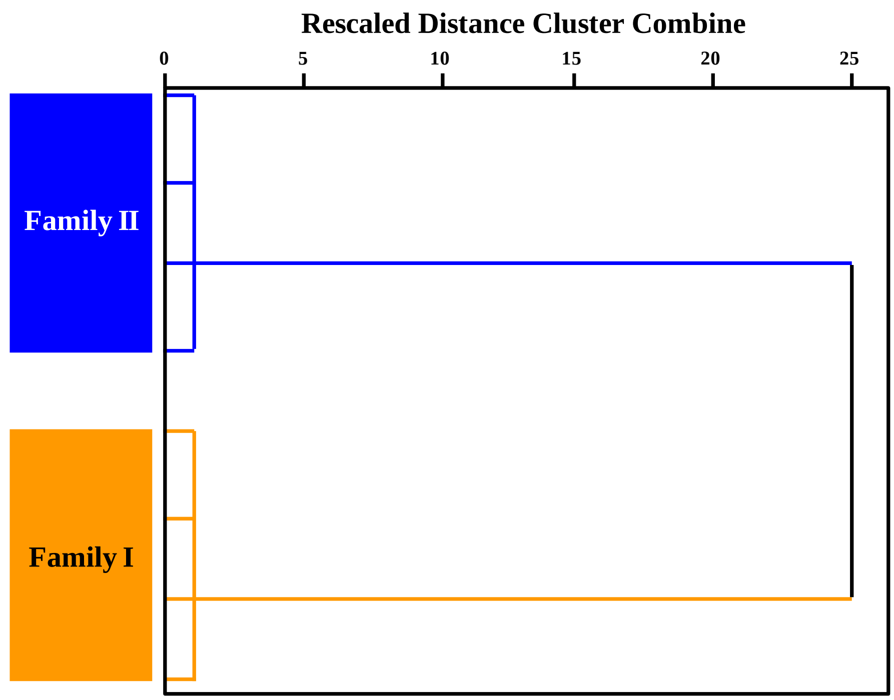

Fig. 3.6: Dendrogram from cluster analysis (Ward method) of the studied crude oils.

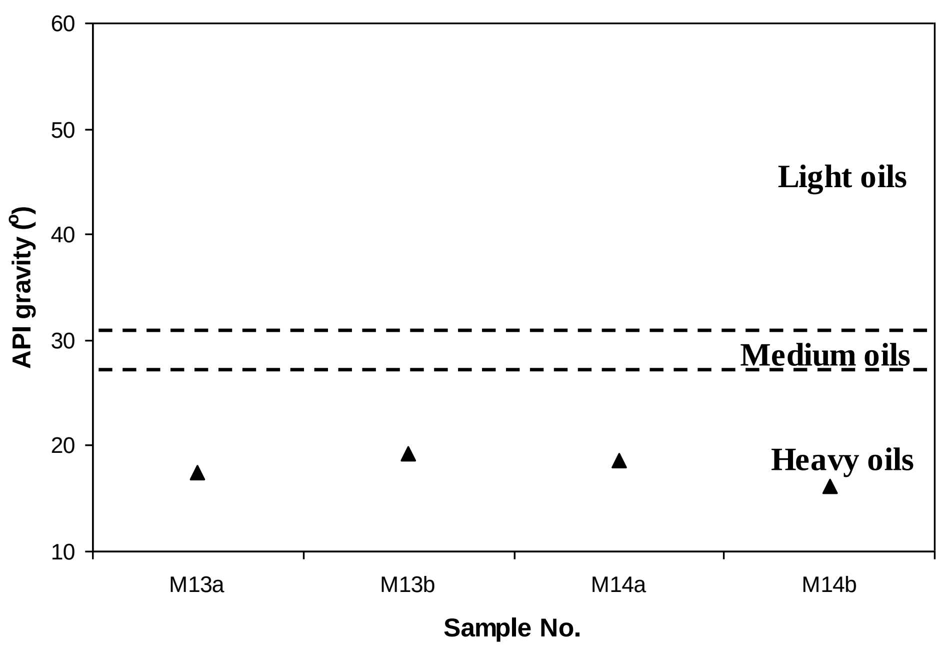

Fig. 3.7: API gravity values of the studied crude oil (Family I) (fields after Martinez et al., 1984).

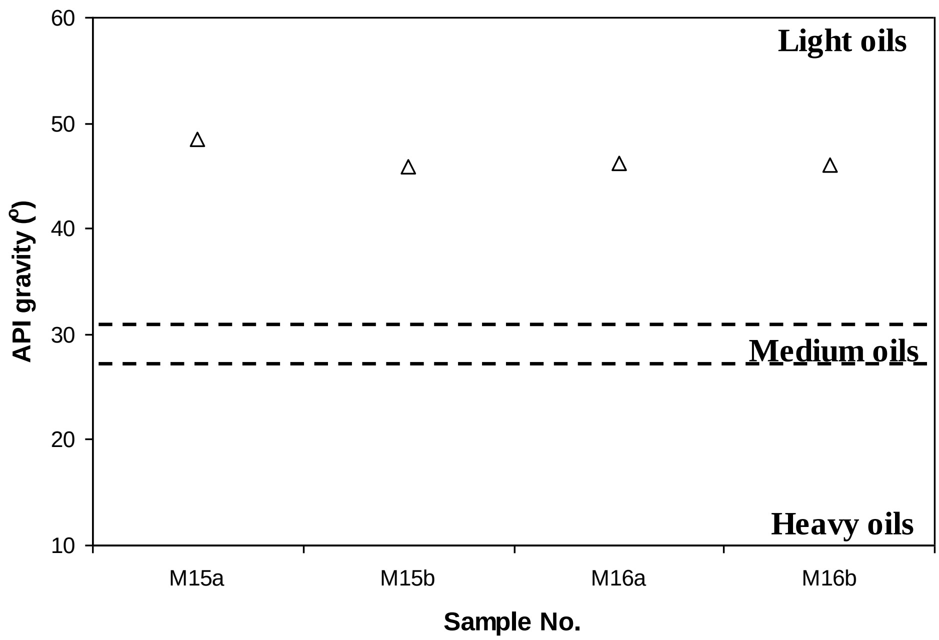

Fig. 3.8: API gravity values of the studied crude oil (Family II) (fields after Martinez et al., 1984).

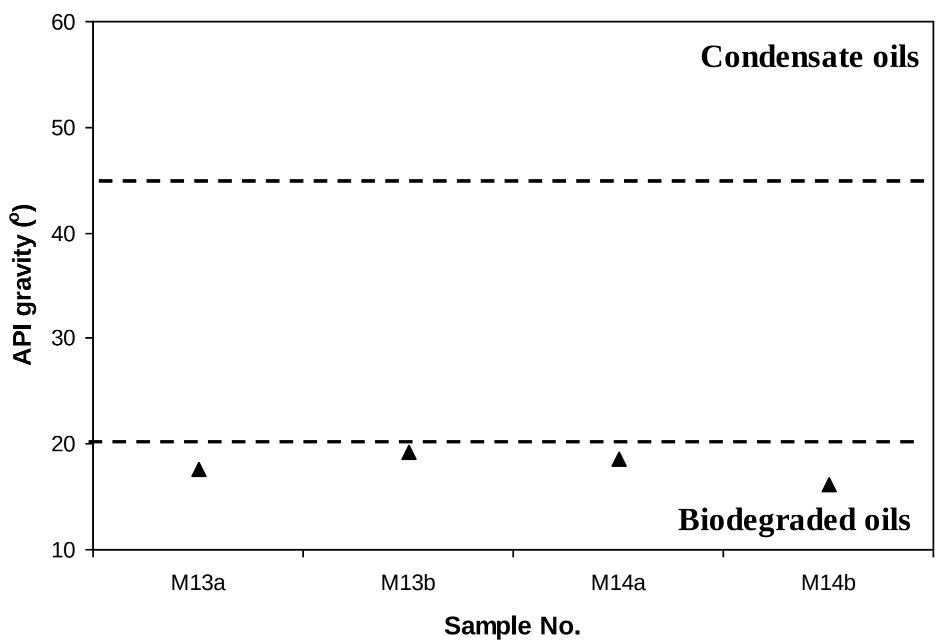

Fig. 3.9: API gravity values of the studied crude oil (Family I) (fields after Waples, 1985).

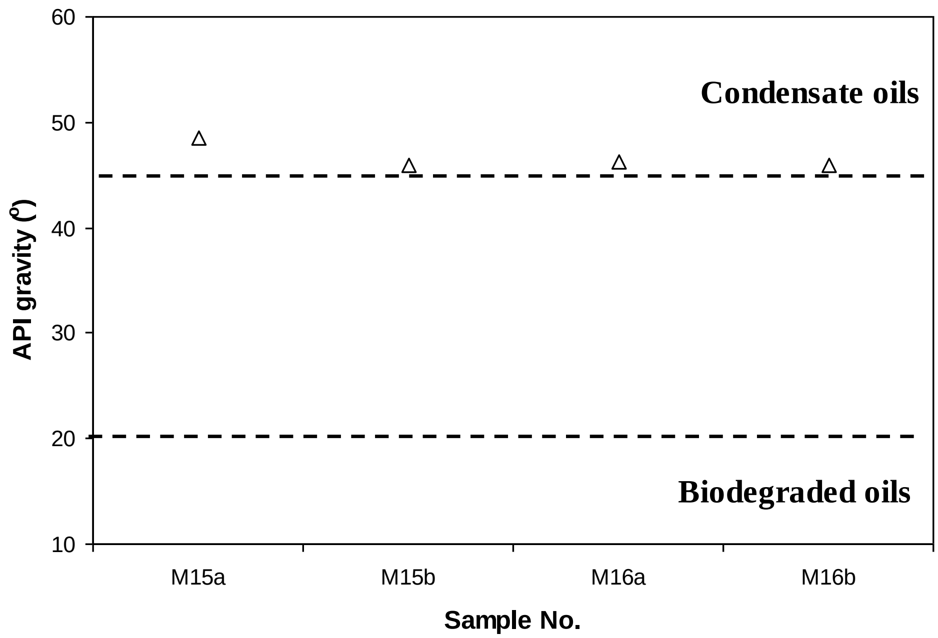

Fig. 3.10: API gravity values of the studied crude oil (Family II) (fields after Waples, 1985).

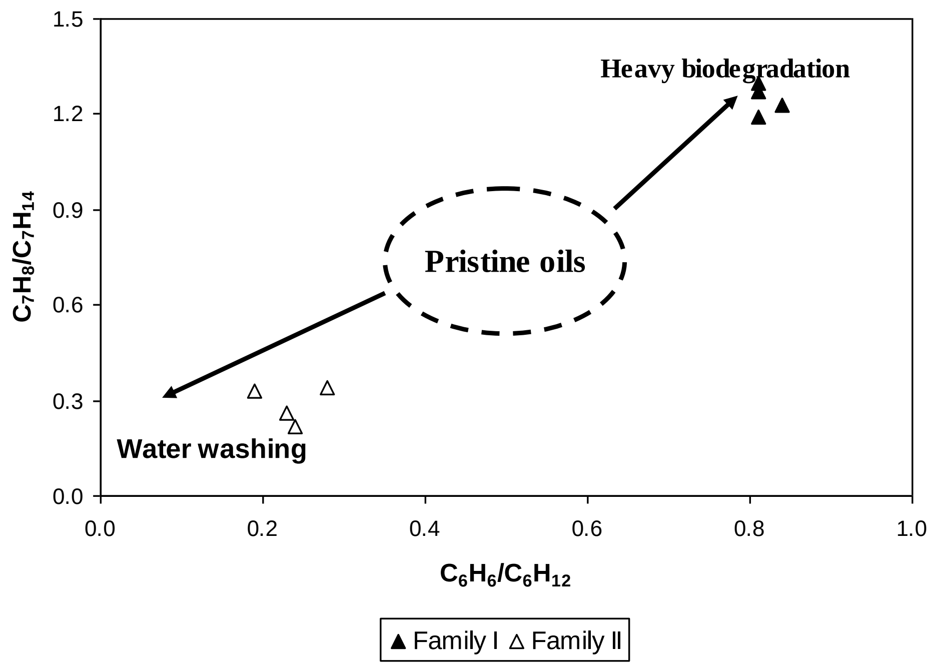

Fig. 3.11: Plot of C_6H_6/C_6H_{12} vs. C_7H_8/C_7H_{14} showing the oil-water interactions Family II oils (fields after Ziegs et al., 2018).

Source-related parameters were employed for the studied crude oil (Fig. 3.12). In general, the source-related parameters indicate that there is a significant difference in the distribution of biomarker ratios. Moreover, Family I oils display higher values of HOP/STER, 21/23TRI, TRIC/HOP, and H28/H29, and lower values of GAM/H30 and TET24/TR26 in comparison to Family II oils. In addition, the biomarker ratios suggest that the crude oils in the Makhbaz Reservoir inclusions have different source rocks.

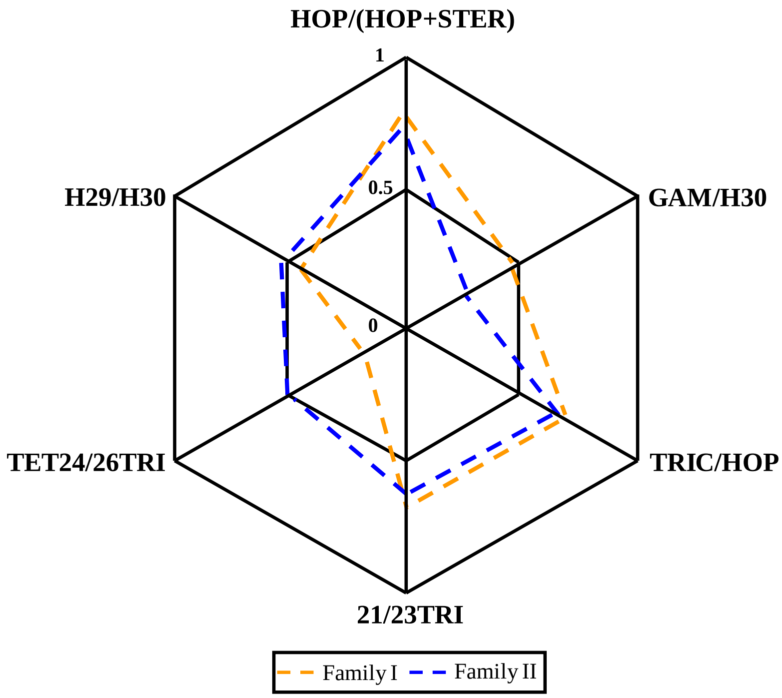

Fig. 3.12: Source-related parameters for the studied crude oil.

3.5. Oil-Source rock Correlation

There are many biomarker ratios that can be used to identify oil-source rock correlation such as Pr/Ph, C_{35}/C_{34} homohopanes, C_{31} 22R/H, C_{30} sterane index, $(C_{19}+C_{20})/(C_{23}+C_{24})$ TT, C_{24} TeT/C_{26} TT, $(C_{19}+C_{20})/C_{23}$ TT, C_{23}/C_{21} TT, C_{29} TT/C_{30} hopane, C_{28} TT/C_{30} hopane, C_{25} TT/C_{24} TeT, C_{24} TeT/(C_{24} TeT+C_{26} TT), C_{30} diahopane/C_{30} hopane and C_{29} diahopane/C_{29} hopane (Zumberge, 1987; Tuo *et al.*, 1999; Zhang and Huang, 2005 Hao *et al.*, 2009; Korkmaz *et al.*, 2013; Ziegs *et al.*, 2018). (Figs. 3.13-19) indicate that Family I oils were generated from the Makhbaz Shale, whereas Family II oils were derived from another source rock. Diamondoid patterns are also considered as an effective source or facies-related parameter according to Schulz *et al.*, (2001), who suggested that two parameters (DMDI =dimethyldiamantane index) based on dimethyldiamantanes are virtually unaffected by thermal maturation:

$$\text{DMDI-1} = (3,4\text{-DMD})/(3,4\text{-DMD} + 4,9\text{-DMD})$$
$$\text{DMDI-2} = (4,8\text{-DMD})/(4,8\text{-DMD} + 4,9\text{-DMD})$$

The binary plot of DMDI-1 versus DMDI-2 (Fig. 3.20) enables the distinction of Family I oils as derived from clay-rich source rock (Makhbaz Shale), in contrast to Family II oils which are generated from carbonate-rich source rock. According to Hallett and Clark-Lowes (2016) the Bilal Formation (Early Eocene carbonates) is one of the main source rocks in the Sabratah Basin. Consequently, the author believes that Family II oils were probably derived from the Bilal Formation.

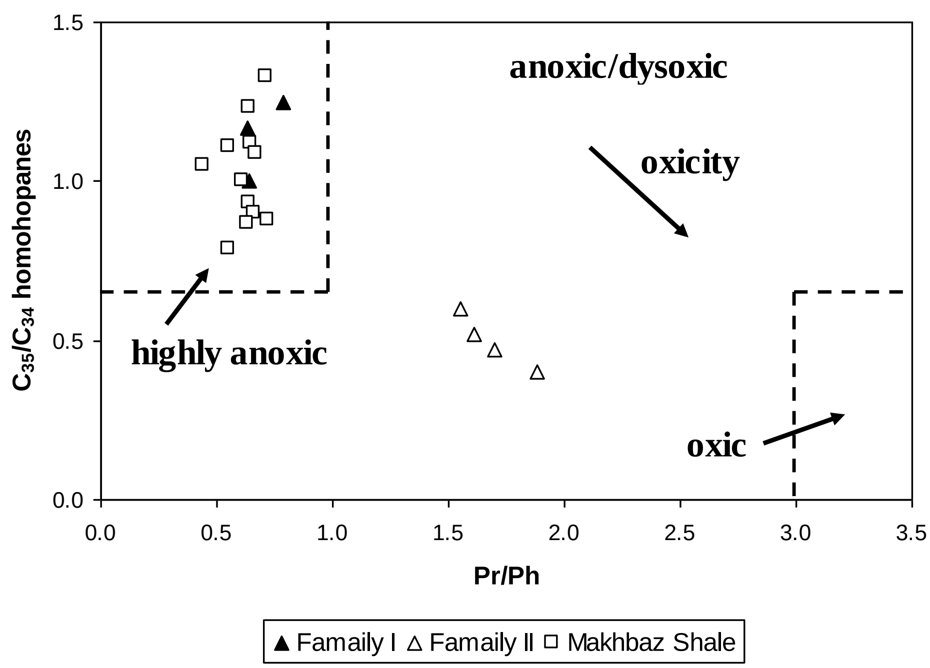

Fig. 3.13: Plot of C_{31} 22R/H vs. C_{30} sterane index showing the source rock for the studied crude oil (fields after Ziegs et al., 2018).

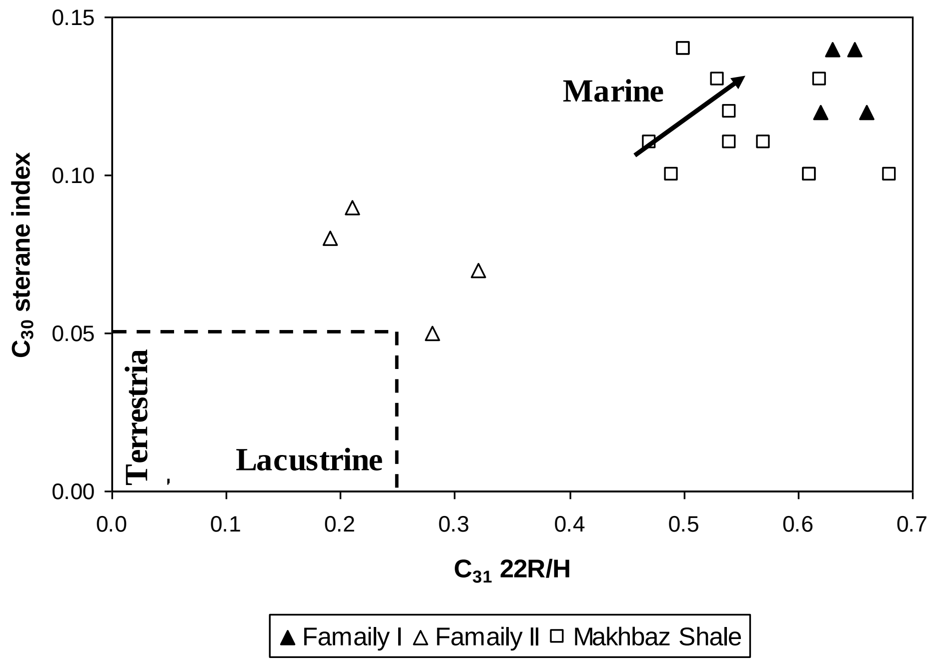

Fig. 3.14: Plot of C_{31} 22R/H vs. C_{30} sterane index showing the source rock for the studied crude oil (fields after Ziegs et al., 2018).

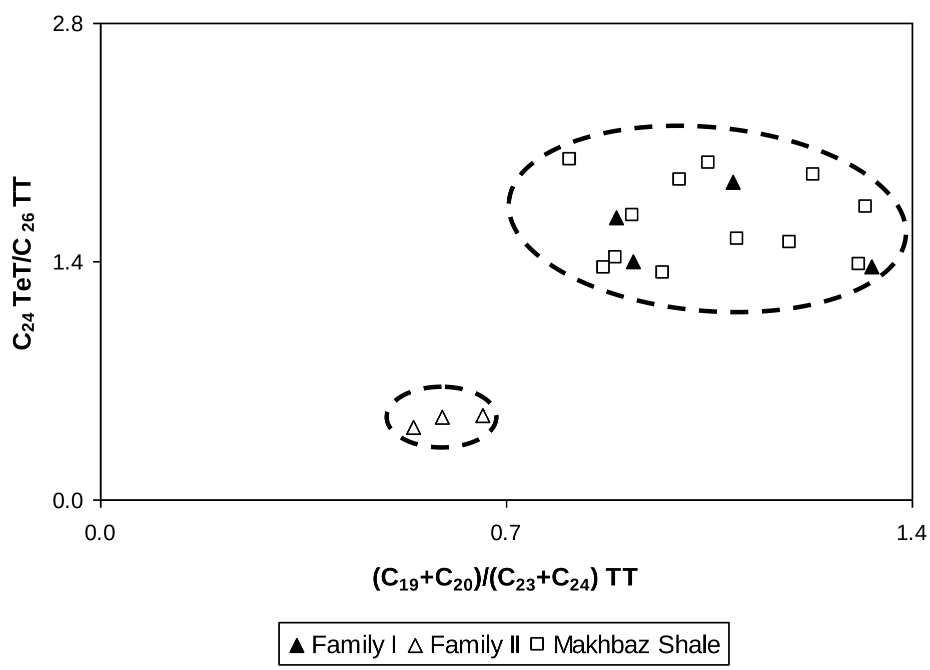

Fig. 3.15: Plot of $(C_{19}+C_{20})/(C_{23}+C_{24})$ TT vs. C_{24} TeT/C_{26} TT showing the source rock for the studied crude oil.

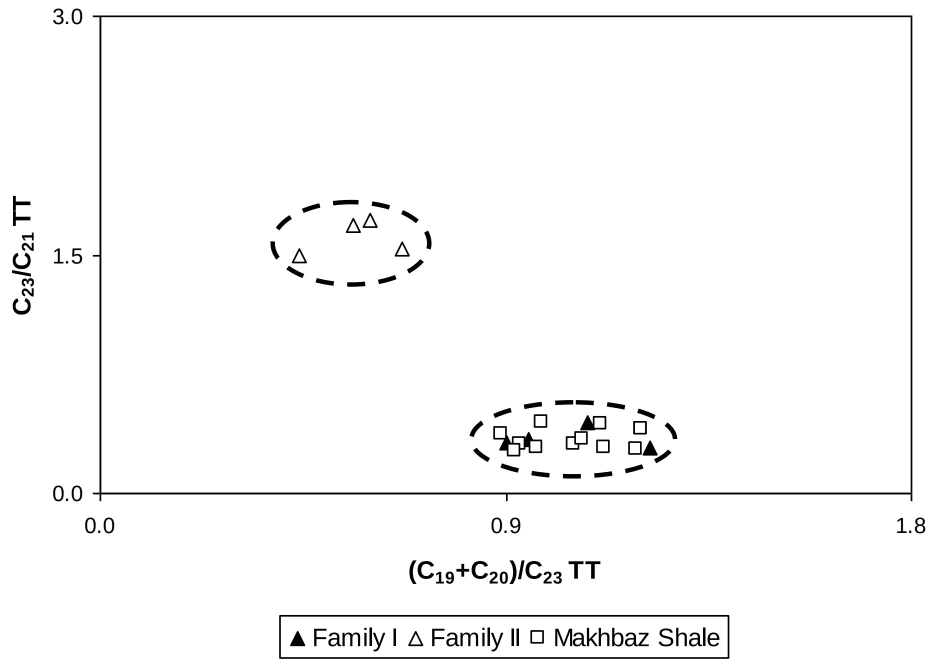

Fig. 3.16: Plot of $(C_{19}+C_{20})/C_{23}$ TT vs. C_{23}/C_{21} TT showing the source rock for the studied crude oil.

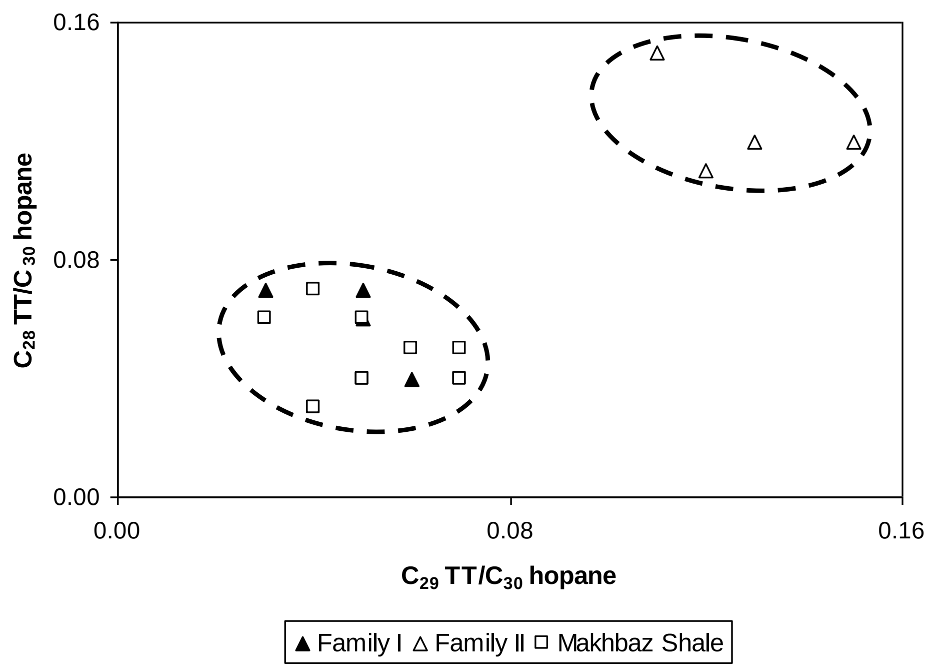

Fig. 3.17: Plot of C_{29} TT/C_{30} hopane vs. C_{28} TT/C_{30} hopane showing the source rock for the studied crude oil.

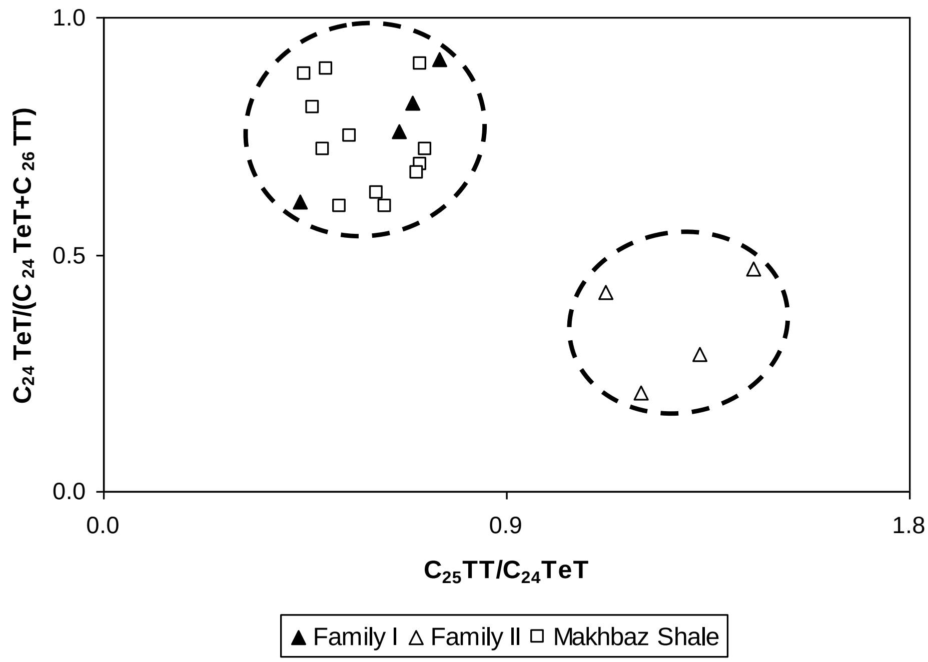

Fig. 3.18: Plot of C_{25} TT/C_{24} TeT vs. C_{24} TeT/(C_{24} TeT+C_{26} TT) showing the source rock for the studied crude oil.

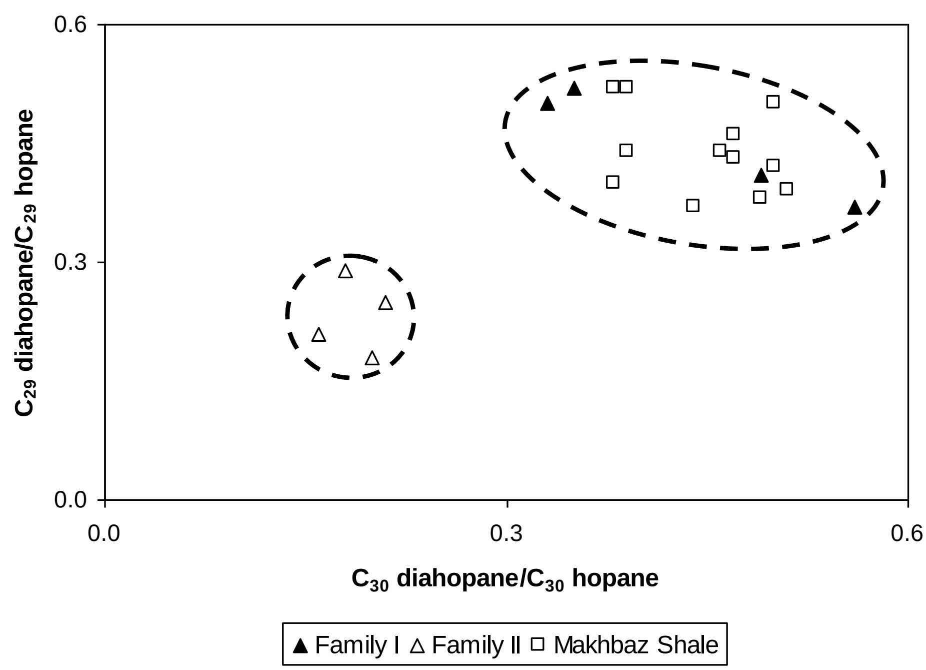

Fig. 3.19: Plot of C_{30} diahopane/C_{30} hopane vs. C_{29} diahopane/C_{29} hopane showing the source rock for the studied crude oil.

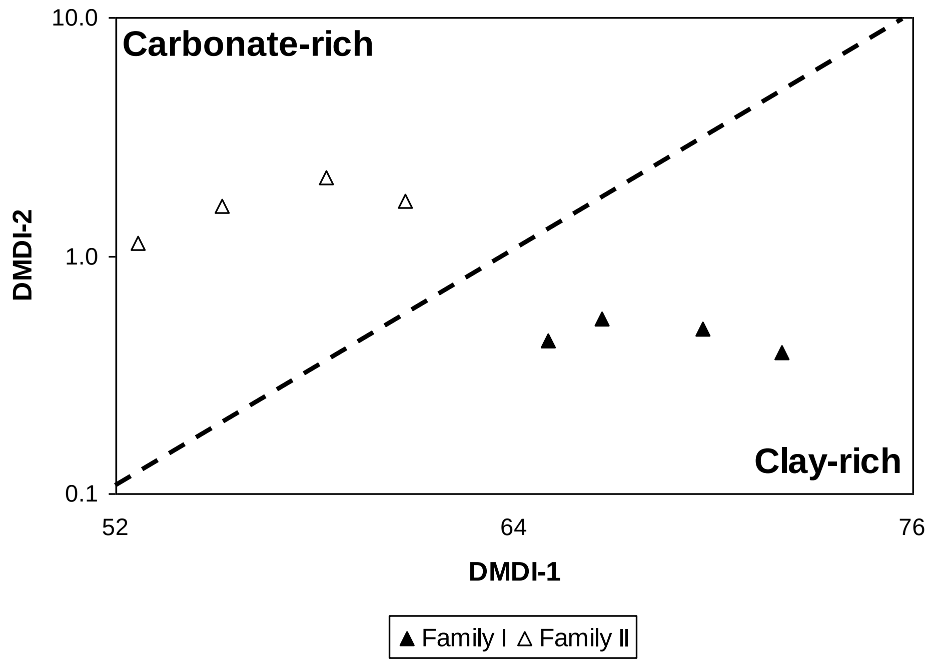

Fig. 3.20: Plot of DMDI-1 vs. DMDI-2 showing the source rock lithology for the studied crude oil (fields after Aldahik et al., 2017).

3.6. Thermal Maturity

Diamondoid-based indices have been widely utilized to determine the thermal maturity of highly mature source rocks and crude oils (Chen *et al.*, 1996; Li *et al.*, 2000; Zhang *et al.*, 2005; Jiang *et al.*, 2019), to estimate the extent of oil cracking (Dahl *et al.*, 1999), and to evaluate biodegradation (Grice *et al.*, 2000; Zhang *et al.*, 2005; Jiang *et al.*, 2019).

In the current study, the thermal maturity of the studied crude oil was assessed using several models such as the ternary plot of SARA and the binary plots of Ts/(Ts+Tm) versus 29Ts/(29Ts+30NH), C_{29} steranes:ßß/(αα+ßß) versus C_{29} steranes:20S/(20S+20R), MDI versus MAI, DMAI-2 versus TMAI-2, MDI versus total diamondoids and DMAI-2 versus total diamondoids (Fig. 3.21-27). All oil families fall in the field of mature. Moreover, the diamondoid indices are mutually correlated, reflecting high mature oil.

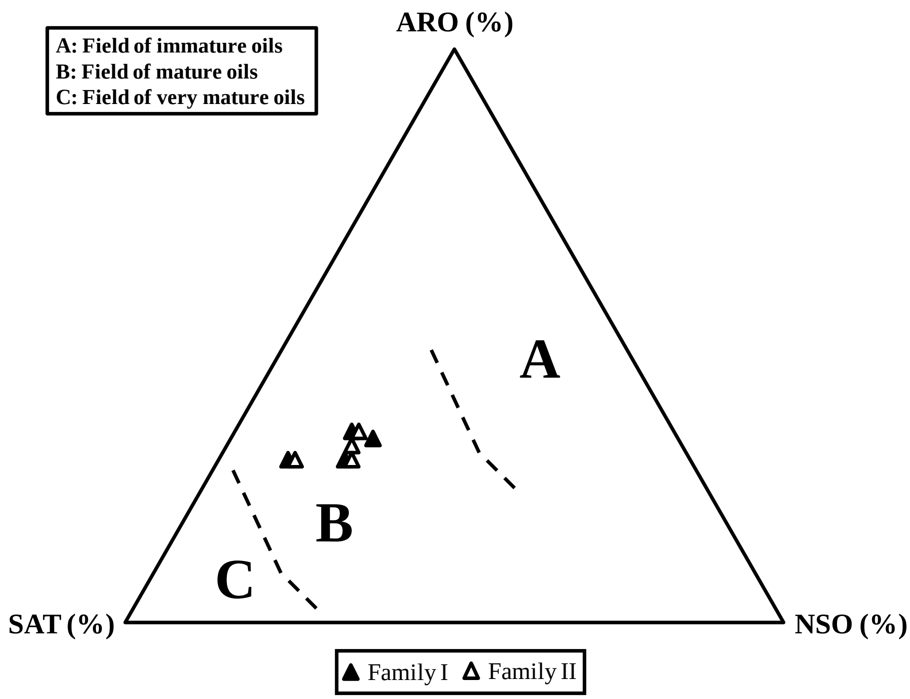

Fig. 3.21: Ternary plot of SARA showing the maturity for the studied crude oil (fields after Peters et al., 2005).

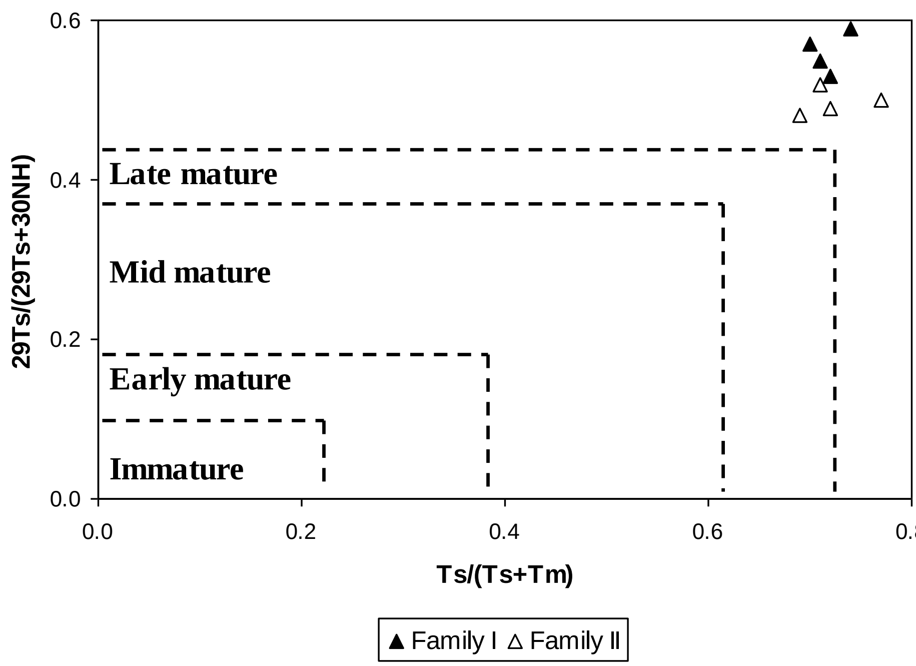

Fig. 3.22: Plot of Ts/(Ts+Tm) vs. 29Ts/(29Ts+30NH) showing the maturity for the studied crude oil (fields after Peters et al., 2005).

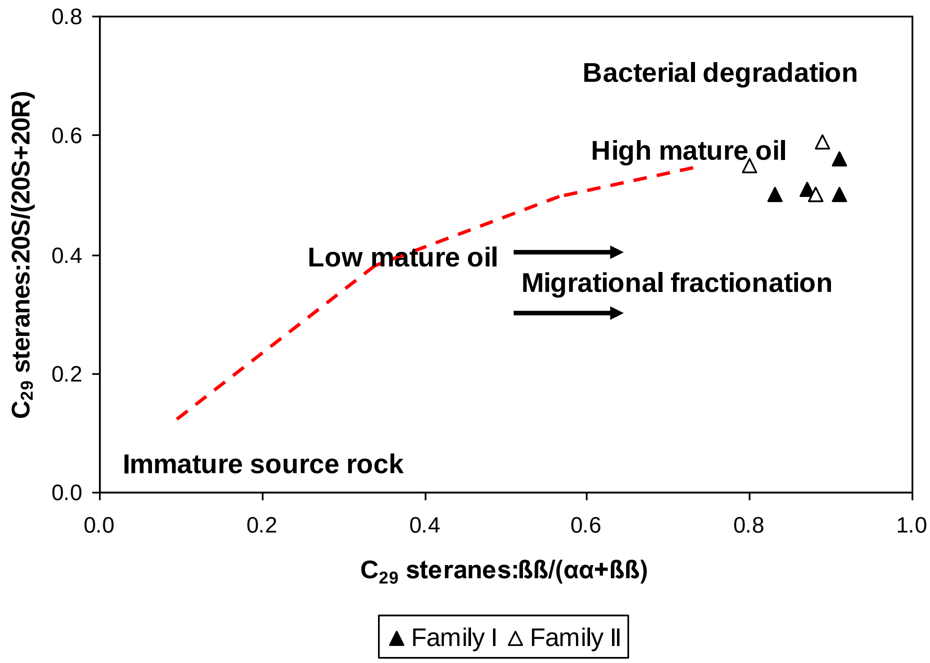

Fig. 3.23: Plot of C_{29} steranes:ßß/(αα+ββ) vs. C_{29} steranes:20S/(20S+20R) showing the maturity for the studied crude oil (fields after Waples and Machihara, 1990).

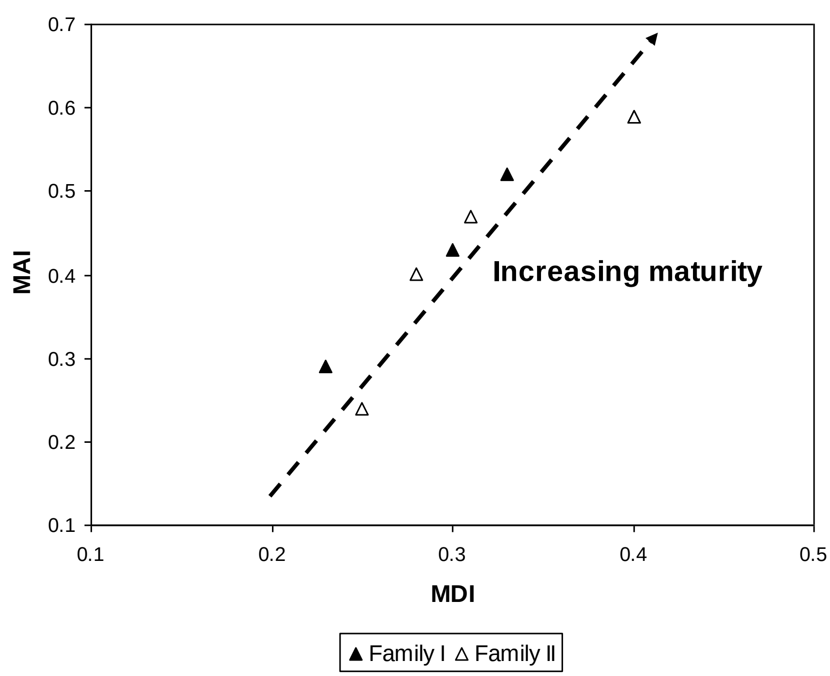

Fig. 3.24: Plot of MDI vs. MAI showing the maturity for the studied crude oil.

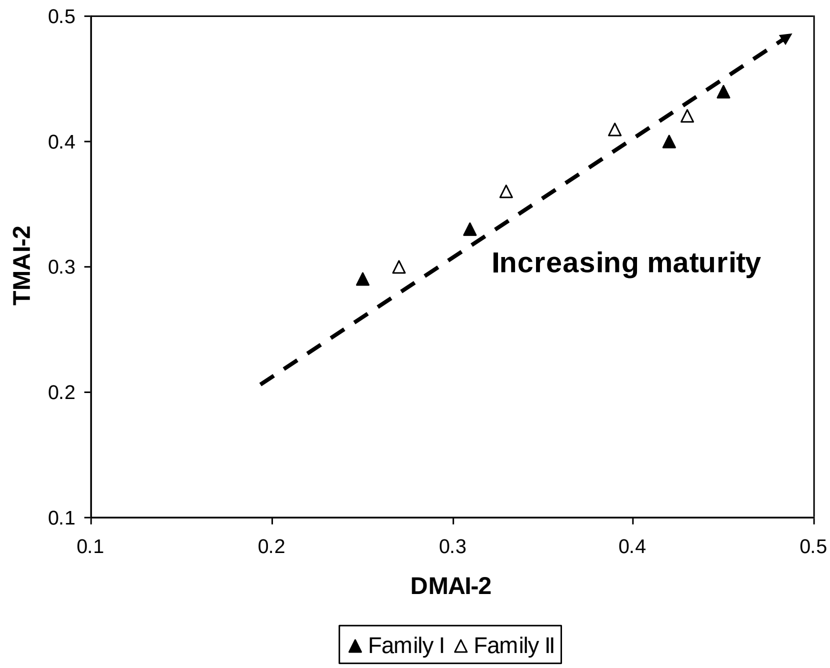

Fig. 3.25: Plot of DMAI-2 vs. TMAI-2 showing the maturity for the studied crude oil.

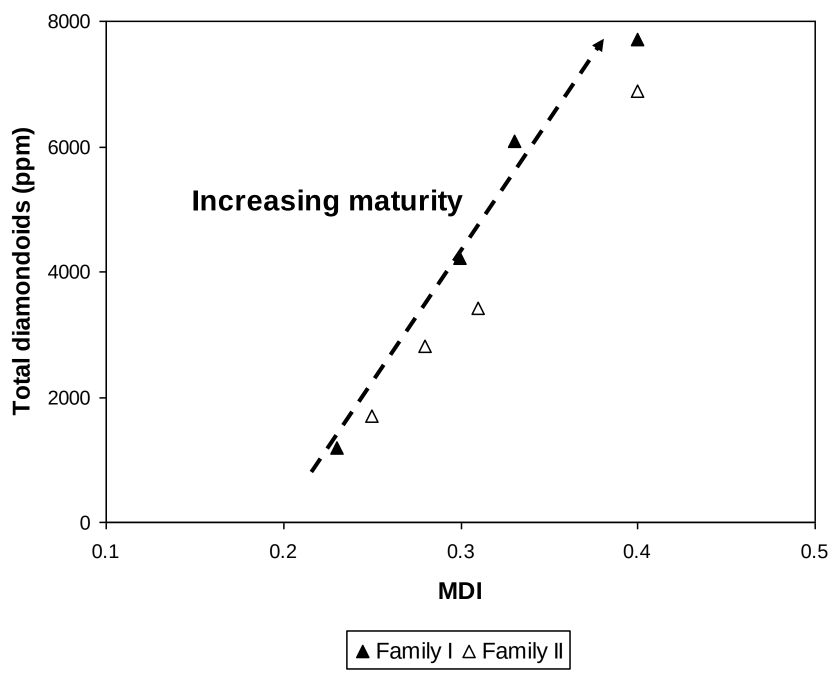

Fig. 3.26: Plot of MDI vs. total diamondoids showing the maturity for the studied crude oil.

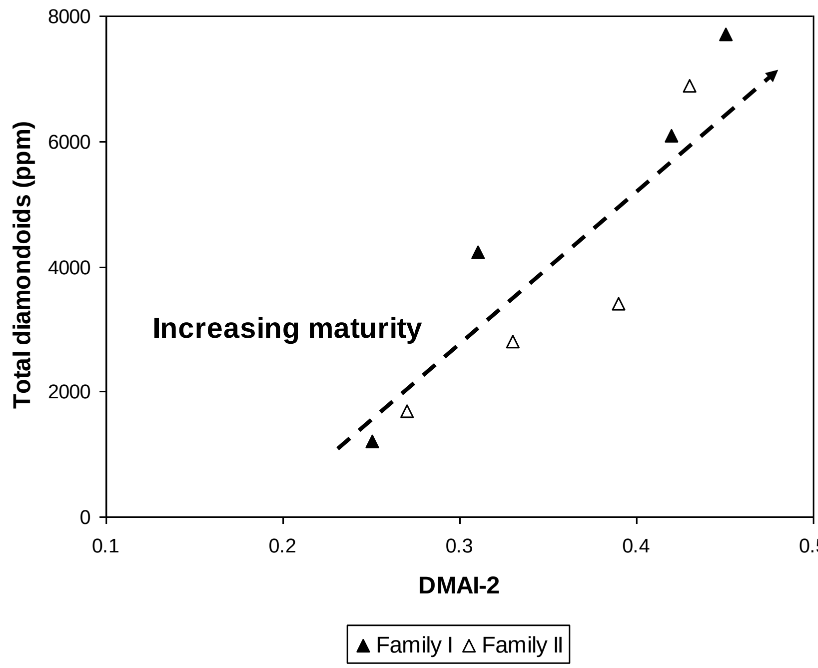

Fig. 3.27: Plot of DMAI-2 vs. total diamondoids showing the maturity for the studied crude oil.

3.7. Charging Episodes

Hydrocarbon charging processes are one focus of research on hydrocarbon formation and distribution (Jiang *et al.*, 2000; Xu *et al.*, 2017). Many authors (e.g., Xu *et al.*, 2017) used the peak wavelength (λ_{max}) and the micro-beam fluorescence spectra parameters ($Q_{650/500}$ and Q_{F535}) to determine the charging episodes of hydrocarbons. Q_{F535} is defined as the area ratio between the area of wavelengths within 720-535nm and the area of wavelengths within 535-420nm (Si *et al.*, 2013). $Q_{650/500}$ is defined as the fluorescence intensity ratio between the fluorescence intensity of a wavelength of 650nm (I_{650}) and the fluorescence intensity of a wavelength of 500nm (I_{500}) (Li *et al.*, 2010). In the present study, the CIE color chart (Fig. 3.28) and the binary plots of $Q_{650/500}$ versus λ_{max} and Q_{F535}versus λ_{max} (Figs. 3.29-30) suggest that at least two episodes of oil charging took place in the Makhbaz Reservoir.

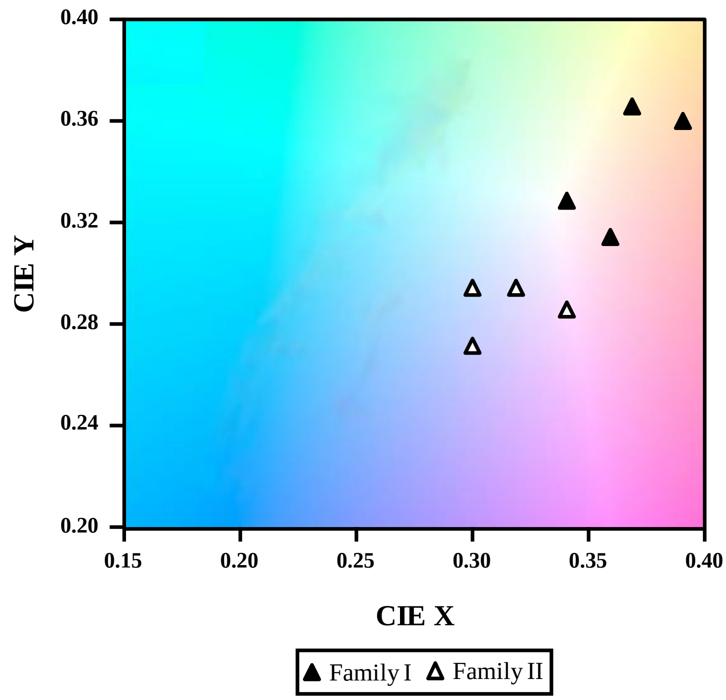

Fig. 3.28: CIE color chart for the studied crude oil.

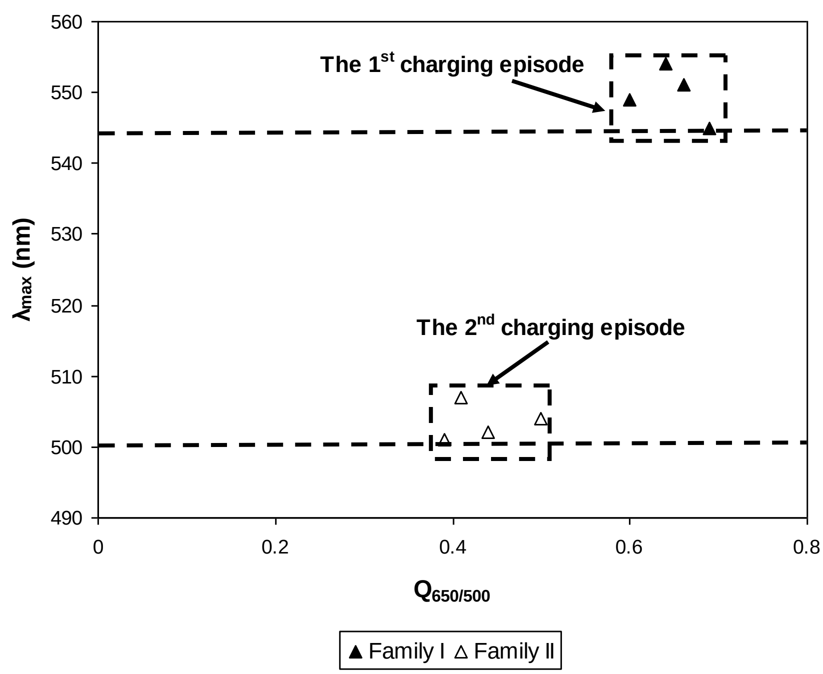

Fig. 3.29: Plot of $Q_{650/500}$ vs. λ_{max} showing the charging episodes for the Makhbaz Reservoir.

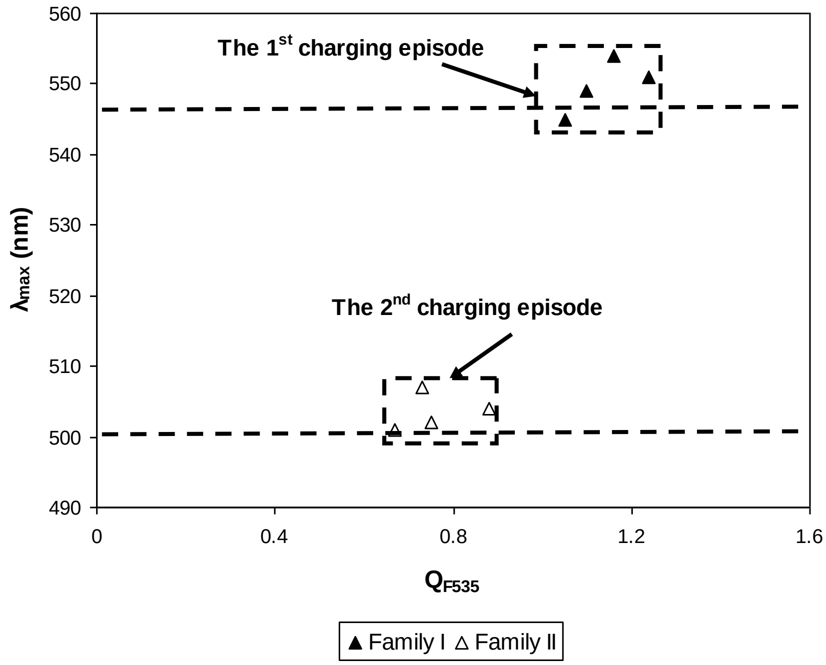

Fig. 3.30: Plot of $Q_{650/500}$ vs. λ_{max} showing the charging episodes for the Makhbaz Reservoir.

CHAPTER FOUR

CONCLUSIONS

The current work is an organic geochemical assessment of source rock and reservoir. The Makhbaz Formation in the offshore well K-137 in the Sabratah Basin was selected as a case study. To achieve this assessment, several techniques were used such as petrographic analysis, scanning electron microscope (SEM), LECO analysis, Rock-Eval pyrolysis, gas chromatography-mass spectrometry (GC-MS) and fluorescence spectrophotometry. The conclusions of this work are as follows:

1) The Makhbaz Shale (source rock) has an excellent quality. It is a potential source rock.

2) There is a slight difference in the organic parameter values (except for HI and OI), indicating the homogeneity of the organic chemical composition of the Makhbaz Shale.

3) Mature organic matter of type II kerogen is dominant in the Makhbaz Shale.

4) C_1 is the main gas in the petroleum inclusions of the Makhbaz Limestone (reservoir).

5) The petroleum inclusions of the Makhbaz Limestone contain two oil families.

6) Family I oils are heavy oils (biodegraded oils) derived from the Makhbaz Shale while Family II oils are of light oils (condensate oils) probably generated from the Bilal Formation.

7) The oil families are thermally mature.

8) At least two episodes of oil charging took place in the Makhbaz Limestone.

9) The Makhbaz Formation was deposited in a medium-saline marine environment.

REFERENCES

Abarghani, A., Ostadhassan, M., Gentzis, T., Carvajal-Ortiz, H. and Bubach, B. (2018): Organofacies study of the Bakken source rock in North Dakota, USA, based on organic petrology and geochemistry. International Journal of Coal Geology; 188: 79-93.

Ahmed, M., Lehnert, O., Fuentes, D. and Meinhold, G. (2014): Origin of oil and bitumen in the Late Devonian Siljan impact structure, central Sweden. Organic Geochemistry; 68: 13-26.

Akinlua, A., Ajayi, T.R. and Adeleke, B.B. (2007): Organic and inorganic geochemistry of northwestern Niger Delta oils. Geochemical Journal; 41: 271-281.

Aldahik, A., Schulz, H.M., Horsfield, B., Wilkes, H., Dominik, W. and Nederlof, P. (2017): Crude oil families in the Euphrates Graben (Syria). Marine and Petroleum Geology; 86: 325-342.

Anketell, J.M. and Mriheel, I.Y. (2000): Depositional environment and diagenesis of the Eocene Jdeir Formation, Gabes-Tripoli Basin, western offshore, Libya. Journal of Petroleum Geology; 23: 425-447.

Arouri, K.R., Al-Saleh, S.H. and Al-Hilal, Z.M. (2009): Residual oil as a tool in migration and filling history analysis of petroleum reservoirs, Ghazal Field, Saudi Arabia. Organic Geochemistry; 40(5): 617-627.

Asomaning, J., Mussone, P. and Bressler, D.C. (2014): Thermal cracking of free fatty acids in inert and light hydrocarbon gas atmospheres. Fuel; 126: 250-255.

Atta-Peters, D. and Garrey, P. (2014): Source rock evaluation and hydrocarbon potential in the Tano basin, South Western Ghana, West Africa. International Journal of Oil, Gas and Coal Engineering; 2(5): 66-77.

Aviles, M.A., Ardakani, O.H., Cheadle, B.A. and Sanei, H. (2019): Organic petrography and geochemical characterization of the Upper Cretaceous Second White Specks and Upper Belle Fourche alloformations, west-central Alberta: Analysis of local maturity anomalies. International Journal of Coal Geology; 203: 60-73.

Baba, M., Parnell, J., Muirhead, D. and Bowden, S. (2019): Oil charge and biodegradation history in an exhumed fractured reservoir, Devonian, UK. Marine and Petroleum Geology; 101: 281-289.

Bailey, H.W., Dungworth, G., Hardy, M., Scull, D. and Vaughan, R.D. (1989): A fresh approach to the Metlaoui. Actes des IIeme journees de geologie tunisienne appliquee a la recherche des hydrocarbures. Mem. ETAP, No. 3, Tunis; pp. 281-307.

Balbinot, M. and Kalkreuth, W. (2010): Organic geochemistry and petrology of the Gomo Member, Recôncavo Basin, Brazil. International Journal of Coal Geology; 84(3-4): 286-292.

Baydjanova, S. and George, S.C. (2019): Depositional environment, organic matter sources, and variable 17α(H)-diahopane distribution in Early Permian samples, southern Sydney Basin, Australia. Organic Geochemistry; 131: 60-75.

Bennett, B., Larter, S., Carbognani, L. and Pereira-Almao, P. (2008): Identification and characterization of reaction proxies for monitoring the progress of thermal processing of heavy oils and tar sands under vis-breaking conditions. Energy and Fuels; 22(1): 440-448.

Bishop, W.F. (1988): Petroleum Geology of east-central Tunisia. Bulletin-AAPG; 72: 1033-1058.

Bishop, W.F. and Debono, G. (1996): The hydrocarbon geology of southern offshore Malta. Journal of Petroelum Geology; 19: 129-160.

Burruss, R.C. (1981): Hydrocarbon fluid inclusions in studies of sedimentary diagenesis. In: Hollister, L.S., Crawford, M.L. (Eds.), Fluid Inclusions: Applications to Petrology; pp. 138-156.

Chen, J.H, Fu, J.M., Sheng, G.Y., Liu, D.H. and Zhang, J.J. (1996): Diamondoid hydrocarbon ratios: novel maturity indices for highly mature crude oils. Organic Geochemistry; 25: 179-190.

Chinn, E.W. (1991): The role of organic geochemistry in petroleum exploration: Basin Research Institute Bulletin, Louisiana State University, Baton Rouge, LA; pp. 15-23.

Claypool, G.E. and Kvenvolden, K.A. (1983): Methane and other hydrocarbon gases in marine sediment. Annual Review of Earth and Planetary Sciences; 11: 299-327.

Curtis, J.B., Kotarba, M.J., Lewan, M.D. and Wieclaw, D. (2004): Oil/source rock correlations in the Polish Flysch Carpathians and Mesozoic basement and organic facies of the Oligocene Menilite Shales: insights from hydrous pyrolysis experiments. Organic Geochemistry; 35(11-12): 1573-1596.

Dahl, J.E., Moldowan, J.M., Peters, K., Claypool, G., Rooney, M., Michael, G., Mello, M. and Kohnen, M. (1999): Diamondoid hydrocarbons as indicators of oil cracking. Nature; 399: 54-56.

Dembicki, H.J. (2009): Three common source rock evaluation errors made by geologists during prospect or play appraisals. AAPG Bulletin; 93(3): 341-356.

Dutta, S., Hartkopf-Froder, C., Witte, K., Brocke, R. and Mann, U. (2013): Molecular characterization of fossil palynomorphs by transmission micro-FTIR spectroscopy: Implications for hydrocarbon source evaluation. International Journal of Coal Geology; 115: 13-23.

El Diasty, W.S. and Moldowan, J.M. (2012): Application of biological markers in the recognition of the geochemical characteristics of some crude oils from Abu Gharadig Basin, north Western Desert–Egypt. Marine and Petroleum Geology; 35:28-40.

El-Ghoul, A. (1991): A modified Farwah Group type section and its application to understanding stratigraphy and sedimentation along an E-W section through NC 35A, Sabratah Basin. Third Symposium on the Geology of Libya. vol. 4. (eds. M.J. Salem, O.S. Hammuda and B.A. Eliagoubi), Elsevier, Amsterdam; pp. 1637–1656.

El-Kammar, M.M., Hussein, F.S. and Sherwani, G.H. (2015): Organic petrological and geochemical evaluation of Jurassic source rocks from north Iraq. Asian Review of Environmental and Earth Sciences; 2(1): 1-8.

El Nady, M.M., Hussein, S.A., Sharaf, L.M. and Ghanem, M.F. (2016): Quantity, thermal maturity of organic matter and relation to prospective source rock horizons in Tut-1x well, North Western Desert, Egypt. Energy Sources, Part A: Recovery, Utilization, and Environmental Effects; 38(21): 3187-3194.

Finetti, I. (1982): Structure, stratigraphy and evolution of central Mediterranean. Bollettino di Geofisica Teorica e Applicata; 24: 247-312.

Fornaciari, M. (2007): Petroleum geology in the NC 41 area (Western Libyan offshore). 3rd EAGE North African/Mediterranean Petroleum and Geosciences Conference and Exhibition, Tripoli extended abstract.

George, S.C., Volk, H. and Ahmed, M. (2007): Geochemical analysis techniques and geological applications of oil-bearing fluid inclusions, with some Australian case studies. Journal of Petroleum Science and Engineering; 57: 119-138.

Ghori, K.A.R. (2002): Modeling the hydrocarbon generative history of the Officer Basin, Western Australia. Journal of Philosophy of Education Society of Australasia (PESA); 29: 29-42.

Grice, K., Alexander, R. and Kagi, R.I. (2000): Diamondoid hydrocarbon ratios as indicators of biodegradation in Australian crude oils. Organic Geochemistry; 31: 67-73.

Grotheer, H., Greenwood, P.F., McCulloch, M.T., Bottcher, M.E. and Grice, K. (2019): $\delta^{34}S$ character of organosulfur compounds in kerogen and bitumen fractions of sedimentary rocks. Organic Geochemistry; 110: 60-64.

Hall, L.S., Boreham, C.J., Edwards, D.S., Palu, T.J., Buckler, T., Hill, A.J. and Troup, A. (2016): Cooper Basin source rock geochemistry: Regional hydrocarbon prospectivity of the Cooper Basin. Geoscience Australia, Part2; 62p.

Hallett, D. (2002): Petroleum geology of Libya. Amsterdam, Elsevier Inc., 503p.

Hallett, D. and Clark-Lowes, D. (2016): Petroleum geology of Libya. 2nd edition, Amsterdam, Elsevier Inc., 404p.

Hammuda, O.S., Sbeta, A.M., Mouzughi, A.J. and Eliagoubi, B.A. (1985): Stratigraphic nomenclature of the northwestern offshore of Libya. Earth Sciences Society of Libya, 166p.

Hao, F., Zhou, X., Zhu, Y. and Yang, Y. (2009): Mechanisms for oil depletion and enrichment on the Shijiutuo uplift, Bohai Bay Basin, China. AAPG Bulletin; 93: 1015-1037.

Haq, B.U., Hardenbol, J. and Vail, P.R. (1988): Mesozoic and Cenozoic chronostratigraphy and eustatic cycles. SEPM Special Publication vol. 42. (eds. C.K.

Wilgus, H. Posamentier, C.K. Ross, C.G.S. Kendall), Sea-Level Changes: An Integrated Approach, pp. 71-108.

Hartkopf-Froder, C., Konigshof, P., Littke, R. and Schwarzbauer, J. (2015): Optical thermal maturity parameters and organic geochemical alteration at low grade diagenesis to anchimetamorphism: a review. International Journal of Coal Geology; 150-151: 74-119.

Hassan, H.H. and Kendall, C. (2014): Hydrocarbon provinces of Libya: A petroleum system study. (eds. L. Marlow, C. Kendall, L. Yose), Petroleum Systems of the Tethyan Region. American Association of Petroleum Geologists, Tulsa, pp. 101-141 Memoir No. 106.

Holba, A.G., Dzoub, L.I., Wood, G.D., Ellisd, L., Adame, P., Schaeffere, P., Albrechte, P., Greenef, T. and Hughes, W.B. (2003): Application of tetracyclic polyprenoids as indicators of input from fresh-brackish water environments. Organic Geochemistry; 34: 441-469.

Huang, W.Y. and Meinschein, W.G. (1979): Sterols as ecological indicators. Geochimica et Cosmochimica Acta; 43: 739-745.

Hunt, J.M. (1996): Petroleum geochemistry and geology, 2nd edition, vol. 743. New York: Freeman and Company.

Jiang, W., Li, Y. and Xiong, Y. (2019): Source and thermal maturity of crude oils in the Junggar Basin in northwest China determined from the concentration and distribution of diamondoids. Organic Geochemistry; 128: 148-160.

Jiang, Z.X., Pang, X.Q. and Huang, Z.L. (2000): Oil and gas migration periods and accumulation process in Shanshan Oil Field of Turpan-Hami Basin. Journal of the University of Petroleum (China); 34(1): 1-11.

Korkmaz, S., Kara-Gulbay, R. and Iztan, Y.H. (2013): Organic geochemistry of the Lower Cretaceous black shales and oil seep in the Sinop Basin, Northern Turkey: An oil-source rock correlation study. Marine and Petroleum Geology; 43: 272-283.

Kruge, M.A., Mastalerz, M., Solecki, A. and Stankiewicz, B.A. (1996): Organic geochemistry and petrology of oil source rocks, Carpathian Overthrust region, southeastern Poland—implications for petroleum generation. Organic Geochemistry; 24(8-9): 897-912.

Larter, S., Adams, J., Gates, I. D., Bennett, B. and Huang, H. (2008): The origin, prediction and impact of oil viscosity heterogeneity on the production characteristics of tar sand and heavy oil reservoirs. Journal of Canadian Petroleum Technology; 47(1): 52-61.

Larter, S.R., Aplin, A.C., Corbett, P.W.M., Ementon, N., Chen, M. and Taylor, P.N. (1997): Reservoir geochemistry: A link between reservoir geology and engineering? SPE Reservoir Engineering; 12(1):12-17.

Larter, S., Jiang, C., Snowdon, L., Bennett, B., Oldenburg, T., Huang, H., Gates, I. and Adams, J. (2010): Some Future Directions in Reservoir Fluid Geochemistry. AAPG Hedberg Conference (Applications of Reservoir Fluid Geochemistry); pp.1-5.

Lewan, M.D. and Roy, S. (2011): Role of water in hydrocarbon generation from Type-I kerogen in Mahogany oil shale of the Green River Formation. Organic Geochemistry; 42(1): 31-41.

Li, C.Q., Chen, H.H. and Liu, H.M. (2010): Identification of hydrocarbon charging events by using micro-beam fluorescence spectra of petroleum inclusion. Earth Science-Journal of China University of Geosciences; 35(4): 657-662.

Li, J.G., Philp, P. and Cui, M.Z. (2000): Methyl diamantane index (MDI) as a maturity parameter for Lower Palaeozoic carbonate rocks at high maturity and overmaturity. Organic Geochemistry; 31: 267-272.

Li, M., Liu, X., Wang, T.G., Jiang, W., Fang, R., Yang, L. and Tang, Y. (2018): Fractionation of dibenzofurans during subsurface petroleum migration: Based on molecular dynamics simulation and reservoir geochemistry. Organic Geochemistry; 115: 220-232.

Liu, K., George, S.C., Lu, X., Gong, S., Tian, H. and Gui, L. (2014): Innovative fluorescence spectroscopic techniques for rapidly characterising oil inclusions. Organic Geochemistry; 72: 34-45.

Liu, Y., Hu, K., Cao, J., Yang, S., Bian, L., Wang, L. and Chen, Y. (2008): Organic biofacies of Jurassic source rocks in northern Qaidam Basin, NW China. Petroleum Exploration and Development; 35(3): 281-288.

Longbottom, T.L., Hockaday, W.C., Boling, K.S., Li, G., Letourmy, Y., Dong, H. and Dworkin, S.I. (2019): Organic structural properties of kerogen a predictors of source rock type and hydrocarbon potential. Fuel; 184: 792-798.

Longford, F.F. and Blanc-Valleron, M.M. (1990): Interpreting Rock–Eval pyrolysis data using graphs of pyrolyzable hydrocarbons vs. total organic carbon, AAPG Bulletin; 74: 799-804.

Martinez, A.R., Ion, D.C., Desorcy, G.J. and Dekker, H. (1984): Classification and nomenclature systems for petroleum and petroleum reserves. 11th World Petroleum Congress, London, Wiley, Chichester; 2: 325-343.

Moldowan, J.M., Dahl, J., Jacobson, S.R., Huizinga, B.J., Fago, F.J., Shetty, R., Watt, D.S. and Peters, K.E. (1996): Chemostratigraphic reconstruction of biofacies: Molecular evidence linking cyst-forming dinoflagellates with pre-Triassic ancestors. Geology; 24: 159-162.

Munz, I.A. (2001): Petroleum inclusions in sedimentary basins: systematics, analytical methods and applications. Lithos; 55(1-4): 195-212.

Pestilho, A.L.S., Monteiro, L.V.S., Carbonezi, C.A., Jorge, S.B. and Neto, E.V.S. (2018): Linking the geochemistry of crude oils and petroleum inclusions in the Ubarana and Lorena oilfields, Potiguar Basin, Brazilian Equatorial Margin. Organic Geochemistry; 124: 133-150.

Peters, K.E. and Cassa, M.R. (1994): Applied source rock geochemistry. In: Magoon, L.B., Dow, W.G. (Eds.): The petroleum system from source to trap, AAPG, Mem.; 60: 93-117.

Peters, K.E., David, J.C. and Marek, K. (2012): An overview of basin and petroleum system modeling: Definitions and concepts. In: Peters, K.E., David, J.C., Marek, K. (Eds.), Basin Modeling: New Horizons in Research and Applications. AAPG Hedberg Series; 4: 1-16.

Peters, K.E. and Moldowan, J.M. (1993): The biomarker guide: Interpreting molecular fossils in petroleum and ancient sediments. Prentice-Hall, Inc, Englewood Cliffs, New Jersey.

Peters, K.E., Walters, C.C. and Moldowan, J.M. (2005): The biomarker guide: Biomarkers and isotopes in petroleum exploration and Earth history. 2nd edition, vol. 2. Cambridge University Press, Cambridge.

Pironon, J., Pagel, M., Walgenwitz, F. and Barres, O. (1995): Organic inclusions in salt. Part 2: oil, gas and ammonium in inclusions from the Gabon margin. Organic Geochemistry; 23(8): 739-750.

Pratsch, J. (1994): Tunisia’s oil and gas potential and future plays. In: Proc. 4th. Conf Tunisian Pet. Explor. (Ed. A. Chine and K. Ben Hassine). ETAP, Tunis; pp. 1-25.

Rabbani, A.R. and Kamali, M.R. (2005): Source rock evaluation and petroleum geochemistry, offshore SW Iran. Journal of Petroleum Geology; 28(4): 413-428.

Racey, A., Bailey, H.W., Beckett, D., Gallagher, L.T., Hampton, M.J. and Mcquilken, J. (2001): The petroleum geology of the Early Eocene El Garia Formation, Hasdrubal field, offshore Tunisia. Journal of Petroleum Geology; 24: 29-53.

Ricchiuto, T. and Pajola, M. (2003): Libya NC 41: Integration of chemical and isotopic analyses. Second Symposium on the Sedimentary Basins of Libya, The geology of northwest Libya, vol. 3. (eds. M.J. Salem, K.M. Oun and H.M. Seddiq), Earth Science Society of Libya, Tripoli, pp. 55-64.

Samani, N.N., Miforughy, S.M., Safari, H., Mohammadzadeh, O., Panahbar, M.H. and Zendehboudi, S. (2019): Solubility of hydrocarbon and non-hydrocarbon gases in aqueous electrolyte solutions: A reliable computational strategy. Fuel; 241: 1026-1035.

Sbeta, A.M. (1990): Stratigraphy and lithofacies of Farwah Group and its equivalent: offshore NW Libya. Journal of Petroleum Research (Tripoli); 2: 42-56.

Schulz, H.M., Sachsenhofer, R.F., Bechtel, A., Polesny, H. and Wagner, L. (2002): The origin of hydrocarbon source rocks in the Austrian Molasse Basin (Eocene-Oligocene transition). Marine and Petroleum Geology; 19(6): 683-709.

Schulz, L. K., Wilhelms, A., Rein, E. and Steen, A.S. (2001): Application of diamondoids to distinguish source rock facies: Organic Geochemistry; 32: 365-375.

Seiter, K., Hensen, C., Schroter, J. and Zabel, M. (2004): Organic carbon content in surface sediments—defining regional provinces. Deep Sea Research Part I: Oceanographic Research Papers; 51(12): 2001-2026.

Selley, R.C. (1998): Elements of Petroleum Geology. 2nd edition, Academic Press, 470p.

Shaltami, O.R. (2012): Mineral composition and environmental geochemistry of the beach sediments along the Mediterranean Coast from Benghazi to Bin Jawwad, Northeast Libya. Unpublished PhD Thesis, Cairo University, Egypt.

Shaltami, O.R., Liu, Y., Jorgensen, L., Elkjaer, C., Fares, F.F., Errishi, H., EL Oshebi, F.M. and Souza, R. (2019): Organic geochemistry of shale and marl: A case study of the Miocene deposits in the Cyrenaica Basin, NE Libya. World Chemistry 2019, Philadelphia, USA, Proceeding Book; pp. 70-82.

Shaltami, O.R., Siasia, G.D., Fares, F.F., Errishi, H. and EL Oshebi, F.M. (2018): Petroleum geochemistry of reservoir: A case study of the Achabiyat and Hawaz formations in the Dur Al Qussah area, SW Libya. Deloitte Oil and Gas Conference, Houston, Texas, USA, Proceeding Book; pp. 22-31.

Shaltami, O.R., Siasia, G.D., Fares, F.F., Errishi, H., EL Oshebi, F.M. and Souza, R. (2018): Petroleum geochemistry of the Akakus Formation in the Dur Al Qussah area, Murzuq Basin, SW Libya. 4th Annual IoT in Oil and Gas Conference, Houston, Texas, USA, Proceeding Book; pp. 11-23.

Shanmugam, G. (1985): Significance of coniferous rain forests and related organic matter in generating commercial quantities of oil, Gippsland Basin, Australia. American Association of Petroleum Geologists Bulletin; 69: 1241-1254.

Shea, R.C., Habicht, S.C., Vaughn, W.E. and Kenttamaa, H.I. (2007): Design and characterization of a high-power laser-induced acoustic desorption (LIAD) probe coupled with a fourier-transform ion cyclotron resonance mass spectrometer. Analytical Chemistry; 79(7): 2688-2694.

Si, S.H., Chen, H.H., Feng, Y. and Wang, Y.L. (2013): Two sources and three charging events of hydrocarbons in Lower Cretaceous reservoirs in Shaya Uplift, Tarim Basin: Evidence from fluid inclusion analysis. Acta Petrolei Sinica; 34(1): 12-21.

Sousa, E.S., Junior, G.R.S., Silva, A.F., Reis, F.A.M., de Sousa, A.A.C., Cioccari, G.M., Capilla, R., de Souza, I.V.A.F., Imamura, P.M., Rodrigues, R., Lopes, J.A.D. and de Lima, S.G. (2019): Biomarkers in Cretaceous sedimentary rocks from the Codó Formation - Parnaíba Basin: Paleoenvironmental assessment. Journal of South American Earth Sciences; 92: 265-281.

Stach, E. (1982): Stach’s text book of coal petrology, 3rd edition. Gebruder Borntraeger, Berlin/Stuttgart; 535p.

Tahoun S.S. and Mansour, A. (2019): The first record of reworked Upper Palaeozoic palynomorphs in the Raha Formation, Gulf of Suez, Egypt. Journal of African Earth Sciences; 153: 67-71.

Tiem, V.T.A., Horsfield, B. and Sykes, R. (2008): Influence of in-situ bitumen on the generation of gas and oil in New Zealand coals. Organic Geochemistry; 39(11): 1606-1619.

Tissot, B.P. and Welte, D.H. (1984): Petroleum formation and occurrence, second edition. Springer Verlag, Berlin, 699p.

Tuo, J., Wang, X. and Chen, J. (1999): Distribution and evolution of tricyclic terpanes in lacustrine carbonates. Organic Geochemistry; 30: 1429-1435.

Van Krevelen, D.W. (1961): Coal: typology-chemistry-physics-constitution: Elsevier Science, Amsterdam; 514p.

Volk, H. and George, S.C. (2019): Using petroleum inclusions to trace petroleum systems – A review. Organic Geochemistry; 129: 99-123.

Volk, H., George, S.C., Killops, S.D., Lisk, M., Ahmed, M. and Quezada, R.A. (2002): The use of fluid inclusion oils to reconstruct the charge history of petroleum reservoirs – an example from the Taranaki Basin. New Zealand Petroleum Conference; pp. 221-233.

Waples, D.W. (1985): Geochemistry in petroleum exploration. Boston, MA: International Human Resources Development Corporation, 232p.

Waples, D.W. and Machihara, T. (1990): Application of sterane and triterpane biomarkers in petroleum exploration. Bulletin of Canadian Petroleum Geology; 38: 357-380.

Yandoka, B.M.S., Abdullah, W.H., Abubakar, M.B., Hakimi, M.H. and Adegoke, A.K. (2015): Geochemical characterisation of Early Cretaceous lacustrine sediments of Bima Formation, Yola Sub-basin, Northern Benue Trough, NE Nigeria: Organic matter input, preservation, paleoenvironment and palaeoclimatic conditions. Marine and Petroleum Geology; 61: 82-94.

Yang, Z., Li, M., Cheng, D., Xiao, H., Lai, H. and Chen, Q. (2019): Geochemistry and possible origins of biodegraded oils in the Cretaceous reservoir of the Muglad Basin and their application in hydrocarbon exploration. Journal of Petroleum Science and Engineering; 173: 889-898.

Xia, L., Cao, J., Hu, S., Li, S. and Shi, C. (2019): Organic geochemistry, petrology, and conventional and unconventional hydrocarbon resource potential of Paleogene saline source rocks in eastern China: The Biyang Sag of the Nanxiang Basin. Marine and Petroleum Geology; 101: 343-354.

Xiao, H., Li, M., Liu, J., Mao, F., Cheng, D. and Yang, Z. (2019): Oil-oil and oil-source rock correlations in the Muglad Basin, Sudan and South Sudan: New insights from molecular markers analyses. Marine and Petroleum Geology; 103: 351-365.

Xu, Z., Liu, L., Wang, T., Wu, K., Gao, X., Dou, W., Xiao, F., Zhang, N., Song, X. and Ji, H. (2017): Application of fluid inclusions to the charging process of the lacustrine tight oil reservoir in the Triassic Yanchang Formation in the Ordos Basin, China. Journal of Petroleum Science and Engineering; 149: 40-55.

Zhang, S. and Huang, H. (2005): Geochemistry of Palaeozoic marine petroleum from the Tarim Basin, NW China: Part 1. Oil family classification. Organic Geochemistry; 36: 1204-1214.

Zhang, S.C., Huang, H.P., Xiao, Z.Y. and Liang, D.G. (2005): Geochemistry of Palaeozoic marine petroleum from the Tarim Basin, NW China. Part 2: maturity assessment. Organic Geochemistry; 36: 1215-1225.

Zhou, S. and Huang, H. (2008): Controls on alkylphenol occurrence and distribution in oils from lacustrine rift basins in East China. Science in China Series D: Earth Sciences; 51(7): 976-983.

Ziegs, V., Noah, M., Poetz, S., Horsfield, B., Hartwig, A., Rinna, J. and Skeie, J.E. (2018): Unravelling maturity- and migration-related carbazole and phenol distributions in Central Graben crude oils. Marine and Petroleum Geology; 94: 114-130.

Zumberge, J.E. (1987): Prediction of source rock characteristics based on terpane biomarkers in crude oils: A multivariate statistical approach. Geochimica et Cosmochimica Acta; 51: 1625-1637.

جيوكيمياء النفط لتكوين مخباز في البئر البحري

ك – 137، حوض صبراته، شمال غرب ليبيا

قدمت من قبل :

عبد الرحمن حمد علي السنوسي

تحت إشراف :

د. أسامة الشلطامي

الملخص

إن هذه الدراسة عبارة عن تقييم جيوكيميائي لتشكيل مخباز في البئر البحري ك –137، حوض صبراتة، شمال غرب ليبيا. أشار محتوى الكربون العضوي الكلي إلى أن مخباز الطين الصفائحي هو صخر مصدري ممتاز. المادة العضوية ناضجة حرارياً وتتميز بسيادة النوع الثاني من الكيروجين. إن الغاز الأكثر وفرة في المستحضرات البترولية من الحجر الجيري في مخباز هو C_1 مع وجود كميات أقل من C_2، C_3، nC_4 iC_4، N_2 ، CO_2 و H_2S. هناك نوعان من عائلات النفط في الادراج البترولية. يعتبر مخباز الصخر المصدر الرئيسي لزيوت العائلة 1 (الزيوت الثقيلة)، في حين أن زيوت العائلة 2 (الزيوت الخفيفة) قد تكون مشتقة من تكوين بلال. جميع الزيوت ناضجة حراريا. حدثت حالتان لشحن النفط في خزان مخباز.

الكلمات الدالة:

جيوكيمياء النفط ، صخور المصدر ، خزان نفطي ، تكوين مخباز ، حوض صبراته ، ليبيا.

جيوكيمياء النفط لتكوين مخباز في البئر البحري

ك – 137، حوض صبراته، شمال غرب ليبيا

قدمت من قبل :

عبد الرحمن حمد علي السنوسي

تحت إشراف :

د. أسامة الشلطامي

قدمت هذه الرسالة استكمالا لمتطلبات الحصول على درجة الماجستير في علم الجيوكيمياء

جامعة بنغازي

كلية العلوم

ديسمبر 2019